Experimental and Numerical Study on Flow and Heat Transport in Partially Frozen Soil

by

MD Montasir Islam

A Thesis submitted to the Faculty of Graduate Studies of

The University of Manitoba

in partial fulfillment of the requirements of the degree of

MASTER OF SCIENCE

Department of Civil Engineering

University of Manitoba

Winnipeg

ABSTRACT

Frozen soil has a major effect in many hydrologic processes, and its impacts are difficult to predict. A prime example is flood forecasting during spring snowmelt within the Canadian Prairies. One key driver for the extent of flooding is the antecedent soil moisture and the possibility for water to infiltrate into (partly) frozen soils. Therefore, these situations are crucial for accurate flood prediction at every spring. The main objective of this study was to evaluate the water flow and heat transport within available hydrological models to predict the impact of frozen and partly frozen soil on infiltration and percolation. A standardized data set was developed for water flow and heat transport into (partial) frozen soil by laboratory experiments using fine sand within a one-dimensional (1-D) soil column. A 1-D soil column having a length of 107 cm and diameter of 35.6 cm was built and equipped with insulation to limit heat exchange only through the soil surface. A data logger collected the moisture content and temperature by five FDR sensors which have been installed at a distance of 15 cm from each other. During the experiments, temperature, soil moisture, and percolated water was observed at different freezing conditions (-5°C, -10°C, and -15°C) as well as at thawing conditions when the air temperature was increased to +5°C. Distribution of soil moisture and soil temperature in the soil column was plotted for the experimental data over the freezing and thawing period. As some of the water in the soil begins to freeze, a decrease in water content was observed with a sudden increase in soil temperature near 0°C or slightly below of 0°C. This was, in fact, only a decrease in unfrozen water, not a decrease in total water content and was caused by the latent heat during freezing. Soil temperature showed noticeable differences at the top and the bottom of soil column during the change of state of water. The heat flux at the lower soil column was strongly limited due to

the overlying soil. Thus, the soil temperature at the lowest sensors stayed in a freezing condition over several days and was not changing the temperature due to the latent heat which was released during the freezing process. Significant variation in soil moisture content was found between the top and the bottom of the soil column at the starting of the thawing period. However, with increasing temperature, the lower depth of the soil column showed higher moisture content as the soil was enriched with moisture with higher transmission rate due to the release of heat by soil particles during the thawing cycle. The soil system did not remain in the isothermal state during the thawing cycle. Although gravitational gradient was mainly responsible for the infiltration rate into the partially frozen soil, the distribution of moisture was greatly influenced by the temperature gradient. Vadose zone modeling using HYDRUS-1D was applied to the data set. Numerical results of the modeling were calibrated using the experimental results. It showed that the newly developed benchmark data set were useful for the validation of numerical models. The use of such a validated freezing and thawing module implemented into larger scale hydrologic models will directly reduce the prediction uncertainty during flood forecasting. Moreover, these benchmark data sets will be useful for the validation of numerical models and for developing scientific knowledge to suggest potential code variations or new code development in numerical models.

ACKNOWLEDGEMENT

I would like to express my deepest and sincere gratitude to my supervisor Dr. Hartmut Holländer, Ph.D., P.Eng., Associate Professor in the Department of Civil Engineering at the University of Manitoba, for his guidance, continuous encouragement and unlimited support throughout the course of this research program. The assistance of Dr. Seifu Guangul, Ph.D., P.Eng., Dr. Shawn Clark, Ph.D., P.Eng., Dr. Wole Akinremi, Ph.D. and Dr. Jirka Šimunek, Ph.D. are also tremendously appreciated.

I would like to express my gratitude and sincere appreciation for the financial support received from the Natural Science and Engineering Research Council of Canada (NSERC), through Dr. Hartmut Holländer, Ph.D., P.Eng.and Stantec. The help received from the technical staff of the Geotechnical Laboratory and the Hydraulics Research and Testing Facilities Laboratory in the Department of Civil Engineering and the Soil Physics Laboratory in the Department of Soil Science at the University of Manitoba are also acknowledged.

I would like to thank Mr. Kerry Lynch, Mr. Alexander Wall, Mr. Rob Ellis, Mr. Zijian Wang, Ms. Yingwen Tan, Ms. Cindy Nguyen, Ms. Theresa Adesanya and Mr. Konstantinos Velegrinos for their support and encouragement.

Finally, I would like to express my deepest gratitude to my parents and my elder brother for their invaluable support throughout my academic career.

LIST OF ALL VARIABLES

A	amplitude of the temperature sine wave at soil surface [K]
b	weights associated with a particular measurement set or point [-]
b_1	empirical parameters [-]
b_2	empirical parameters [-]
b_3	empirical parameters [-]
C	free space electromagnetic wave [-]
C_i	volumetric heat capacities of the ice [$ML^{-1}T^{-2}K^{-1}$] (e.g., $Jm^{-3}K^{-1}$)
C_n	volumetric heat capacities of the solid [$ML^{-1}T^{-2}K^{-1}$] (e.g., $Jm^{-3}K^{-1}$)
C_p	volumetric heat capacity of the soil [$ML^{-1}T^{-2}K^{-1}$] (e.g., $Jm^{-3}K^{-1}$)
C_v	volumetric heat capacities of the vapour [$ML^{-1}T^{-2}K^{-1}$] (e.g., $Jm^{-3}K^{-1}$)
C_w	volumetric heat capacities of the liquid [$ML^{-1}T^{-2}K^{-1}$] (e.g., $Jm^{-3}K^{-1}$)
D_a	length (mm) in which the surface force will influence the water permittivity [L]
E	maximum potential rate of infiltration or evapotranspiration [LT^{-1}]
h	pressure head [L] (e.g., cm)
h*	reference pressure head [L]
h_A	minimum pressure head at the soil surface [L]
h_c	heat transfer coefficient [$WL^{-2}k^{-1}$](e.g., $Wm^{-2}k^{-1}$)
h_{ref}	pressure head at reference temperature T_{ref} [L]
h_s	maximum pressure head at the soil surface [L]

h_T	pressure head at temperature T [L]
K	unsaturated hydraulic conductivity [LT^{-1}]
K_a	dielectric permittivity [-]
K_r	relative hydraulic conductivity [-]
K_s	saturated hydraulic conductivity [LT^{-1}]
K_T	hydraulic conductivity at soil temperature T [LT^{-1}]
K^*	reference unsaturated hydraulic conductivity [-]
K_{Lh}	water flows due to pressure head and gravity [LT^{-1}]
K_{LT}	water flow due to temperature gradient [$L^2 T^{-1}K^{-1}$]
K_{vh}	vapor flows due to pressure head [LT^{-1}]
K_{vT}	vapor flows due to temperature [$L^2 T^{-1} K^{-1}$]
K_{flh}	hydraulic conductivity for liquid phase in partially frozen soil [LT^{-1}]
K_{ice}	dielectric constant of ice [-]
K_{ref}	hydraulic conductivity at reference temperature T_{ref} [LT^{-1}]
K_{soil}	dielectric constant of soil [-]
k_0	matching point which can be fitted at saturation [L/T] (e.g., cm day^{-1})
L	empirical parameter [-]
L_0	volumetric latent heat of the water [ML^1T^{-2}] (e.g., J m^{-3})
L_f	latent heat of freezing [L^2T^{-2}] (e.g., J kg^{-1})
L_w	latent heat due to the vaporization of water [$ML^{-1}T^{-2}$] (e.g., J kg^{-1})
m	empirical parameter [-]
m_p	number of different sets of measurements for soil hydraulic properties [-]

m_q	number of different sets of measurements [-]
n	measure of pore size distribution [-]
n_i	observation day [T]
$n_{p\,j}$	number of measurements in a particular measurement sets for soil hydraulic properties [-]
$n_{q\,j}$	number of measurements in a particular measurement sets [-]
o	organic matter [-]
o_i	observed values at the i^{th} day [-]
o_l	mean observed value [-]
P_W	density of water [ML^{-3}]
$p_j(\theta_i, b)$	corresponding model predictions for the vector of optimized parameters for soil hydraulic properties [-]
$p_j^*(\theta_i)$	specific measurements at water content θ_i for the j^{th} measurement for soil hydraulic properties [-]
Q	ratio of the ice content to the total water content [-]
q	Darcian fluid flux density [LT^{-1}]
q_h	heat flux [WL^{-2}] (e.g., Wm^{-2})
$q_j*(x,t)_i$	specific measurements at time t_i for the j^{th} measurement [-]
$q_j*(x, t_i, b)$	corresponding model predictions for thevector of optimized parameters [-]
r^2	co-efficient of determination [-]
S	specific surface area [L^2/M]
S_e	effective saturation [-]

s	sink term in the flow equation [T^{-1}] (e.g., $m^3m^{-3}day^{-1}$)
s_i	simulated values at the i^{th} day [-]
T	temperature, [K] (e.g., ºC)
t	time [T]
T_i	initial temperature [K]
t_0	time when the simulation starts [T]
T_0	daily fluctuations in soil temperature [K]
T_t	travel time [T]
T_{avg}	average temperature at the soil surface [K]
$T_{coolant}$	temperature of the incoming fluid [K]
T_{ref}	reference temperature [K]
T_{top}	temperature of the soil surface [K]
v	propagation velocity [L/T] (e.g., m/s)
v_j	weights associated with a particular measurement set or point [-]
$\overline{v_j}$	weights associated with a particular measurement set or point for soil hydraulic properties [-]
W_u	unfrozen water content [-]
$w_{i,j}$	weights associated with a particular measurement set or point [-]
$\overline{w_{i,j}}$	weights associated with a particular measurement set or point for soil hydraulic properties [-]
x	spatial coordinate [L]
x(r,z)	coordinates of a location [-]

z	spatial coordinate positive upward [L]
α	geometric factor [-]
α_k*	temperature scaling factor for the hydraulic conductivity [-]
β	angle between the flow direction and the vertical axis [º]
β_t	thermal dispersity [L]
γ	surface tension of soil water [MT^{-2}]
ε	dielectric permittivity or dielectric constant [-]
ϵ_a	permittivity of air [-]
ϵ_i	permittivity of ice [-]
ϵ_r	relative dielectric permittivity of soil [-]
ϵ_s	permittivity of soil [-]
ϵ_{bw}	permittivity of ice above 0ºC [-]
θ	temperature at freezing point depression [ºC]
$\theta(h)$	measured volumetric water content [-](e.g., cm^3cm^{-3})
θ_i	volumetric ice content [-]
θ_r	residual water content [-]
θ_r*	reference residual water content [-]
θ_s	saturated water content [-]
θ_m	gravimetric moisture content [-]
θ_u	unfrozen water content in soil [-]
θ_v	volumetric water content [-]
θ_{va}	volumetric vapor content [-]

θ_v^*	reference volumetric water content [-]
θ_{vl}	volumetric liquid water content [-]
θ_{tot}	unfrozen water content + frozen ice [-]
λ	latent heat of fusion of water [L^2T^{-2}] (e.g., kJ kg^{-1})
$\lambda(\theta)$	coefficient of the apparent thermal conductivity [$MLT^{-3}K^{-1}$]
$\lambda_0(\theta)$	thermal conductivity [$MLT^{-3}K^{-1}$]
μ_h	scaling factors for the pressure head [-]
μ_k	scaling factors for hydraulic conductivity [-]
μ_T	dynamic viscosity at temperature$T$ [$ML^{-1}T^{-1}$]
μ_{Tref}	dynamic viscosity at reference temperature T_{ref} [$ML^{-1}T^{-1}$]
μ_θ	scaling factors for the water content [-]
ρ_i	density of the ice [ML^{-3}]
ρ_T	density of soil water at temperature$T$ [ML^{-3}]
ρ_w	density of liquid water [ML^{-3}]
ρ_t	period of time [T]
ρ_{ref}	density of soil water at reference temperatureT_{ref} [ML^{-3}]
Ψ_i	ice potential [L^2T^{-2}] (e.g., J kg^{-1})
σ	surface tension at the interface of air-water [MT^{-2}]
σ_T	surface tensions at temperature T [MT^{-2}]
σ_{ref}	surface tensions at reference temperature T_{ref} [MT^{-2}]
Φ	objective function [-]
Ω	impedance factor [-]

ACRONYMS

CHWT	Coupled Heat Water Transfer
EM	Electromagnetic
EMI	Electromagnetic Induction
EC	Electrical Conductivity
FDR	Frequency Domain Reflectometry
GMER	Geometric Mean Error Ratio
MAE	Mean Absolute Error
ME	Mean Error
NMR	Nuclear Magnetic Resonance
NSE	Nash-Sutcliffe Efficiency
OSM	Observed soil moisture
OST	Observed soil temperature
PVC	Polyvinyl Chloride
RMSE	Root Mean Square Error
SFC	Soil Freezing Characteristic
SWAT	Soil and Water Assessment Tool
SWC	Soil Water Retention Curve
SWE	Snow Water Equivalent
SHE	Systeme HydrologiqueEuropeen
SSM	Simulated soil moisture

SST	Simulated soil temperature
TDR	Time Domain Reflectometry
tt	Travel Time
VWC	Volumetric Water Content
VGM	van Genuchten-Mualem
WaSiM	Water Balance Simulation Model
1-D	One-Dimensional

TABLE OF CONTENTS

LIST OF TABLES

LIST OF FIGURES

CHAPTER 1

INTRODUCTION

1.1 Motivation

Sudden snow melt and strong precipitation are the key factors behind flooding situation. A prime example is flood forecasting during spring snowmelt within the Canadian Prairies. Impacts of snowmelt are associated with large uncertainties: a key factor is the effect of frozen and thawing soils and how water can infiltrate into them. Soils can drastically reduce the infiltration rate since water expands in frozen conditions by about 9%(Paterson 1995) and can effectively seal the open pores. The corresponding reduction of the pore space directly increases the amount of meltwater that is then available at the surface and can lead to overland flow and flooding situations which occur mainly during spring time in Canadian Prairies. Spring runoff depends on the soil moisture level in the preceding fall(Suzuki 2013). Runoff regime can be affected by the high water saturation and early frost penetration, or heavy rain on the still frozen soil in spring(Stähli et al. 2001).Therefore, understanding the freezing and thawing processes of soils and the infiltration into them is of major importance for forecasting using hydrological models. While considerable research work in this area has been carried out, no panacea to the problem has yet emerged. For example, a comparison of hydrological prediction using ten different hydrological models showed that freezing and thawing of soil and the resulting water movement was not adequately integrated into large-scale hydrologic models (Holländer et al. 2009). A general problem in hydrological modeling is that models are all quite flexible because of their high dimensionality. Therefore, virtually any hydrological response can be simulated with “appropriately selected”

parameters by the model users (Holländer et al. 2014). Several studies have proved how model parameters can compensate for model structural errors, often by assuming unrealistic values during parameter estimation procedures (e.g., Clark and Vrugt 2006).Most of the tested models (Hydrus (Simunek et al. 1999),Soil and Water Assessment Tool (SWAT) (Arnold et al. 1998), Water Balance Simulation Model (WaSiM-ETH) (Schulla and Jasper 2007)) used simple freezing/thawing routines, like the "degree-day" approach. Only CoupModel(Jansson and Moon 2001) which was developed in Sweden contains a physical-based method where snow melt/refreeze was based on energy balance including surface heat exchange, radiation, and near surface soil heat flux. However, precipitation was crudely assumed to be snow below temperature $T < 0°C$ and to be a mixture of rain and snow in a temperature range from 0 to +2°C. Moreover, CoupModel was not able to predict the runoff from a massive snowmelt event in the right order of magnitude during the above-mentioned study (Holländer et al. 2009). Even in the last few decades, simulation of subsurface flows became a topic of interest for the large scale hydrological situations (Borsi et al. 2013). Since the freezing and thawing processes of soil and the infiltration into them were not adequately addressed in large-scale hydrological models, this study aimed for a better representation of these processes in meso to large scale hydrological situations. Therefore, there was a need to evaluate the implemented freezing and thawing processes of the models using common sets of criteria and standards, which will allow for parameterization of all models in the same way. A new standardized data set was needed since existing data sets were generally created to verify a certain numerical model (Flerchinger and Saxton 1989b). This attempt was in contrast to the traditional method where each model was independently evaluated and validated using different sets of criteria.

1.2 Objective and scope of research

The aim of this research was to develop a benchmark data set for fine sand in different freezing to thawing cycles that can resemble the physical properties of water flow and heat transport in partly frozen soil when soil water system was moving from a freezing to a thawing cycle (*objective 1*) and later this data set was used for inverse calibration by using vadose zone modeling to optimize the parameters that were mainly responsible for addressing water flow and heat transport in partly frozen soil (*Objective 2*).

In a first phase a standardized data set was developed using laboratory-based experiments for the evaluation of infiltration into (partial) frozen soils and its application of available physical-based numerical models. In order to develop a standardized data set, laboratory experiments were performed using standardized fine sand within a one-dimensional soil column to evaluate the flow and heat transportinpartially frozen soils. Later, a physical-based vadose zone model was used on the laboratory results, which was capable of re-predicting the standardized data to some extent. The applied physical-based relationships in these models can be used for further optimization and application into new numerical codes.

The thesis was organized as follows: In Chapter 2**,** an introduction of laboratory experiments in partially frozen soil and modeling the vadose zone was presented. This was followed by a review of the available literature on water movement into seasonally frozen soils, soil freeze-thaw cycle experiments, direct and indirect method of soil moisture measurement in frozen soil, factors that can affect the accurate measurement of soil moisture, calibration of the soil moisture measurement devices, freezing and thawing characteristics of soil in the unsaturated zone, unsaturated soil hydraulic parameters and how these parameters were addressed in recent hydrological models. In Chapter 3**,** the experimental setup, test conditions, and the measurement

procedure which contained details on Frequency Domain Reflectometry (FDR) to measure the soil moisture content and temperature measurement procedure were described. Moreover, governing equations for coupling of heat and fluid flow in the unsaturated zone by numerical modeling was also discussed in this chapter. Results and discussions are covered in Chapter 4 and Chapter 5 respectively. Specifically observed temperature, soil moisture and percolated water at different freezing conditions as well as thawing conditions were discussed, followed by the results of the simulation to address which physically based relationship in the model can be used for further optimization. The major conclusions from the current study and recommendations for future work were presented in Chapter 6 and Chapter 7 respectively.

CHAPTER 2

LITERATURE REVIEW

The movement of soil water in partially frozen soil largely depends on the change of soil temperature in the unsaturated zone. If water cannot infiltrate due to pore blockage in the unsaturated zone, overland flow can occur which will lead to a flooding situation. In unsaturated zone groundwater fluctuations might happen if the groundwater recharge is not matched by the rate of infiltration and percolation. Therefore, understanding the water flow and heat exchange in partially frozen soil, measuring the moisture content and soil temperature in partially frozen soil and numerical simulation of the coupled heat and fluid flow were the main challenges to address these problems in right scale. Considerable research works were done to address the solutions of these problems. In this chapter, different techniques for measuring soil water movement and temperature change in partially frozen soil, estimation procedure of the unsaturated soil hydraulic properties for the numerical analysis of soil column experiments and different numerical modeling tools to simulate water flow and heat transport in partially frozen soil were discussed based on the previous research works.

2.1 Water flow and measurement technique in the seasonally frozen soil

Numerous components were found responsible for the movement of water into the frozen soil which was difficult to quantify. Especially water movement in the unsaturated zone wascomplicated because of the presence of air (Kane and Stein 1983). Temperature played an important role in the analysis of unsaturated frozen soil as fluid properties changed with temperature. The magnitude of temperature change and its effect were different in the saturated

and unsaturated soil. This was because of the presence of unfrozen water content as thin films on the surface of soil particles. The quantity of unfrozen water content varied according to the soil water content and soil types. Unfrozen water content could be found in greater quantities infine grained soil with larger surface areas. An equation was presented by Anderson and Morgenstern (1973) which was used by Kane and Stein (1983) to predict unfrozen water content (W_u) as a function of temperature and surface are:

$$\ln(W_u) = a + b\ln(S) + cS^d \ln(\theta) \quad (1)$$

In this equation a, b, c and d were empirical coefficients, S was the specific surface area, L^2/M; and θ was the temperature at freezing point depression, ºC. When W_u was equal to the total moisture content or less than that only, then equation 1 was valid (Kane and Stein 1983).

The unsaturated frozen soil has four components: soil, ice, water and air which made studying it complicated. In the case of unsaturated soil, equation 1 was still valid under the same condition. But if W_u was greater than the total moisture content, all water present in the soil was unfrozen. Watanabe and Wake (2009) showed that at sub-zero temperature a certain amount of water remained unfrozen because surface forces of soil particles and the pore geometry among soil particles decreased the free energy of soil water(Miller 1980; Dash et al. 1995; Watanabe and Mizoguchi 2002; Cannell and Gardner 1959; Watanabe and Wake 2009). The measurement of unfrozen water content was always challenging and ended up with empirical equations derived from lab experiments. Watanabe and Wake (2009) measured liquid water content and relative permittivity of unsaturated soils of various types at sub-zero temperatureusing pulse nuclear magnetic resonance (NMR) and time domain reflectometry (TDR). They presented a mixing model that can address unfrozen water content in the frozen sand by including reduced dielectric permittivity due to surface forces and ice formation. However soil water content was commonly

estimated by using the Topp equation based on the dielectric permittivity of soil (Topp et al. 1980; Watanabe and Wake 2009):

$$\theta_v = -5.3 \times 10^{-2} + 2.92 \times 10^{-2} K_a - 5.5 \times 10^{-4} k_a^2 + 4.3 \times 10^{-6} k_a^3 \quad (2)$$

In this equation $\theta_v$was the volumetric water content (-) and $K_a$was the measured dielectric permittivity or dielectric constant (-) which was often addressed as ε in other research works. Watanabe and Wake (2009) showed the following equation to measure the unfrozen water content in frozen condition:

$$\theta_{u=} \sqrt{p_w S D_a \frac{(\varepsilon_r^\alpha - \varepsilon_a^\alpha) - \theta_s(\varepsilon_s^\alpha - \varepsilon_a^\alpha) - \theta_{tot}(\varepsilon_i^\alpha - \varepsilon_a^\alpha)}{\varepsilon_{bw}^\alpha - \varepsilon_i^\alpha}} \quad (T < 0, \theta_u < p_w S D_a) \quad (3)$$

In this equation, $\theta_u$was the unfrozen water content in the soil (-), $p_W$was the density of water (ML^{-3}), S was the specific surface area (L^2M^{-1}), D_a was the length (L) in which the surface force will influence the water permittivity, $\epsilon_r$was the relative dielectric permittivity of the soil (-), $\epsilon_a$was the permittivity of the air (-), $\epsilon_s$was the permittivity of the soil (-), $\epsilon_i$was the permittivity of the ice (-), $\theta_{tot}$was the unfrozen water content (-) + frozen ice , α was the geometric factor (-), $\epsilon_{bw}$was the permittivity of ice above 0ºC(-), and T was the temperature (ºC).

The relation between water content and water potential was one of the most important factors to address hydraulic properties in the vadose zone. At large negative pressure, the hydraulic conductivity of the samples became very low which caused extensive time for equilibrium state. Madsen et al. (1986) found that water potential determined by pressure plates was lower than water potential measured by thermocouple psychrometer. However, the main reason for these discrepancies was a partial interruption of the continuous water phase during pressure plate measurements and lack of thermodynamic equilibrium (Madsen et al. 1986; Campbell et al. 1986). Considering this, an alternative way to determine the moisture characteristics was the

freezing point depression of liquid water. Bouyoucos and McCool (1916) found that the wilting point of the soils could be determined by measuring the freezing point depression. It has been experimentally proven that water potential was the main reason for freezing point depression in the porous media (Cannell and Gardner 1959; Schofield and Da Costa 1938; Day 1942 ; Bittelli et al. 2003). Adsorptive and capillary forces were the two main forces that lower the energy status of water and cause water to remain unfrozen at a temperature well below freezing point (Bittelli et al. 2003). Bittelli et al. (2003) measured temperature and unfrozen water content using a thermistor and a spiral shaped transmission line, and later temperatures were converted to water potential using Clapeyron equation (Spaans and Baker 1996a):

$$d\Psi_L = \left(\frac{\lambda}{T}\right) dT + d\,\Psi_i \tag{4}$$

In the above equation, Ψ_i was the ice potential (L^2T^{-2}), T was the temperature (K), and λ was the latent heat of fusion of water (333.7 kJ Kg^{-1} at 273.15 K), subscript L and i were liquid water and ice respectively. This was possible when liquid water and ice co-existed and ice was assumed to be at atmospheric pressure, then using Clapeyron equation water potential of the liquid phase can be obtained from temperature. The relationship between the quantity and energy status of liquid water in frozen soil can be represented by a soil freezing characteristic (SFC) curve (Spaans and Baker 1996a). They have also used the Clapeyron equation to measure the matric potential of frozen soil. But in that case liquid water content was measured using time domain reflectometry (TDR) method. High matric potential gave better soil moisture characteristics but at the same time it became inaccurate and time consuming when the soil dried. Therefore, water retention properties can be obtained for high matric potentials but with the decrease of temperature as soil can result low matric potential from freezing, TDR could be used to get the moisture content of partially frozen soils. This was because when the temperature dropped, a portion of soil water

changed phase and became frozen in situ. Remaining unfrozen water stayed in adsorbed films around particles. This water content in the partially frozen soil can be directly identified using TDR. At the same time, release of latent heat was an important factor here as it was temperature dependent according to equation 4. In order to address the effect of latent heat in the phase change, it was important to measure the temperature of the vadose zone at frozen condition.

2.2 Measuring soil moisture and temperature using indirect method

Direct or indirect methods could be used to measure soil moisture. One of the direct methods was removing the water by heating which was known as gravimetric method. In case of indirect methods some physical or chemical properties of the soil were measured which were related to the water content of the soil such as frequency domain reflectometry (FDR), time domain reflectometry (TDR) (Rodríguez 2009). According to Dane et al. (2002), some other methods were nuclear magnetic resonance (NMR), electromagnetic induction (EMI), neutron thermalization, gamma ray attenuation, radar scatterometry or active microwave, passive microwave and capacitance devices that can be used to measure soil moisture content indirectly. All these methodologies mentioned so far were costly, required high skill to operate the instruments and were mostly used in large scale field studies because of costly equipments. However, capacitance sensors such as TDR and FDR were relatively cost effective, easy to carry and easy to connect to the data logger which could transmit data without any wire from field sites (Lea-Cox et al. 2008). A capacitance technique was first introduced in the field of agriculture by Smith-Rose (1933) which was further developed with the introduction of micro-electronics (Dane et al. 2002; Rodríguez 2009). A capacitor is a device that measures the dielectric permittivity by storing the electrical energy of a certain volume of soil or substrate surrounding the sensor prongs. The dielectric permittivity is the amount of energy stored in the

soil or substrate of the surrounding medium. Since permittivity has no unit, it was based on a standard (vacuum has permittivity of 1). According to Bogena et al. (2007), a fixed voltage was applied to the surrounding sensor prongs as an electromagnetic wave. Time will be short if there was low water content for the applied voltage to rise up to a threshold point which means there was low permittivity. On the other hand, it will take a longer time to rise up to the threshold point if there was a large amount of water correlating with higher permittivity value.

In order to simplify the calibration procedure of these electromagnetic water content sensors, Blonquist et al. (2005) compared different sensor technologies using an array of media mixtures or liquids of known properties. The sensors used for the trials were ECH_2O and EC-20. The EC-20 sensor was found susceptible to moderate salt concentration when the sensor was immersed in a solution with a dielectric permittivity of 40 as the bulk electrical conductivity was increased from 0 to 2 dS/m. With an increase of output voltage to 200 mV, Bandaranayake et al. (2007) found a drift under similar conditions. A similar situation was found with the ECH_2O i.e., the applied electrical conductivity of the solution was increased from 0 to 3 dS/m which resulted an increase by about 9% of the sensor's output(Nemali et al. 2007). However, the temperature was found as an influencing factor for EC-20 in terms of less drifting which was better than the broadband sensors having higher frequency (Blonquist et al. 2005). Nemali et al. (2007) found an increase in output with the increasing temperature. As reported by Bandaranayake et al. (2007), EC-20 exhibited skin effects (energy concentrated at the close proximity of the sensor only while the propagation of the uniform energy through the substrate is ideal) as well as this sensor required the lowest sampling volume of about 1.99 cm^3. In terms of analyzing the response of the sensor to the supply voltage, Bogena et al. (2007) showed two best fit voltages that can minimize the variation associated with the volumetric water content calibration equation. On the other

hand, a strong reduction in the sensitivity was found while measuring higher permittivity by EC-5. A maximum error of 6%was reported by Bogena et al. (2007) where the bulk electrical conductivity was equal to 1 dS/m with a permittivity of 40. The performance of EC-5 was also evaluated by Parsons and Bandaranayake (2009) using the same methodology as used by Bandaranayake et al. (2007). Although a large influence of bulk density was found on the sensor readings, the volumetric water content measurement was more stable using EC-5 than EC-20. Another experiment was carried out with the EC-5 and the ECH_2O-ET (which was replaced by 5TE later on) by Kizito et al. (2008). They mainly studied the excitation frequency, temperature, and calibration of the sensors. They conducted their experiment in rockwool substrate which reduces the interactions between the sensors and solid materials because of the presence of ions in solution. The study reported that, sensors were much more prone to produce uncertainty in the results in high water content and high EC values as these two factors were responsible to reduce the signal strength of the probe pulse. They also observed the effect of temperature on sensor readings in an air-water environment. The sensor gave more stable result in water than in air. Due to bonding effects, this sensor was sometimes unable to identify water content. When water molecules interacted with the soil particles having large surface area, they cause bonding effect (Rodríguez 2009).

Although measuring soil moisture content using TDR sensors was very common, FDR was becoming more popular for the measurement of the complex dielectric permittivity of the porous material. TDR and FDR both used the same principle of measuring dielectric permittivity but with a different mechanism. FDR measured dielectric permittivity from the difference between the output wave and the return wave frequency while TDR worked in the same way from the difference of time between sending a pulse and receiving it back again. FDR was considered

accurate and faster than TDR but must be calibrated for different soil types. Measuring effective permittivity and converting it into volumetric water content using Toppequation (Topp et al. 1980)was used during this procedure. The importance of accurate measurements of unfrozen water content and accurate simulation of freezing and thawing processes has been recognized using FDR technology. E.g., He and Dyck (2013) developed multiphase dielectric mixing model to measure the unfrozen water content in the frozen soil using TDR technology. The increasing demand of measuring soil moisture led to the development of various techniques to measure it. One popular indirect method for measuring soil moisture was the thermo-gravimetric method which was important for the calibration of measured soil moisture using other methods (Ojo et al. 2015; Walker et al. 2004; Robinson et al. 2008). The electrical properties of the medium were used to measure the dielectric constant at a specific frequency using FDR. Several methods have been followed to determine the dielectric constant of water in literature in the past half century (e.g., Malmberg and Maryott 1956). Malmberg and Maryott (1956) used a low-frequency bridge method to measure the dielectric constant of water with an accuracy of 0.1% at 5ºC intervals within the range of 0ºC to 100ºC. The value of the dielectric constant was found to be 78.30 at 25ºC, which was 0.3% lower than expected. The following equation was used to fit the data from this experiment:

$$\varepsilon = 87.740 - 0.4008T + 9.398(10^{-4})T^2 - 1.410\,(10^{-6})T^3 \quad (5)$$

In this equation,ε was the dielectric constant and T was the temperature in ºC. This equation was used to fit the value of dielectric constant for water measured over the range of 1ºC to 99ºC.

TDR was a predecessor of FDR technology. The TDR technology has been originally used to detect faults in a transmission line, and later it became a very effective methodfor determining the water content of soils (Hivon and Sego 1990). Davis and Annan (1977) carried out the first

investigation of TDR to determine the water content of soils. They showed a technique to measure apparent dielectric constant using a frequency independent TDR sensor which was ranged between 10^6 to 10^9 Hz. According to the electromagnetic theory, the propagation velocity in non-magnetic low loss material was

$$v = \frac{C}{K_a}\ 0.5 \tag{6}$$

Where v was the propagation velocity (L T^{-1}) and C was the free space electromagnetic wave. According to Patterson and Smith (1985), the reflection voltage of the transverse electromagnetic wave and the propagation velocity were measured by the TDR. A step voltage was sent by the TDR which travelled unchanged along the transmission line until it came in contact with a dielectric discontinuity which caused a partial reflection and transmission of the signal. Determination of the travel time of the reflected wave (tt) can be taken from the signal trace along the transmission line, which was the distance AB in Figure 1. Knowing the length of the transmission lines from Figure 1, the propagation velocity can also be calculated using the following equation:

$$V = \frac{1}{tt} \tag{7}$$

The apparent dielectric permittivity can be expressed using the following equations (equation 8 and 9):

$$K_a = \left(\frac{C(tt)^2}{21}\right) \tag{8}$$

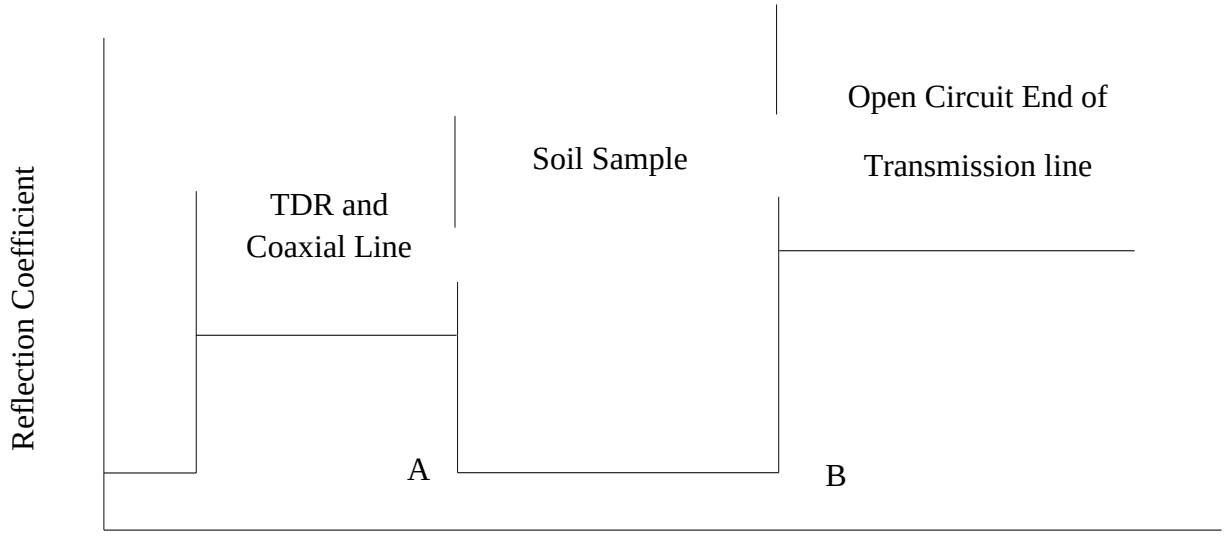

Figure 1: Typical TDR trace(after Hivon and Sego 1990; Topp et al. 1980)

One of the facts about dielectric constant was that soil has a lower value (in the range of 2 to 4) than the dielectric constant of water (80 at 20ºC). Soil type, density, temperature or pore water salinity was not only the dependable factor for dielectric constant but also it was strongly dependent on the liquid water content (Davis and Annan 1977; Hoekstra and Delaney 1974; Hivon and Sego 1990). Apart from equation 2, Topp et al. (1980) also showed an equation based on the relationship between the apparent dielectric constant (K_a) and the volumetric water content (θ_v) of soils:

$$K_a = 3.03 + 9.30\,\theta_v + 146.0\,\theta_v^2 - 76.7\,\theta_v^3 \quad (9)$$

Through equation 9, Topp proved that the relationship between the dielectric constant and the volumetric water content can be held over a wide range of soil types and textures, and it was independent of temperature and salinity (Hivon and Sego 1990). Smith and Tice (1988) found that the value of apparent dielectric constant could be decreased for fine grained soil where the

specific surface area was high which caused absorption of a large amount of water having a dielectric constant lower than 80. However, they also found higher signal attenuation for saline pore fluids since the fluid had a higher electrical conductivity than a non-saline fluid.

Patterson and Smith (1981) used the TDR method to evaluate the volumetric unfrozen water content in frozen soil since ice and soil grains have similar dielectric constant ($K_{ice} = 3.2\ and\ K_{soil} = 2\ to\ 4$). For the validation of equation 9, they used a combination of TDR-dilatometry method on the frozen soil and ice-water mixtures and obtained a good agreement between the two methods (Hivon and Sego 1990). They also found good correlations between the previously published unfrozen water content data using other methods and their TDR results. Therefore, it was considered that the TDR technique is precise within ±2.5% of θ_v for the determination of the volumetric unfrozen water content. They showed that one of the main difficulties with the TDR method was signal losses in high saline soils (salinity > 5 ppt) which were caused due to the increase in pore water electrical conductivity. The determination of the travel time was less accurate when the evaluation of open circuit response from TDR trace became more difficult due to high signal attenuation. By improving the open circuit response and appropriate line length, good agreement between the volumetric unfrozen water content measurement by TDR vs. other methods was obtained (Patterson and Smith 1983, 1985). However, the variation of predicted and experimental values at low or high water content was observed (Topp et al. 1980). Patterson and Smith (1983) found that unfrozen water content was overestimated by TDR because of air ($K_{air} = 1$) which replaced ice. Hivon and Sego (1990) showed the effectiveness of evaluating the unfrozen water content in saline frozen sand and silty sand. They found an increased amount of unfrozen water when there were high salinity and small grain size at a given temperature. At warmer temperatures (> 3ºC) and high salinities the signal

attenuation increased which caused further experimental difficulties and can be offset by using suitable transmission line length (80 mm) (Hivon and Sego 1990).

FDR sensors worked based on the capacitance techniques that worked based on the measurement of the charge time of a capacitor in order to determine the dielectric permittivity of a medium. Rao and Singh (2011) found that repeatability and sensitivity were the two parts of the strength of the capacitance probe technique. The measurement repeatability was reported better than TDR and sensitivity to small changes in volumetric water contents in dry materials was large. However, these two factors: repeatability and sensitivity were found as the two strongest points for FDR, the rapidity and ease of measurements, precise depth resolution, and relative cheapness of the probe were other advantages of using FDR over TDR. Apart from having these advantages, some disadvantages of this technique were the relatively small zone of influence for capacitance probe, the sensitivity to the region adjacent to the probe, and the sensitivity to the air gaps surrounding the probes. They came to a conclusion that FDR was better than TDR in terms of measurement repeatability. Though FDR had the limitation of showing erroneous results in highly saline soils, which was also true for any dielectric technique to measure volumetric water content as well.

2.3 Factors that can affect the determination of VWC using EM sensors

It was already proved that increasing salt concentration could increase electrical conductivity (EC) that can affect the measurement of volumetric water content (VWC) (Nemali et al. 2007; Bandaranayake et al. 2007; Topp et al. 1980). A capacitance sensor was reported by Thompson et al. (2007) which was sensitive to a soil solution where EC > 1.8 dS/m. Sometimes sensors cannot read the energy pulse as it can be dissipated by the increasing concentrations of ions in solution which was also known as dielectric losses. This was originally reported by Kelleners et

al. (2004) when they found the rejection of data due to increased VWC and bulk EC. The same effect was reported by Plauborg et al. (2005). Since the short length of TDR probes (10-15 cm) were susceptible to reduction in signal attenuation, Jones and Or (2004)proposed a model that was related to the modification in sensor design and could extend the TDR measurement in saline soils.

Another important factor that influenced the sensor measurement of VWC was temperature. As found by Polyakov et al. (2005), VWC reading could change at the rate of 0.001 $cm^3/cm^3/^oC$ and 0.003 $cm^3/cm^3/^oC$ for sandy soil if temperature changed. On the other hand, from the findings of Persson and Berndtsson (1998)and also Seyfried and Murdock (2004), a negative temperature correlation was observed for a TDR sensors operating at 45 MHz, which was in contrast to the findings of Polyakov et al. (2005). That means the effect of temperature varied with soil specific substrates. In that case measurement of temperature should be integrated while measuring VWC by the sensors. This was usually done using a thermocouple in the sensor head that provided temperature data. However, this sensor might cause drifting in the observed data due to overheating (> 40ºC) problem because of sunlight in the field measurement as found by Robinson et al. (2004). Another variable that affected the measurement of VWC was the excitation frequency. Kelleners et al. (2005a) reported the maximum frequency used by the most capacitance sensors was 150 MHz. However, VWC could be overestimated or underestimated at nearly saturated sand in low supplying voltage frequency like 50 MHz due to temperature effect. Topp et al. (1980) reviewed a lot of cited research that was done on the determination of water content by an electromagnetic wave. The significant influence of soil properties on VWC measurement was shown there. Topp et al. (2000) showed that, real and imaginary real permittivity can be affected by the soil constituents such as dissolved salts and clay content. This

finding was later proved by the experiments of Hanson and Peters (2000). In their experiments, several electro-magnetic sensors were tested in different soil type location using default calibration equations. The results showed thatdepending on the soil types, all the sensors had a significant amount of variations in their readings. As described by Chandler et al. (2004) and Kelleners et al. (2005b), soil specific calibration equations were also dependent on the soil characteristics. However, Kelleners et al. (2005b) reported that discrepancies between the calculated permittivity using calibration equation and measured permittivity using EM sensors were very little for sand and mostly high when the soil had high ionic constituents. They concluded that measuring VWC using Topp et al. (1980) relationship between VWC and dielectric permittivity was more useful for soils having low electrical conductivity. However, Logsdon (2005) suggested that VWC measurement for soil with high surface area need correction for temperature as he found a correlation between the soil surface area and the average dielectric permittivity.

2.4 Unsaturated soil hydraulic parameters

Determination of unsaturated soil hydraulic properties was one of the most important tasks for the use of numerical models in order to simulate flow and mass transport in the unsaturated zone (Holländer et al. 2009). However, the parameters that were needed in the governing equations of the hydrogeological models were very difficult to characterize in terms of unsaturated flow. Due to a large range of uncertainty and time-consuming and expensive methodology, measuring these parameters in the unsaturated zone was very difficult. Because of these reasons the soil water retention curve (SWC) was being used which was rather easy and quick method to estimate unsaturated soil hydraulic parameters (Van Genuchten 1980). A number of studies showed the successful use of the Millington and Quirk (1961) method in various forms for calculating the

unsaturated hydraulic conductivity from the measured SWC curve (Van Genuchten 1980; Jackson et al. 1965; Jackson 1972; Bruce 1972; Green and Corey 1971). The disadvantage of using this method was that the results seem quite tedious while applying this method to non homogeneous soils in multidimensional unsaturated flows. However, Brooks and Corey (1964) and Jeppson (1974) showed successful use of an analytical expression for theconductivity based on Burdine (1953) theory. Although Brooks and Corey (1966) got good results with their equations, there was some sort of discontinuity at some negative value of pressure head in the slope of both water retention curve and unsaturated hydraulic conductive curve. In numerical unsaturated modeling, this kind of discontinuity could cause rapid convergence. The prediction of unsaturated zone hydraulic parameters was also found less accurate tosome extent than the various modified forms of the Millington and Quirk (1961) method. However, the research from Mualem (1976) showed that hydraulic conductivity can be calculated from the knowledge of the soil water retention curve. As shown by Van Genuchten (1980), it can be done using a closed form analytical expressions which can produce an SWC. The mathematical expression can be used to obtain three independent soil hydraulic parameters by matching the SWC from the formula with the experimental data. By using this closed form equation, Van Genuchten (1980) came to a decision that a dependable description of the SWC at low moisture content was necessary for the accurate prediction of unsaturated hydraulic conductivity. Based on Mualem (1976) pore-size model, the following retention curve was given by Van Genuchten (1980):

$$\theta\,(h) = \theta_r + \frac{\theta_s - \theta_r}{[1 + (\alpha h)^{1-\frac{1}{n}}]} \tag{10}$$

In this equation $\theta(h)$was the measured volumetric water content (L^3/L^3) at the pressure head h (L), θ_s and $\theta_r$were the saturated and residual water content respectively, α was the inverse of the air entry suction (L^{-1}), and n (> 1) was the pore size distribution (Van Genuchten 1980). Once the

equation (10) was combined with Mualem (1976) pore size model it gave the following closed-form equation to calculate unsaturated hydraulic conductivity (Van Genuchten 1980):

$$K(S_e) = k_0\ S_e^L\ (\ 1 - [1 - S_e^{n(n-1)}]^{1-\frac{1}{n}})^2 \tag{11}$$

Where S_e was the effective saturation which can be computed from the following equation:

$$S_e = \frac{\theta(h) - \theta_r}{\theta_s - \theta_r} \tag{12}$$

k_0 was the matching point which can be fitted at saturation (L/T), L (-) was an empirical parameter that can be normally assumed to be 0.5 according to Mualem (1976). Equation 12 can then be re-written as following (van Genuchten and Nielsen 1985):

$$S_e = [1 + (\alpha h)^n]^{-m} \tag{13}$$

In this equation, α (L^{-1}), n and m are empirical parameters.

2.5 Numerical modeling of the unsaturated zone based on laboratory experiment

A numerical solution using an implicit finite-difference technique was found for a mathematical model of one-dimensional, vertical, unsteady, unsaturated flow above a recharging or discharging groundwater flow system which was applicable to homogeneous isotropic soils in which the functional relationships between hydraulic conductivity, moisture content, and soil moisture tensions showed hysteresis properties. The model allowed the solution of cases with upper boundary conditions of constant rate rainfall, ponded water, evaporation, and redistribution. The lower boundary condition was representative of a recharging or discharging groundwater flow system with a dynamic water table (Freeze 1969)**.** The results from this model were correlated later to the results of a laboratory column experiment using a tensiometer-transducer system. It has been found that, on the Canadian Prairies spring snowmelt and heavy

summer rains were available at the surface prior to the thawing of the frost wedge and therefore did not infiltrated (Freeze and Banner 1970). Certain portions of groundwater recharge areas never received direct infiltration to the water table as effective infiltration was mainly depression focused in those areas. It was always an erroneous process to estimate the recharged groundwater without investigating the unsaturated hydrologic properties of the soil during a freezing and thawing cycle of the cold region (Freeze and Banner 1970). However, ROSETTA (a computer program) used five hierarchical pedotransfer functions (PTFs) in order to estimate the unsaturated hydraulic conductivity and the water retention capability of the soil. It also allowed the estimation of van Genuchten water retention parameters (Schaap et al. 2001)

2.6 Hydrology of the boreal zone and reduction of frost depth due to global warming

The hydrology in the Boreal zone in the Northern Hemisphere was greatly affected by the seasonal ground frost. The flow patterns in the unsaturated zone and snowmelt water into runoff and infiltration was highly affected by the changing temperature of this region. A study has been carried out close to Oslo airport, Norway to examine the spatial and temporal variability of snowmelt infiltration using electrodes installed below the ground surface and in shallow boreholes. The results showed rapid and significant changes in the local groundwater levels due to the spatial scale of snowmelt infiltration that required adequate attention in the vulnerable area (French and Binley 2004).

Significant research was found on the decreasing depth of soil frost due to climate warming which implied the importance of understanding the snowmelt infiltration process in the frozen soil as there was the potential impact of the reduction in frost depth on the hydrological cycle (Iwata et al. 2008; Cutforth et al. 2004; Frauenfeld et al. 2004; Hirota et al. 2006). A field study was conducted in Hokkaido, Japan in different snow and soil condition where soil temperature,

water content, matric potential, snow cover and meteorological parameters were monitored for four winters to determine the flux from the snowmelt infiltration. It was found that, in both frozen and unfrozen conditions water from snowmelt infiltrated into the soil due to the decreasing frost depth in that area. The results showed that, the high air temperatures and an absence of freeze back events during the snowmelt period were responsible for the lacking of partially flow impedance in the frozen soil. The results also showed the effect of climate change on the interaction between snow cover and soil (Iwata et al. 2008). A paired plot experiment was carried out later in the same area on a further research project where two plots have been developed by manipulating the depth of snow cover. It has been found that, a thin frozen layer unimpeded the infiltration of meltwater whereas the thick frozen layer impeded the infiltration which generated a 63 mm runoff from the meltwater. These results clearly showed that the soil water dynamics can be changed by the thickness of the snow cover deposition (Iwata et al. 2010).

2.7 Effect of hysteresis on simulation

Although the effect of hysteresis was ignored by several simulation models, it was found that soil water movement was influenced by the hysteresis in the soil water retention curve particularly when wetting to drying changed frequently (Feddes et al. 1988; Milly 1982; Hopmans and Dane 1986).,The presence of entrapped air, the pore space geometry and the thermal gradients were the main reasons of hysteresis in the water retention curve. However, a computer-based hysteresis model was introduced by Mualem (1974) based on the independent domain principal. He introduced a factor which was a ratio of the volume of the actual empty pores and the volume of the pores that had the possibility to be empty if the neighbouring pores could deliver air to all other pores(Feddes et al. 1988). In this model, the volumetric water content can be

calculated using the value of matric head from the curve. Later, this model was used by Hopmans and Dane (1986). They incorporated Mualem's model in a soil-water flow model in order to determine the effect of both the hysteresis and temperature on the movement of soil-water (Feddes et al. 1974). However, a comparison of simulation results with the observed data using the modified Picard iteration method to solve the Richards differential equation showed a successful simulation of both soil temperature and water content profiles (Zhang et al. 2007).

2.8 Freezing and thawing characteristics of soil in the hydrological models

The frozen soil has a crucial impact on the hydrology of many watersheds. Mild rainfall or snowmelt events can create large runoff rates as pore can be blocked by ice greatly which directly reduced the permeability of the soil. A still frozen soil layer under the thawed saturated surface layer was found responsible for the extreme erosion rates from such runoff (Feddes et al. 1988). Freezing of pore water happened gradually with falling ambient temperature (Spaans and Baker 1996b) and no single freezing point for the pore water in soil and rock can be found. Due to the effects of adsorption, capillarity, and osmosis, the freezing point might be depressed which results in unfrozen pore water below the temperature of 0°C (Tian et al. 2014). A passageway might be created due to this unfrozen soil and might have an important effect in characterizing the behaviour of frozen soil during freezing and thawing cycle. In cold regions freezing and thawing process have an impact specifically on agriculture and ecosystem. Since the understanding of freezing and thawing cycle has not been advanced enough, an improved approach combined by lab experiment and simulations was needed under different field conditions. Intertwined relationship between temperature and soil moisture made modeling of soil freeze-thaw process complicated. A comparative study at two agricultural sites between a coupled heat water transfer (CHWT) model simulation and an in situ measurements of soil

temperature and liquid soil water content over two winter seasons in different years showed high accuracy in the prediction of temporal changes in freezing and thawing front migration while low accuracy has been found for the estimation of infiltration rate of snowmelt (Cheng et al. 2014). However, the model was capable of describing the freezing and thawing front migration in layered and homogeneous freezing soil through time series analysis. Often the thawing process became complicated during the spring time due to the spatially distributed ice formations in the subsurface and snowmelt surface water percolated into the subsurface (Li et al. 2012; Cheng et al. 2014). It was also found that a rapid increase of air temperature during springtime had avital impact on the thawing process of shallow soil layers (Cheng et al. 2014). In recent years, evaluation of freezing and thawing characteristics was done by using the pulsed nuclear magnetic resonance technique. Many experimental studies showed the effectiveness of this technique in this field (e.g., Ishizaki et al. 1996; Tian et al. 2014). This technique showed that in fully-saturated frozen soils, the thickness of the water films decreased with the temperature (Tian et al. 2014).

A comparison of snow water equivalent (SWE) and stream flow was done using the hydrological model HYDROTEL (Fortin et al. 2001)and the thermodynamic model CROCUS (Brun et al. 1989). The study showed a strong influence of seasonal snow accumulation and snowmelt on the hydrology of boreal regions (Oreiller et al. 2014). It was reported that CROCUS could underestimate SWE and it had a threshold value of 2°C which was used to separate rain and snow. Therefore, a correction of snowfall was done using a precipitation gauge which was applied to the model, and the results ended with an overestimation of SWE due to lack of addressing the loss in SWE. Blowing snow sublimation and relocation were found responsible for this overestimation of SWE. After a correction to the threshold value of wind speed was

applied in the model, the model performance was found better than the traditional degree day or the energy balance model. However, satisfying generation of streamflow from spring runoff simulation in HYDROTEL demanded homogeneity in input data (Oreiller et al. 2014).

Another study was reported on the ability of quantifying the uncertainties in hydrological prediction by a physically-based distributed model named European Hydrologic System or Systeme Hydrologique Europeen (SHE) (Abbott et al. 1986). SHE does not require a lengthy hydro-meteorological record for calibration and it allows spatial variability of catchment inputs and outputs to be simulated. As significant uncertainties in prediction may arise due to the lack of data or spatial variability in inputs and outputs to be simulated, SHE can address these uncertainties by carrying out a sensitivity analysis over a realistic range of the predictions. It was also found that SHE can be used as a decision-support system tool in case of unavailability of data. The study also reported that extensive further development and refinement is needed for the application of SHE in almost any kind of hydrological problems (Abbott et al. 1986). The first test of the snowmelt component of SHE showed a simulation of snowmelt runoff for a sub-basin and an investigation of the different hypothesis of basin behaviour where previous field studies particularly on that sub-basin were absent. It was reported that a test with temperature-based (degree-day) options resulted in comparable accuracy but only through empirical fitting of parameters. However, the study proved that in the process of operation for SHE-type models' compared to simpler models', a greater hydrological expertise is required as reported by Bathurst and Cooley (1996). A sensitivity analysis was reported by Zhang et al. (2007) where the effects of the ice content on matric potential including the impedance of ice to the soil water flow were found as important factors that need to be addressed in the numerical simulation of thermal and hydrological processes in frozen soil (Zhang et al. 2007). Since sensitivity analysis on

hydrological models were useful to address the interactions between different hydrological process, an investigation was carried out to find the effects of potential changes in the input parameters in modeling results by using the Simultaneous Heat and Water (SHAW) model (Flerchinger and Saxton 1989a; Flerchinger et al. 1996). The SHAW model was developed mainly aiming to simulate soil freezing and thawing. The system was basically integrated into a one-dimensional snow-residue-soil system with a representation of the physics of vegetation cover, snow, and soil. The model can simulate heat, water, and solute fluxes and was capable of soil freezing and thawing. The energy balance equation for multilayered snowpack used in the SHAW model includes latent heat transfer at the surface, solar and long-wave radiation exchange and vapour transfer within the snowpack. This model was tested successfully with a dataset of two years length that was recorded at three sites ranging from shallow snow cover to a deep snow drift. Additionally, it simulated the depth and density of the snow cover along with the magnitude and timing of the snow cover outflow for all three sites (Flerchinger and Cooley 2000). Another study was carried out on the calibration and validation procedures used for SHAW by Flerchinger et al. (2012). Limitations of SHAW model in respect to this study were found that the model was restricted to the Campbell (1974) soil moisture release curve and the model was unable to consider the preferential flow. Therefore, the soil water content simulated by SHAW was unable to ensure optimized results as it had no provisions to consider the influence of preferential flow and the absence of other forms of soil moisture release curve (e.g., Brooks and Corey model and VGM model) which might yield better optimized results (Flerchinger et al. 2012).

The simulation of freezing and thawing behaviour of soil water content in soil column experiment was successfully showed by Hansson et al. (2004) using HYDRUS-1D. The

implemented code was used in HYDRUS-1D and is available for research purposes. The paper presented a new method that can address the phase change of soil water in a numerical model while simulating flow and heat transport both at subzero and above zero temperatures. This method was based on the formulation that mixed both of the water flow and heat transport similar to the governing equation of groundwater flow which was known as Richards equation. The model was calibrated using data obtained from a lab experiment. The lab experiment was carried out in soil columns having a diameter of 8 cm and a length of 20 cm which were exposed to a circulating fluid from the top at a temperature of -6ºC. Freezing was done from top to bottom of the soil column. Based on the calibrated result, a new function was proposed that can better describe the dependence of the ice and water content on the thermal conductivity of the frozen soils. Afterwards, data predicted from the numerical model was compared with the experimental data which showed a good fit. Later, the model was used for simulating heat flow and water transport below a road in Sweden. For that situation, mass and energy conservative based iterative Pichard schemes were implemented into the numerical code and the model simulated reasonable results in terms of frost depth prediction with time. Due to the lack of data set in the site location in Sweeden, the model was not calibrated and validated. However, the model was able to simulate the distribution of water content and temperature with depth in freezing and thawing conditions of the subsurface zone under the road. Considering this, the numerical freezing and thawing module integrated into HYDRUS-1D, which was developed by Hansson et al. (2004)was a successful mass-and-energy conservative based model to address water flow and heat transport in partially frozen soil.

CHAPTER 3

METHODOLOGY

This chapter presents the details of the laboratory test facility, test conditions, the dielectric sensors used to measure the soil temperature, soil moisture content and the measurement procedure of percolation water and air temperature employed in the present study. The theory and equations that were used to model and simulate the physical system in a laboratory experiment are also described.

3.1 Experimental setup, instrumentation, and test conditions

Laboratory experiments have been conducted to develop a standardized data set. In the first stage, the soil column (Figure 2) was built for the laboratory testing and equipped with measurement devices. The soil column was made of a PVC (polyvinyl chloride) pipe. It had a length of 110 cm and a diameter of 35.6 cm. Two PVC plates were installed at the bottom of the pipe: the first one was fixed at the bottom of the PVC pipe. This plate had an outlet in the center of the plate. Another plate was installed 1.2 cm above the first plate. This plate acted as the filter bottom for the sand within the column. A No. 45 sieve (mesh size 0.355 mm) was placed on top of the second plate to retain the fine sand in the PVC pipe. Overall, the total filter (both the second PVC plate and the mesh) had a thickness of 1.8 cm. Therefore, the total length of the soil column was 107 cm. The distribution system at the top of the soil column was a porous pipe which wasinstalled on a metal mesh. The porous pipe was laid out as an Archimedes spiral at the mesh to allow a spatially constant distribution of water to the sand. A peristaltic pump (Masterflex L/S Digital Pump System) was used to pump the water to the distribution system at

the rate of 10 ml/min. Pure fine sand was used (99.44% retaining on the No.200 sieve) in the soil column. There was no chemical or organic material in the fine sand.The whole setup was placed in the ice chamber of the Hydraulics Research and Testing Facility of the Department of Civil Engineering where temperature can be controlled within a range of +25°C to -30°C.A data logger (Decagon EM-50) collected the moisture content and temperature data measured by five 5TE FDR sensors. All sensors were installed horizontally in the soil column so that the sensors prong faced 90º from the vertical axis. Sensor 1 was installed at a depth of 27 cm from the top. Then the sensor 2, sensor 3, sensor 4, and sensor 5 were installed at a distance of 15 cm from each other accordingly. Therefore, sensor 2, sensor 3, sensor 4, and sensor 5were installed at depths of 42, 57, 72, and 87 cm, respectively from the top of the PVC pipe. 5TE sensors should be installed at a distance of > 20 cm to eliminate any interference problems. However, this distance is only applicable for vertically placed sensors. For sensors that are horizontally placed, the selected placement having 15 cm spacing did not lead to any overlapping problems (Decagon Devices 2007-2010; Chambers 2016; Travis 2015).

The whole pipe was covered with insulation materials in order to allow freezing and thawing of the soil column only from the top. The operating environment of all the sensors was within a temperature range of -40°C to +60°C. The accuracy of each sensor is ±0.03 cm^3/cm^3 (using manufacturer based Topp equation), ±0.01 to ±0.02 cm^3/cm^3(using medium specific calibration equation) for soil volumetric water content (VWC) and ±1°C for temperature(Decagon Devices 2007-2010). A pressure transducer (Diver D1 243) manufactured by Schlumberger Water Services was used to measure the percolated water during the thawing period of the soil. A bottle probe sealed in a miniature bottle filled with nontoxic glycol was used to measure the air temperature along with a data logger manufactured by Thermo Scientific which can monitor

readings for any time period. The data logger also allowed recording data according to a user-defined logging interval of one observation. Temperature-buffered bottle sensor eliminated rapid changes when the door of the ice chamber was opened.

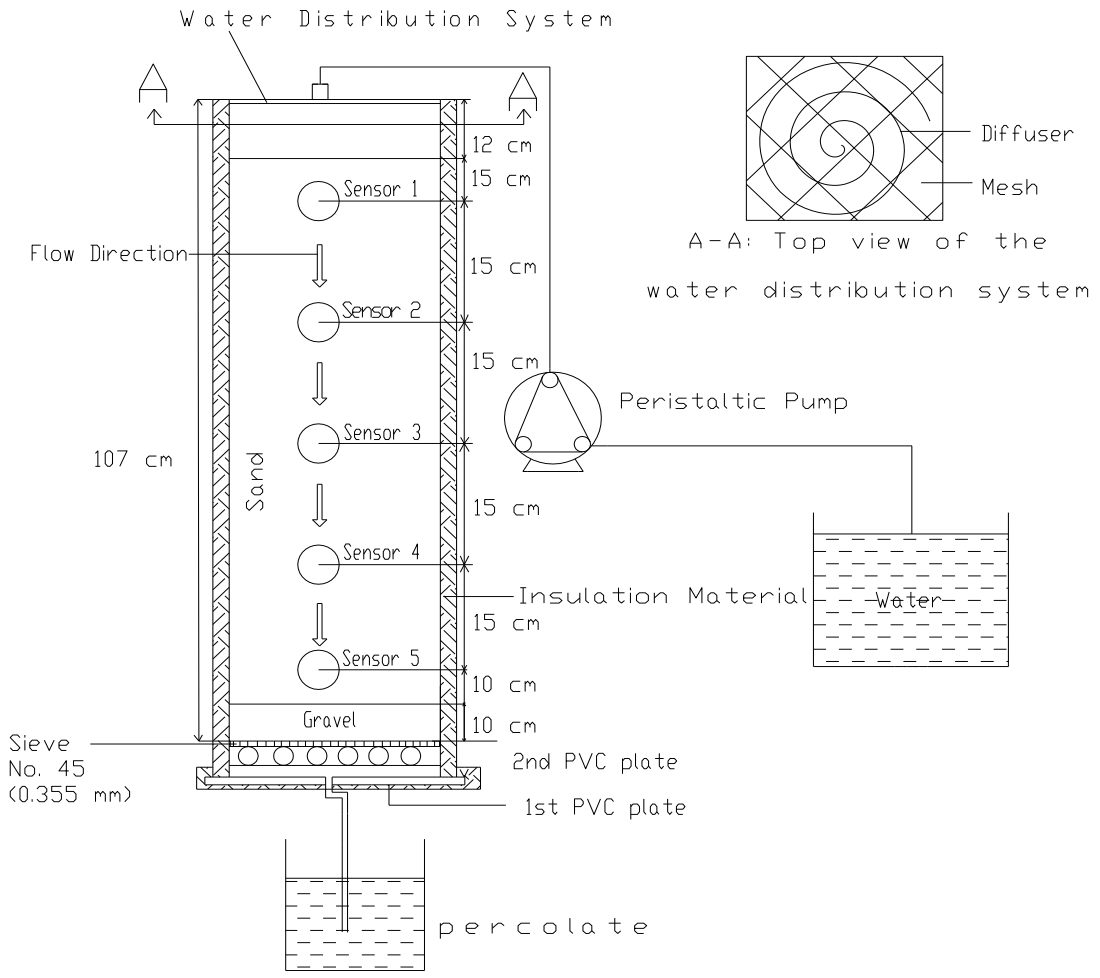

Figure 2: Schematic diagram of the laboratory setup

3.2 Measurement procedure of the sensors and calibration of the sensors

Decagon 5TE dielectric sensors were used to measure soil moisture and temperature at different depths of the soil column. Apart from the water content and temperature, electrical conductivity of the soil can be also measured using the 5TE. 5TE used an oscillator running at 70 MHz in order to measure the dielectric permittivity of soil to determine the water content. A thermistor attached with the sensor prongs measured the soil temperature while EC was measured using the screws on the surface of the sensor which formed a two-sensor electrical array (Figure 3)(Decagon Devices 2007-2010).

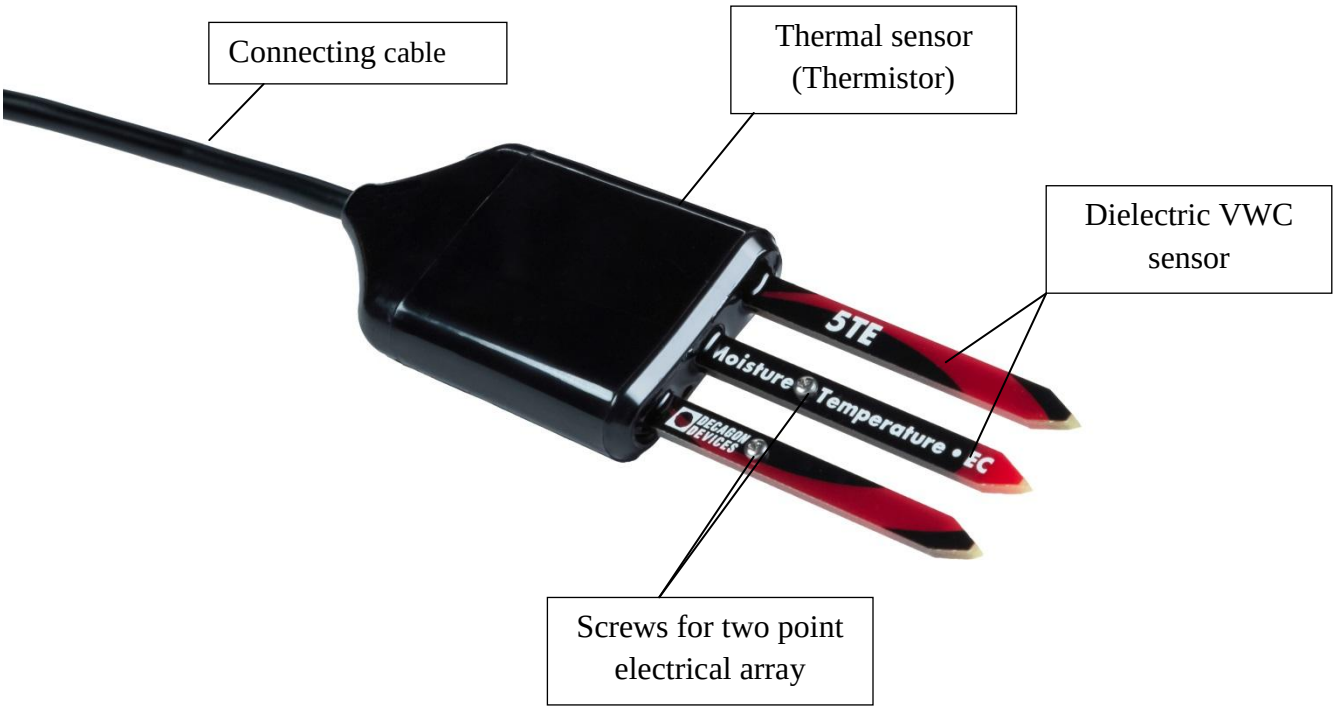

Figure 3: 5TE components 5TE components (Decagon Devices 2007-2010)

The 5TE sensor measured the dielectric permittivity of the surrounding medium using an electromagnetic field. A 70 MHz oscillating wave was supplied to the sensor prongs by the sensor that charges depending on the dielectric permittivity of the material. The soil dielectric permittivity and the soil volumetric water content were proportional to stored charge. This charge was measured by the 5TE microprocessor and a value of dielectric permittivity from the sensor came as an output(Decagon Devices 2007-2010).Later, this dielectric permittivity were converted to VWC using the Topp equation (equation 2) (Topp et al. 1980). For this study, all five 5TE sensors were calibrated to measure dielectric permittivity (K_a) accurately in the range of 1 (air) to 80 (water) values of dielectric permittivity. The dielectric permittivity values recorded by the 5TE in standard serial communication had units of K_a*50. Tests conducted by Decagon Devices showed that for a 5TE sensor installed properly in a normal mineral soil with electrical conductivity <10 dS/m, the Topp equation will provide measurements within ±3% VWC of the actual soil VWC. Calibration of the 5TE was done by following the modified procedure described in Spelman et al. (2013)and using a calibration container of known volume. Laboratory calibration of the sensors was conducted by placing the soil sample into a container while compaction was applied to bring the sample to the bulk density. A sensor was inserted into the soil, and a reading of the raw counts was obtained. A precise volume of the soil was then extracted to measure the bulk density and the actual volumetric water content using oven dry method. After that, the soil was shifted from the container to a bowl where 200–400 cm^3 of water was added to 11031.8 cm^3 of soil. Then, the soil and water were mixed until homogeneity was obtained. Then this whole procedure of placing the soil into the container up to obtaining a precise volume of the soil to measure the bulk density and the actual volumetric water content and the mixing of soil with the same amount of water until the homogeneity obtained was

repeated until the reasonable amount of data (5% to 40% of VWC) was obtained. Once enough measurements were taken, a plot of sensor's raw counts and corresponding volumetric water content was developed for each sensor. All data were plotted on a graph. Afterwards, regression analysis was done to find the best fit line in this data which resulted an equation. This equation was then used as the calibration equation for each sensor for the particular soil (Spelman et al. 2013). All five sensors were calibrated in the same way separately. It is better not to calibrate all sensors at the same time in the same container as it may create the interference error. If the five sensors were going to be placed in the same container at the same time then the sensors should be far enough away from each other and the side of the container so that they will not get any interference(Chambers 2015). The volume of soil that the sensor integrated into the volumetric water content (VWC) measurement was also important to evaluate when selecting a soil moisture sensor. Cobos (2014) described the results of tests which were conducted to find the measurement volume of Decagon's VWC sensors. According to that note, the maximum measurement volume of the5TE sensor was approximately 715ml. The application note also mentioned an idealized measurement volume of Decagon 5TE sensor (Figure 4).

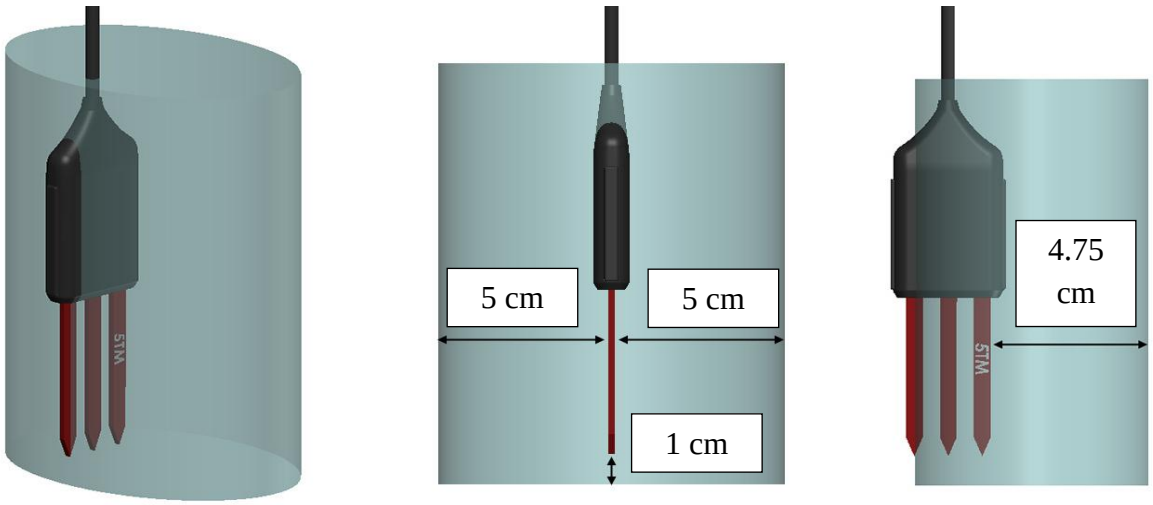

Figure 4: Idealized measurement volume of Decagon 5TM and 5TE sensors(Cobos 2014)

After calibrating the sensors and obtaining the calibration equation for each of the five FDR sensors, the soil column was moved into the ice chamber to initiate the freezing and thawing experiments. At first, some preliminary tests at the non-frozen condition to validate the reliability of the soil column equipped with different measurement devices were carried out. The field capacity was an important threshold value since soil water can gravitationally flow inside the unsaturated zone if the water content reaches this threshold value. The soil column has been drained with water initially in order to achieve field capacity at different depth of the soil column. The initial moisture content was in a range of 5% to 10% for all five sensors at the different depths of the soil column. After that, the soil column was frozen at -5°C, -10°C and -15°C separately. When all sensors showed together no decline in temperature, the temperature in the ice chamber was changed to +5°C to simulate thawing conditions. Pumping was started when the air temperature reached at 0°Cat a flow rate of 10 ml/min. The infiltration water temperature was at +3°C. Pumping of water stopped when all the five sensors were showing soil temperatures close to +5°C. All temperatures and moisture contents from different depths of the soil column during these freezing and thawing conditions were recorded by the EM-50 data logger.

3.3 Sieve analysis, permeability test and unsaturated soil hydraulic parameterization from SWC curve

Sieve analysis and constant head permeability test were conducted in order to determine the properties of the soil. The sieve analysis was conducted according to the ASTM C 136-06 (ASTM 2006a). The result from the sieve analysis experiment was applied to ASTM soil types and average grain size classification in order to determine the sand, silt and clay composition. The soil was characterized by a major portion of fine sand (99.44%) based on the sieve analysis.

Therefore, the amount of silt and clay was negligible in the soil used for the laboratory experiments. The constant head permeability test was carried out in accordance to ASTM D 2434-68 (ASTM 2006b). The soil was tested three times at three different hydraulic head differences which resulted an average hydraulic conductivity of 709.17 cm/day having a standard deviation of 50.7 cm/day.

A soil water characteristics curve (SWC) was developed for the soil using pressure plates. SWC curve relates volumetric water content with matric potential. The relationship between soil water content and matric potential under equilibrium condition can be described by the SWC. SWC was related to some important soil properties such as the distribution of pore spaces, sizes, interconnectedness and they were strongly affected by the soil texture, structure and some other factors including organic matter content (Connecticut). For fine soil particles usually, SWC showed highly nonlinear behavior and was difficult to be obtained accurately. This was because matric potential can extend over several orders of magnitudes so the SWC was usually plotted on the logarithmic scale for a certain range of water contents. SWC estimation can be done by several methods. One of the primary problems for developing the SWC curve was the time and determination of equilibrium state under the low matric potential values related to the level of wetness of the soil. For the fine sand in the soil column, laboratory measurements with pressure flow cell and pressure plates were used to determine the SWC curve (Figure 5a and Figure 5c). The pressure plate apparatus consisted of a pressure chamber that enclosed a saturated porous plate, which allowed water flow but prevented air flow through it's pores. Usually, porous plates stayed open to atmospheric pressure at the bottom surface. On the other hand, the top surface stayed at the applied pressure of the chamber(Connecticut). After sieving the fine sand, the sand samples were placed in retaining rubber rings (Figure 5b), which were in contact with the porous

plate and left overnight for getting saturated in the water. After saturation of the soil was done, the saturated soil samples in the porous plate were placed in the chamber. Then, a known gas pressure was applied to the soil for forcing water out from the soil through the plate. between the Once the force exerted by the air pressure and the force by which soil water was held by the soil particles reached to an equilibrium stage, water flow stopped. For this particular experiment 0.05 bar, 0.1 bar, 0. 3 bar, 1 bar, 3 bar, 6 bar, 10 bar, and 15 bar were applied, and the VWC content was calculated for these pressure points. Soil pore distribution and soil structure can influence the soil water retention in the low suction range of 0.05 bar to 1 bar (Connecticut). Therefore, undisturbed soil samples could yield better results than lab repacked sample. However, in this experiment lab based compacted samples were used. For the low-pressure range of 0.05 bar to 1 bar, the air pressure was applied while for a pressure range of 3 bar to 15 bar, nitrogen gas was applied to force water out of the soil. When the equilibrium stage was established between the suction and applied air pressure, the soil samples were taken from the pressure plate, weighted and oven dried for gravimetric moisture content (θ_m) of the soil samples. Later θ_m was converted to $\theta_v$using the estimated bulk density of the soil sample and unit weight of water. Outflow from cells was monitored continuously in order to relate them to the change in water content of the sample.

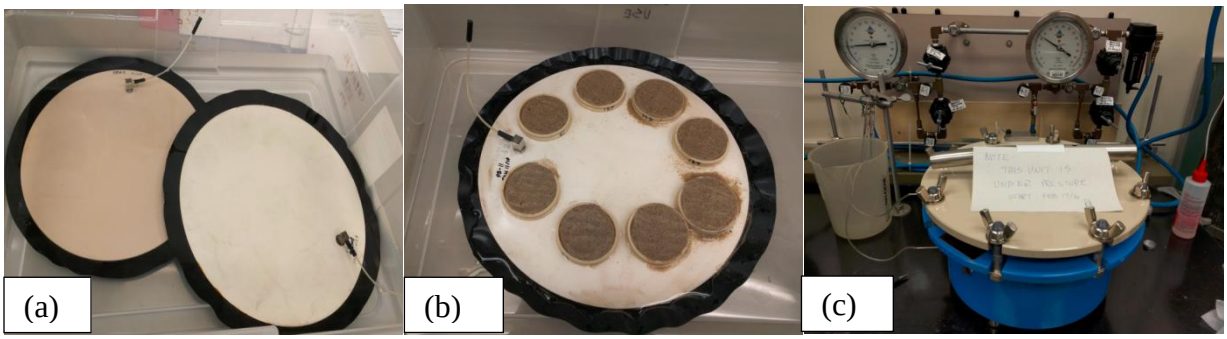

Figure 5: Pressure plates and flow cell apparatus used to desaturated soil sample to desired matric potential: (a) porous plates soaked in water, (b) soil samples on porous plate, (c) pressure chamber

After getting the VWC for each pressure points, a SWC curve was developed in logarithmic scale and then van Genuchten model (equation 10) (Van Genuchten 1980) was fitted to the experimental SWC using the Excel inbuilt optimization program in order to estimate unsaturated soil hydraulic properties ($\theta_r, \alpha, n,$ and m).

3.4 Numerical analysis of the laboratory-based physical model

HYDRUS-1D version 4.16 (Simunek et al. 2013)which was a physically based vadose zone modeling was used to model and simulate the flow and heat transport in the 1-D soil column and re-predict the experimental data set of moisture content and temperature profile in the partially frozen soil. There were four governing equations that were used to simulate moisture and heat transport. HYDRUS-1D used the modified form of Richard's equation (equation 14) for simulating uniform water movement in a partially saturated rigid porous medium. In order to minimize the mass balance errors without affecting the modeling performance at the saturation

level, the modified form of Richard's equation was solved using the Galerkin-type linear finite element schemes (Celia et al. 1990; Simunek et al. 2013) in HYDRUS-1D:

$$\frac{d\theta_v}{\partial t} = \frac{\partial}{\partial x}\left[k\left(\frac{\partial h}{\partial x} + cos\beta\right)\right] - s \quad (14)$$

Where θ_v was the volumetric water content [L^3L^{-3}],*t* was time [T], *h* was the water pressure head [L], *x* was the spatial coordinate [L] (positive upward), *s* was the sink term [$L^3L^{-3}T^{-1}$], and the angle between the flow direction and the vertical axis was α. When β became 0°that means the vertical flow was applied while β = 90°was representing horizontal flow. Therefore, in case of inclined flow, β should be between 0°and 90°, and *K* was the unsaturated hydraulic conductivity function [LT^{-1}] (Simunek et al. 2013):

$$K(h,x) = K_s\,(x)\,K_r\,(h,x) \quad (15)$$

In equation 15, K_s was the saturated hydraulic conductivity [LT^{-1}] and K_r was the relative hydraulic conductivity [-].

HYDRUS-1D can use five different analytical models for hydraulic properties. Among them, the van Genuchten-Mualem (VGM)(Van Genuchten 1980; Mualem 1976) model was chosen to represent the water retention behaviour of the soil as the unsaturated soil hydraulic properties. θ_v (h) and K(h) in equation 14 were usually highly non-linear functions of the pressure head. The VGM model was discussed in section 2.4 (equations 10 and 11). For this study, the parameters of the VGM model were determined by laboratory experiment which was discussed in section 3.4. In order to simplify the description of the spatial variability in the unsaturated soil hydraulic properties in the flow domain, HYDRUS-1D implemented a scaling procedure. By this procedure, the code assumed the variabilities in the hydraulic properties of a given soil profile in

HYDRUS-1D and made an approximation using a set of linear scaling transformations. This method can relate the reference soil hydraulic properties $\theta_v^*(h^*)$ and $K^*(h^*)$ with the soil hydraulic properties $\theta_v(h)$ and K(h) of the individual soil layer in the soil profile (Simunek et al. 2013). This method was originally introduced by Miller and Miller (1956) for porous media. There were three independent scaling factors used to define a linear model of the actual spatial variability in the soil hydraulic properties by HYDRUS-1D as follows (Simunek et al. 2013; Vogel et al. 1991):

$$K(h) = \mu_k k^* h^* \tag{16}$$

$$\theta_v(h) = \theta_r + \mu_\theta [\theta^*(h^*) - \theta_r^*]$$

$$h = \mu_h h^*$$

In equation 16, μ_k , μ_θ and μ_h wereinterrelated independent scaling factors for the hydraulic conductivity, the water content, and the pressure head, respectively. In the original scaling method of Miller and Miller (1956), scaling was obtained by assuming μ_θ =1 (with $\theta_r* = \theta_r$), and $\mu_k = \mu_h - 2$ (Simunek et al. 2013). However, more details of the scaling method of equation 16 and how they were usually applied to represent the hydraulic properties of soil profiles can be found inVogel et al. (1991).

Soil hydraulic properties can also be dependent on the temperature which was addressed by HYDRUS-1D through a similar scaling technique as discussed above. However, it was based on capillary theory. The Prediction of the influence of temperature on the soil water pressure head can be done using the influence of temperature on surface tension which was derived by Philip and De Vries (1957):

$$\frac{dh}{dT} = \frac{h}{\sigma}\frac{d\sigma}{dT} \tag{17}$$

In equation 17, σ was the surface tension at the interface of air-water [MT^{-2}], and T was temperature [K]. So that h_T became (Simunek et al. 2013):

$$h_{\mathrm{T}} = \frac{\sigma_T}{\sigma_{ref}} h_{ref} = \alpha_h^* h_{ref} \tag{18}$$

In equation 18, σ_T and σ_{ref} were surface tensions and h_{T} and h_{ref} were pressure heads at temperature T and reference temperatureT_{ref}. From the equation of Constantz (1982), the temperature dependence of hydraulic conductivity can be written as:

$$K_T(\theta) = \frac{\mu_{ref}\,\rho_T}{\mu_T \rho_{ref}} K_{ref}(\theta) = \alpha_k^* K_{ref}(\theta) \tag{19}$$

$$\mu_T = \frac{1.787 - 0.007T}{1 + 0.03225T}$$

$$\rho_T = 1 - 7.37.10^{-6}(T-4)^2 + 3.79.10^{-8}(T-4)^3$$

In equation 19, K_{ref} and K_T were the hydraulic conductivities at reference temperature T_{ref} and at soil temperature T [°C] respectively. ρ_T and ρ_{ref} were the density of soil water [ML^{-3}] at temperature T and T_{ref} respectively and μ_T and μ_{ref} were the dynamic viscosity [$ML^{-1}T^{-1}$] at temperature T and T_{ref} respectively. The temperature scaling factor for the hydraulic conductivity was α_k^* (Simunek et al. 2013).

The governing heat transport equation without considering the transfer of latent heat by vapor movement and as described with a convection-dispersion equation by the Simunek et al. (2013)was as follows:

$$\frac{\partial C_p(\theta)T}{\partial t} = \frac{\partial}{\partial x}\left[\lambda(\theta)\frac{\partial T}{\partial x}\right] - C_w \frac{\partial qT}{\partial x} - C_w ST \tag{20}$$

According to Sophocleous (1979), equation 20 can also be written as following

$$C_p(\theta)\frac{\partial T}{\partial t} = \frac{\partial}{\partial x}\left[\lambda\,(\theta)\frac{\partial T}{\partial x}\right] - C_w q\frac{\partial T}{\partial x} \tag{21}$$

Where $C_p(\theta)$ and C_w were volumetric heat capacities [$ML^{-1}T^{-2}K^{-1}$] of the porous medium and the liquid phase respectively, $\lambda\,(\theta)$was the coefficient of the apparent thermal conductivity of the soil [$MLT^{-3}K^{-1}$]. Volumetric heat capacity came as an output of the bulk density and gravimetric heat capacity. The first two term of equation 20 on the right hand side represented the heat flow due to conduction and the heat transported by the flowing water. The third term on the right hand side of equation 20 stood for energy uptake by plant roots associated with root water uptake (Simunek et al. 2013). Equation 21 was derived from equation 20 making use of the continuity equation that described the isothermal Darcian flow of water in a variably saturated porous medium which was as follows (Simunek et al. 2013):

$$\frac{\partial \theta}{\partial t} = -\frac{\partial q}{\partial x} - S \tag{22}$$

However, the volumetric heat capacity was also described by DeVries (1963) as follows:

$$C_p(\theta) = C_n\theta_n + C_0\,\theta_0 + C_w\,\theta + C_a a_v \tag{23}$$

$$\approx (1.92\theta_n + 2.51\theta_0 + 4.18\theta)10^6\,(JM^{-3}\ {}^0C^{-1})$$

In the above equation the subscripts n, o, a, w were representing solid phase, organic matter, gas phase and liquid phase, respectively.

The apparent thermal conductivity $\lambda\,(\theta)$was expressed by the following equation which was a linear function of the velocity (De Marsily 1986) and it was a combination of the thermal conductivity of the porous medium (both solid and water) without the presence of water and macrodispersivity:

$$\lambda\,(\theta) = \lambda_0(\theta) + \beta_t C_w |q| \quad (24)$$

In the above equation $\beta_t$stood for thermal dispersivity [L] and in order to had the dimensions of the thermal dispersivity in length units, the volumetric heat capacity of the liquid phase as C_w included in this equation (Simunek et al. 2013). However, the thermal conductivity was expressed using the Chung and Horton (1987) equation:

$$\lambda_0(\theta) = b_1 + b_2\theta + b_3\theta^{0.5} \quad (25)$$

In this equation $b_1, b_2\ and\ b_3$were empirical parameters which were determined by Chung and Horton (1987) based on the soil texture. In this research, values of these parameters for fine sand was used from HYDRUS-1D which were taken from the study of Chung and Horton (1987) such as 1.47054E+016 $Wm^{-1}K^{-1}$for b_1, -1.5518E+017 $Wm^{-1}K^{-1}$for b_2 and3.16617E+017 $Wm^{-1}K^{-1}$ for b_3.

3.4.1 Water flow boundary conditions

According to Simunek et al. (2013), within the flow domain the initial distribution of pressure head or water content were required for the solution of Richard's equation (equation 14). In this study, it was water content which can be expressed as follows:

$$\theta(x, t) = \theta_i\,(x) \quad t=t_0 \quad (26)$$

In the above initial condition, t_0 was the time when the simulation began. Apart from this, two boundary conditions (BCs) were selected i.e. one at the soil surface where x = L and another one at the bottom of the soil column where x = 0. HYDRUS-1D had the option to select either system-independent or system-dependent boundary conditions. Due to the variations of external parameters in this study such as constant water flow, distinct temperature variations at different temperature cycle, change of soil moisture conditions from the field capacity, the upper

boundary condition in the soil column was defined as “atmospheric BC with surface runoff”. In consideration of potential surface ponding, the numerical solution of equation 14 was obtained by following two conditions: prescribed fluxor prescribed pressure head which were used to limit the absolute value of the flux(Neuman et al. 1974):

$$-\mathrm{k}\frac{\partial \mathrm{h}}{\partial \mathrm{x}} - k \leq E \; at \; x = L \tag{27}$$

and

$$h_A \leq h \leq h_s \;\; at \; x = L \tag{28}$$

In the above equations, E was the maximum potential rate of infiltration or evapotranspiration under current atmospheric condition [LT^{-1}], and h_A and h_s were minimum and maximum pressure head at the soil surface [L]. A prescribed head boundary condition was used to calculate the actual surface flux, when one of the end points of equation 27 was reached. Another option in HYDRUS-1D for this type of boundary condition was to assume that, above 0º temperature any excess water on soil surface will be immediately removed (Simunek et al. 2013). Another system dependent type boundary condition “seepage face” was used as the lower BC at the bottom of the soil column. According to this boundary condition, water can leave the saturated part of the flow domain. This type of boundary condition was also ideal for soil columns when the bottom of the soil column was exposed to the atmosphere such as gravity drainage of a finite soil column. There was also an option in HYDRUS-1D for this boundary condition where a value other than zero can be specified for triggering flux across the seepage face (Simunek et al. 2013).

3.4.2 Heat transport boundary conditions

The solution for governing equation of heat transport at equation 20 required knowledge of the initial temperature within the flow region (Simunek et al. 2013):

$$T(x, t) = T_i\,(x) \text{ at } t=0 \tag{29}$$

In the above equation, T_i was a prescribed function of x. For the upper BC at the top of the soil column, Cauchy type boundary condition was selected where the temperature is prescribed as (Simunek et al. 2013):

$$T(x, t) = T_0\,(t) \tag{30}$$

For the bottom of the soil column, zero gradient boundary condition was selected as lower BC. A zero-gradient boundary condition was usually used to simulate the freely draining soil column profile. In field studies of water flow and drainage in the vadose zone, this type of situation often occurs. A sine function (Kirkham and Powers 1972) was used as atmospheric boundary condition for the daily fluctuations in soil temperature which was expressed as follows:

$$T_0 = T_{avg} + A \sin\left(\frac{2\pi t}{\rho_t} - \frac{7\pi}{12}\right) \tag{31}$$

In this equation ρ_t was a period of time[T] which was required to complete one cycle of the sine wave i.e. 1 day, T_{avg} was the average temperature at the soil surface [K] during the period ρ_t and the amplitude of the sine wave [K] was A (Simunek et al. 2013).Since the detailed temperature values were observed in the laboratory experiment, these values were used directly in the model so that A became 0. Thus the second part in the right hand side of the equation became 0.

3.5 Inverse calibration by HYDRUS-1D

Parameter optimization was an important factor in modeling which was an indirect approach for the estimation of soil hydraulic parameters or heat transport parameters from the transient flow in HYDRUS-1D (Simunek et al. 2013) by implementing an inverse solution. HYDRUS-1D has an inverse method which was based on minimizing the suitable objective function. That function represented the discrepancy between the observed values and predicted values. In this method

the initial estimate of the optimized parameters were improved by an iterative process until a degree of precision was obtained in the calibrated results. This method was successfully applied to a laboratory column based outflow data byKool et al. (1985) and Van Dam et al. (1994).

The objective function that will be minimized by HYDRUS-1D during the parameter estimation process was defined bySimunek et al. (1998):

$$\Phi(b,q,p) = \sum_{j=1}^{m_q} v_j \sum_{i=1}^{n_{q\,j}} w_{i,j}\left[q_j^*(x,t_i) - q_j(x,t_i,b)\right]^2 + \sum_{j=1}^{m_p} \overline{v_j} \sum_{i=1}^{n_{p\,j}} \overline{w_{i,j}}\left[p_j^*(\theta_i) - p_j(\theta_i,b)\right]^2 + \sum_{j=1}^{n\,b} \widehat{v_j}\,[b_j^* - b_j]^2 \quad (32)$$

In equation 32, the right-hand side represented the deviations between measured and calculated variables that were spatial or temporal such as water contents, temperatures or pressure head at different locations or different time in the flow domain. The first term of equation 32 can be defined for different equilibrium and non-equilibrium water flow conditions using HYDRUS-1D inbuilt options. In the first term of this equation, m_q, was the number of different sets of measurements, $n_{q\,j}$was the number of measurements in a particular measurement sets, $q_j^*(x,t_i)$represented specific measurements at time $t_i$for the j^{th} measurement set at location $x(r,z)$, $q_j^*(x,t_i,b)$were the corresponding model predictions for the vector of optimized parameters b (e.g., θ_r, θ_s, α, n, K_s) and v_j and $w_{i,j}$were weights associated with a particular measurement set or point, respectively. The second term of equation 32 expressed the differences between the independently measured and predicted soil hydraulic properties. The terms $m_p, n_{p\,j}, p_j^*(\theta_i), p_j(\theta_i,b), \overline{v_j}, \overline{w_{i,j}}$ had similar meanings in second terms as for the first term but for soil hydraulic properties. The third and last term were a penalty function for deviations between prior knowledge of the soil hydraulic parameters, b_j^*, and their final

estimates, b_j, where nb was the number of parameters with prior knowledge and $\hat{v}_j$ was the preassigned weights (Simunek et al. 2013). As there could be difference in weighting between different data types because of the extent of number and values of the data set involved in calibration, a weighting coefficients v_j as used to minimize the differences (Clausnitzer and Hopmans 1995):

$$v_j = \frac{1}{n_j \sigma_j^2} \tag{33}$$

This equation 33 caused the objective function to become the average weighted squared deviation which was normalized by the measurement variances σ_j^2 (Simunek et al. 2013). Using the Levenberg-Marquardt nonlinear minimization method which was originally a weighted least-squares approach based on Marquardt's maximum neighborhood method (Marquardt 1963), minimization of the objective function Φ was done. In this method the Newton and steepest descend methods were combined and resulted in confidence intervals for the optimized parameters. Optimizing parameters by using this method was considered as a standard in nonlinear least-squares fitting among soil scientists and hydrologists (Van Genuchten 1981; Kool et al. 1985, 1987; Simunek et al. 2013). In order to adjust the calibrated parameters of HYDRUS-1D inverse calibration method applied some statistical analysis tool such as correlation matrix which specified the degree of correlation between the fitted coefficients, goodness of fit r^2 which represent the regression of the observed and fitted values, mean, standard error, T-value and the lower and upper confidence limits. For each fitted parameters of b_j HYDRUS specified the upper and lower bounds of the 95% confidence level. By using the optimization program an estimated mean of the parameters as obtained and if the actual value of the specific parameter

stayed in a narrow interval of that estimated mean value that means the result was sensitive to the value of that particular parameter. If large confidence limits was found, that means that particular parameter was not very effective on the results (Simunek et al. 2013). Although HYDRUS-1D inverse calibration was well equipped with statistical analysis, performance criteria were also used in the modeling results in order to minimize the misfit between the observed and simulated values. RMSE (root mean square error) was used in meteorology, air quality, and climate research studies as a standard method to measure model performance(Chai and Draxler 2014). It was considered as a standard metric for model errors (e.g., McKeen et al. 2005; Savage et al. 2013; Chai et al. 2013)). The RMSE was calculated using the following formula (Hyndman and Koehler 2006):

$$RMSE = \sqrt{\frac{n_{i=1}\,(s_i - o_i)^2}{n}} \tag{34}$$

In the equation 34, $n_i$was the observation day [T], $s_i$was the simulated values at the ith day and $o_i$was the observed values at the ith day. If the RMSE value was zero that means the predicted values were the same as the observed values.

To evaluate the model performance and accuracy, the mean absolute error (MAE)was another useful measure that was widely used. It gave an idea that how close the predicted values were to the observed values (Chai and Draxler 2014):

$$\mathrm{MAE} = \frac{1}{n}\sum_{i=1}^{n}|s_i - o_i| \tag{35}$$

The last method that was used to evaluate model performance was the Nash-Sutcliffe Efficiency (NSE). It was usually used to evaluate the predictive power of hydrological models. It can be calculated by using the following equation (Nash and Sutcliffe 1970):

$$\mathrm{NSE} = 1 - \frac{n_{i=1}(o_i - s_i)^2}{n_{i=1}(o_i - o_l)^2} \tag{36}$$

In equation 36, $o_l$was the mean observed value. The NSE value can range from -∝ to 1. The model performance was as better as much the efficiency value was close to 1.

3.6 Hansson's model for simulating temperature profile

A method was presented by Hansson et al. (2004)where the implemented code was designed for dealing with phase change in water by coupling equations of governing heat transport and variably saturated flow in both positive and negative temperature. This method was applied successfully to simulate the soil temperature which showed better fit with the observed data than the standard code of HYDRUS with the presence of latent heat at different depth of the soil column during the phase change of water. Governing equation for water flow in above and subzero temperature was shown using the modified Richard's equation(Hansson et al. 2004):

$$\frac{\partial \theta_u(h)}{\partial t} + \frac{\rho_i}{p_w}\frac{\partial \theta_i(T)}{\partial t} = \frac{\partial}{\partial x}\left[K_{Lh}(h)\frac{\partial h}{\partial x} + K_{Lh}(h) + K_{LT}(h)\frac{\partial T}{\partial x} + K_{vh}(\theta)\frac{\partial h}{\partial x} + K_{vT}(\theta_{vl})\frac{\partial T}{\partial x}\right] - S \tag{37}$$

In the above equation,$\theta_u$was the volumetric unfrozen water content [L^3L^{-3}] (= $\theta_{vl} + \theta_{va}$), $\theta_{vl}$was the volumetric liquid water content [L^3L^{-3}], $\theta_{va}$was the volumetric vapor content [L^3L^{-3}], $\theta_i$was the volumetric ice content [L^3L^{-3}], t was time [T], x was the spatial coordinate [L],

ρ_i wasthe density of the ice [ML^{-3}], (931 kgm^{-3}) ρ_w was the density of liquid water [ML^{-3}] (approximately 1000 kgm^{-3}), h was the pressure head [L], T was the temperature [K] and s was a sink term [T^{-1}] for root water uptake. Due to freezing and thawing effects that relates the ice content with the temperature, and due to the dependence of the water content and hydraulic conductivity on the pressure head, equation 32 showed a highly non-linear behaviour. The water flow was simulated considering five different processes using equation 37 (Hansson et al. 2004): first two terms on the right hand side was for water flows due to pressure head and gravity ($K_{Lh}[LT^{-1}]$), the third term was water flow due to temperature gradient ($K_{LT}[L^2T^{-1}K^{-1}]$), and the last two terms were for vapor flows due to pressure head ($K_{vh}[LT^{-1}]$) and temperature ($K_{vT}[L^2T^{-1}K^{-1}]$) . The equation for soil hydraulic properties were same as used in the standard HYDRUS-1D code which is given in section 2.4 (equations 10 and 11). However, equation 11 worked for hydraulic conductivity in water flows for pressure head and gravity ($K_{Lh}\left[LT^{-1}\right]$) only. That was why another equation for hydraulic conductivity on water flows due to temperature gradient ($K_{LT}[L^2T^{-1}K^{-1}]$)was used (Fayer 2000; Noborio et al. 1996; Hansson et al. 2004):

$$K_{LT} = K_{Lh}\left(hG_{wT}\frac{1}{\gamma_0}\frac{d\gamma}{dT}\right) \tag{38}$$

In the above equation, $\gamma$was the surface tension of soil water [MT^{-2}] which can be determined from a quadratic equation as follows while $\gamma_0$was 71.89 gs^{-2} in 25°C(Hansson et al. 2004):

$$\gamma = 75.6 - 0.1425T - 2.38 \times 10^{-4}T^2 \tag{39}$$

The hydraulic conductivities of vapour flows due to pressure head ($K_{vh}[LT^{-1}]$) and temperature gradient ($K_{vT}[L^2T^{-1}K^{-1}]$) can be determined using the equations by Fayer (2000) and Scanlon et al. (2003). Since this study does not consider any vapour flow, it was not discussed here. Hansson's model gave another advantage to consider the resistance of the porous media to water

flow due to ice blocking in freezing conditions by introducing an impedance factor, Ω (Lundin 1990) which was used to reduce the hydraulic conductivity. In Hansson et al. (2004), it was multiplied by Q which was the ratio of the ice content to the total water content. This parameter Q made the blocking more effective if the water content decreased as the ice content part of the total water content increased. Thus the hydraulic conductivity for liquid phase in partially frozen soil$K_{flh}$was reduced by the following equation (Hansson et al. 2004):

$$K_{flh} = 10^{-\Omega Q} K_{Lh} \tag{40}$$

Using the above equation, a small value of the impedance factor will have a significant effect on the hydraulic conductivity of the liquid phase due to the portion of ice content in the total water content of the soil pores(Hansson et al. 2004).

The governing equation in this model for heat transport in porous media was:

$$\frac{\partial C_p T}{\partial t} - L_{f\rho_i}\frac{\partial \theta_i}{\partial t} + L_o(T)\frac{\partial \theta_v(T)}{\partial t} = \frac{\partial}{\partial x}\left[\lambda(\theta)\frac{\partial T}{\partial x}\right] - C_w\frac{\partial q_l T}{\partial x} - C_v\frac{\partial q_v T}{\partial x} - L_0(T)\frac{\partial q_v}{\partial x} - C_w S T \tag{41}$$

In the above equation, the first term on the left side stood for the change in energy content while second and third term were represented a change in the latent heat of the frozen and vapor phase of water, respectively. The five terms on the right-hand side of the above equation represented: soil heat flow by conduction, convection heat flow with flowing water, heat flow due to diffusion of water vapor, transfer of latent heat due to diffusion of water vapor and energy uptake by root water uptake, respectively(Hansson et al. 2004). In equation 41, the volumetric heat capacity of the soil which was denoted by C_p($Jm^{-3}k^{-1}$, $ML^{-1}T^{-2}K^{-1}$) was expressed by the following equation

which was basically the sum of volumetric heat capacities of the solid C_n, liquid C_w, vapor C_v and ice C_i, multiplied by their volumetric fractionθ (Hansson et al. 2004):

$$C_p = C_n\theta_{in} + C_w\theta_w + C_v\theta_v + C_i\theta_i \quad (42)$$

Apart from these, in equation 41, $L_f$was the latent heat of freezing (J kg^{-1},L^2T^{-2}) which was approximately 3.34 $\times 10^5$ J kg^{-1}, $L_0$was the volumetric latent heat of the water (J m^{-3}, $ML^{-1}T^{-2}$) which was determined by $L_0 = L_{w\rho_w}$ where $L_w$was the latent heat due to the vaporization of water which was 2.501 $\times$ 10^6-2.369.2 T [°C](Hansson et al. 2004). More breakdowns on the each term on the both sides of equation 41 can be found atHansson et al. (2004).

CHAPTER 4

RESULTS

In this chapter,the calibrated equations for the 5TE sensors from the lab experiments of the sensor calibration were shown. The soil hydraulic properties were determined from the SWC curve using the VGM model. The relation between VWC vs. pressure head was established from the lab experiment and unsaturated hydraulic conductivity was determined from the VGM model and plotted against the pressure head. Soil moisture and soil temperature data were plotted for the soil column experiment over the freezing and thawing period. Later vadose zone modeling using HYDRUS-1D was applied to the standardized data set to identify to what extent they were predictable. Results from the numerical model and simulation were plotted and the benchmark data set was used for the inverse calibration of the numerical model to reduce uncertainty and more accurate prediction from the simulation. Results of the error analysis, development of calibrated equations, findings on the unsaturated soil hydraulic properties from the lab experiments and the calibrated soil hydraulic and heat transport parameters from the numerical analysis were shown in the tables.

4.1 Soil specific calibration of FDR sensors

In order to calibrate the FDR sensor, it was important to validate the relation between VWC and dielectric permittivity, as VWC calculated by FDR sensor was actually based on the Topp equation that converted the measured dielectric permittivity into VWC. For the calibration, data points were collected for both dielectric permittivity and Topp equation based VWC of fine sand for each of the five sensors. VWC was calculated as a product of the gravimetric moisture

content and bulk density divided by the density of water for the sample of each trial which was defined as Actual VWC. VWC calculated from each trial as a product of the gravimetric moisture content (Actual VWC)and sensor's output based on Topp equation (Sensor's VWC)were plotted against the dielectric permittivity for all five sensors. The data points from the Actual VWC and dielectric permittivity were used in a linear regression analysis to produce calibration equations. Plots for Actual VWC versus dielectric permittivity, Sensor's VWC versus dielectric permittivity and ±3% deviations of Sensor's VWC versus dielectric permittivity were shown in Figure 6toFigure 10for sensor 1 to sensor 5 respectively. These plots illustrated if the Actual VWC was located within ±3% of Sensor's VWC as VWC from the sensors will be accepted if they lie within the ±3% of the Actual VWC.

The actual VWC showed generally a linear trend of increasing VWC with increasing dielectric permittivity values. The manufacturer supplied Sensor's VWC showed the similar trend of increasing moisture content with increasing dielectric permittivity. However, from the graphs, it was found that in most cases the manufacturer supplied Sensor's VWC did not lie within ±3% of the Actual VWC.Table 1showed the error analysis that was carried out to find out the deviation between the Actual VWC and the manufacturer supplied Sensor's VWC based on mean deviation and average error. The largest averaged error was 39.1% while the smallest averaged error was 16.3% (Table 1). Table 1also showed the calibration equation and the R^2 values from each of the determined calibration equation. The R^2 values for the calibrated equation ranged from 0.91 to 0.94. That means the dielectric permittivity measurements remained close to each other for all five FDR sensors. Therefore, the sensors were good for using in the experimental set up to measure VWC in the1-D soil column at different depths with the calibrated equation as

there was a significant difference between the Actual VWC and manufacturer equation based Sensor's VWC.

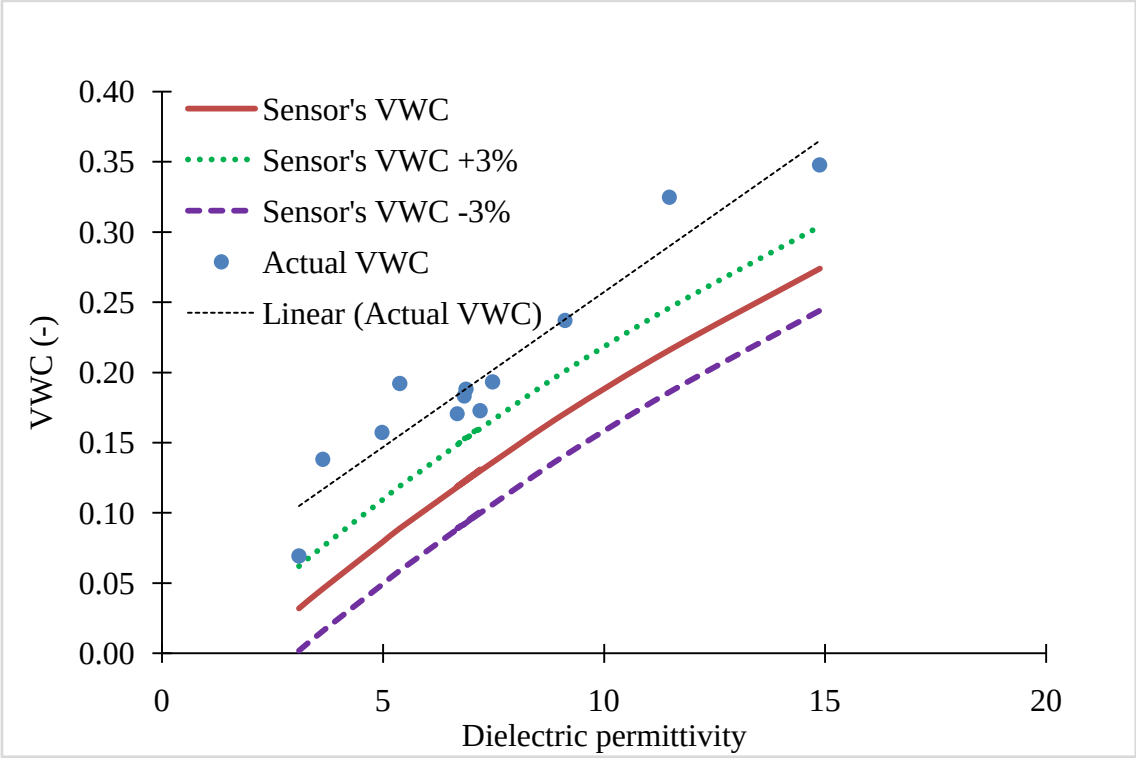

Figure 6: Actual VWC and measured dielectric permittivity along with the ±3% of the sensor's VWC for Sensor 1

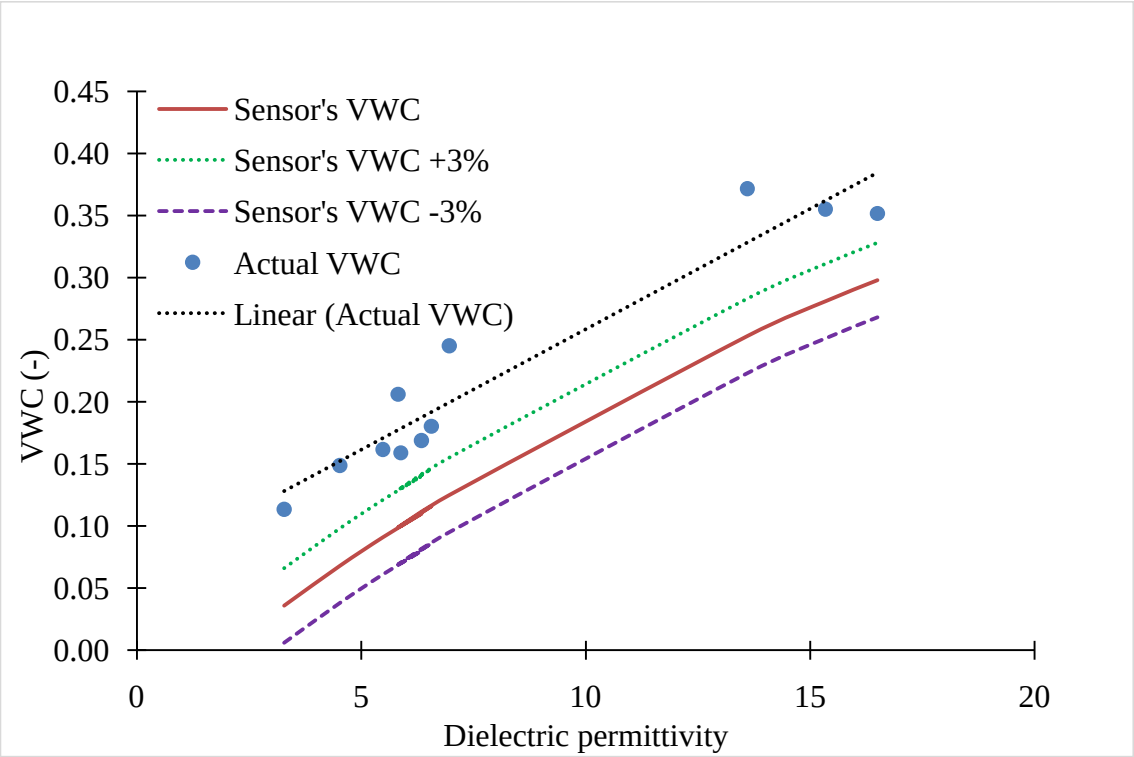

Figure 7: Actual VWC and measured dielectric permittivity along with the ±3% of the sensor's VWC for Sensor 2

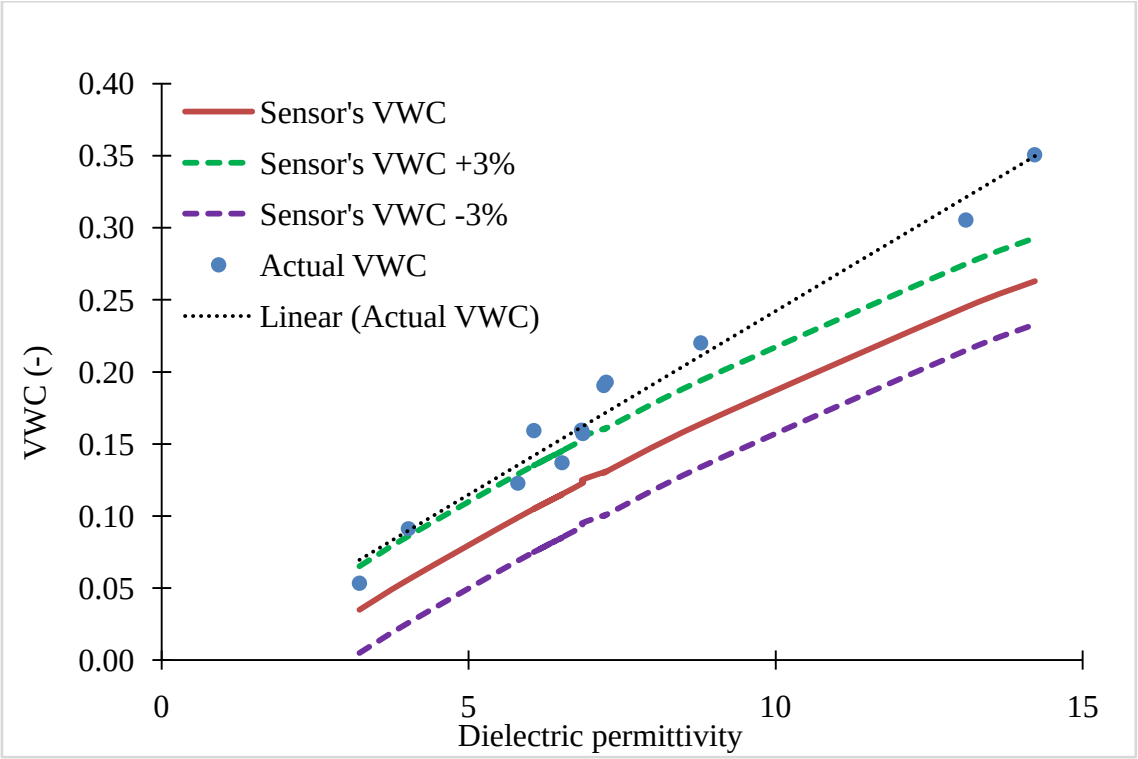

Figure 8: Actual VWC and measured dielectric permittivity along with the ±3% of the sensor's VWC for Sensor 3

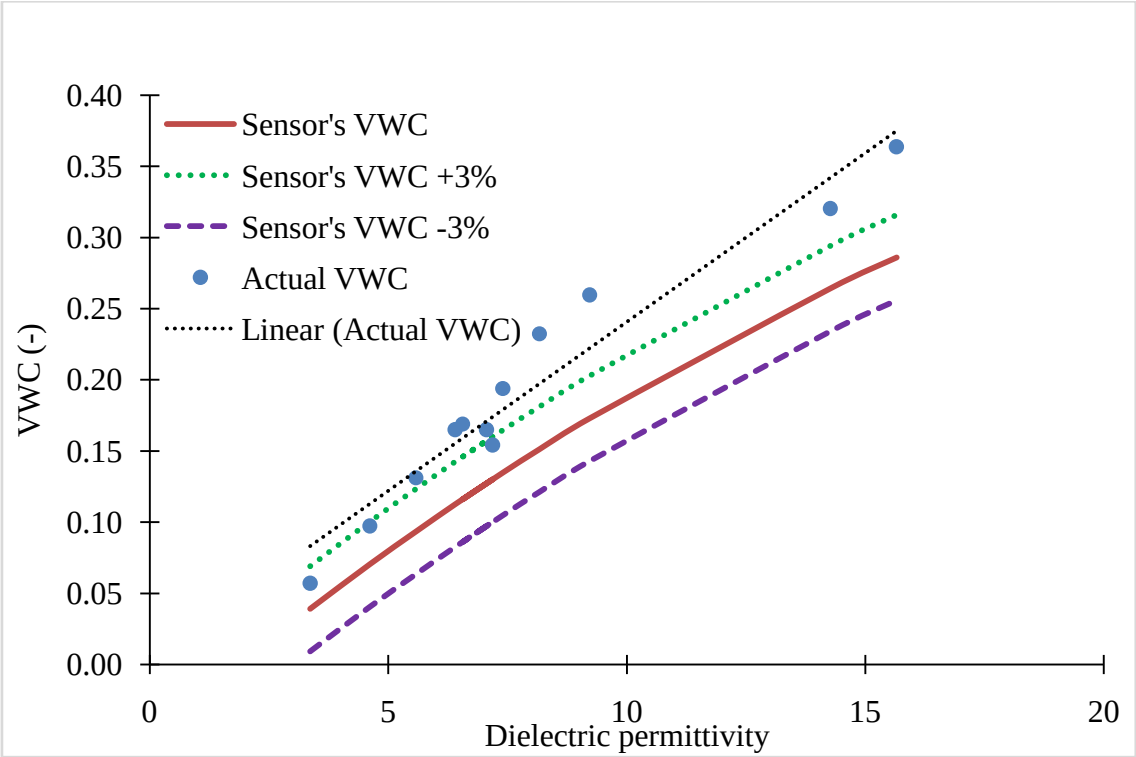

Figure 9: Actual VWC and measured dielectric permittivity along with the ±3% of the sensor's VWC for Sensor 4

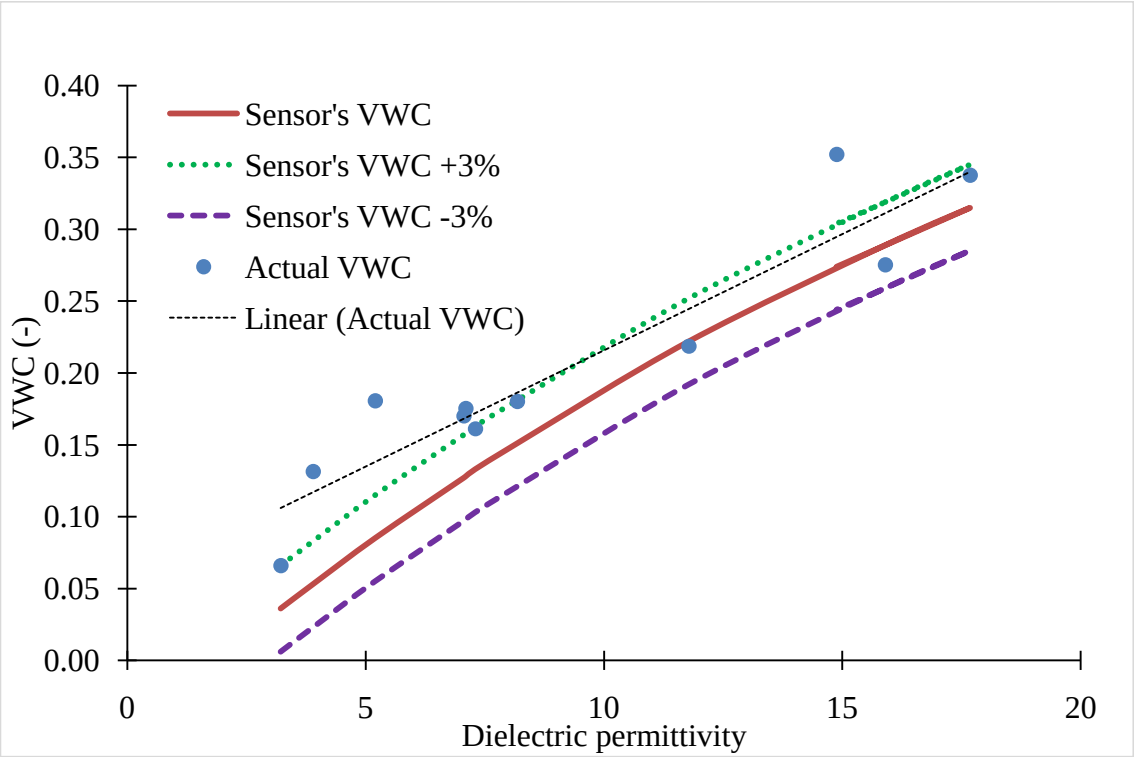

Figure 10: Actual VWC and measured dielectric permittivity along with the ±3% of the sensor's VWC for Sensor 5

Table 1: Measured Actual VWC and Sensor's VWC with the sensor specific calibration equation

FDR sensor No.	Mean deviation (-)	Average error (%)	R^2 of the calibrated equation	Calibration equation
1	0.070	16.30	0.91	VWC= 0.0221 × (raw counts) + 0.0365
2	0.077	39.07	0.93	VWC= 0.0201 × (raw counts) + 0.0614
3	0.046	26.68	0.97	VWC= 0.0255 × (raw counts) – 0.0124
4	0.051	27.23	0.94	VWC= 0.0237 × (raw counts) + 0.0034
5	0.056	30.24	0.95	VWC= 0.0186× (raw counts) + 0.0475

4.2 Experimental results from soil column experiments at different freezing and thawing periods

Calibrated equations for each FDR sensor were used to measure the VWC in the thawing and freezing experiments of the soil column in the ice chamber. There were total three freezing and thawing cycle carried out in the ice chamber: -5°C to +5°C, -10°C to +5°C, and -15°C to +5°C. Foreach of the cycles, two plots were made based on the soil moisture, soil temperature, air temperature and percolated water. Figure 11, Figure 13 and Figure 15showed the soil temperature in respect of air temperature for each of the freezing to thawing cycle while Figure 12, Figure 14 and Figure 16showedthe soil moisture in respect of percolated water in different freezing to thawing cycle. It took 17, 28 (due to technical problems of the ice chamber) and 16days to freeze the whole soil column in -5°C, -10°C and -15°C respectively, so that steady state temperatures for each cycle were achieved in the soil column. Once the temperature at all depths of the soil column reached the desired freezing temperature, the thawing period started.

After the air temperature reached to +5°C from -5°C,-10°C and -15°C respectively (within ~6 hrs since the room temperature in the ice chamber was set to +5°C), snowmelt simulation started by pumping water from the top surface of the soil column (Figure 11 to Figure 16). Pumping of water was continued for the next 9, 9 and 13daysrespectively for each of the cycles until soil temperature at all depths reached to +5°C. After pumping wasstopped, the soil column was left at+5°C temperature for 12, 12 and 8 more daysuntil soil moisture throughoutthe soil column reached to ±10% moisture content at all depths for each of the thawing cycle respectively (Figure 12, Figure 14 and Figure 16).Figure 17illustratedthe rate of percolation in respect of soil moisture at the last 20 cm of the soil column in different freezing and thawing cycle andwhen the percolation rate reached to aconstant value for each of the different cycles. Based on the graphs inFigure 11to Figure 17, the flow of water and heat transport were discussed in the section Discussion.

Once air temperature increased to +5°C, soil temperatures increased in all experiments (Figure 11, Figure 13 and Figure 15). In the case of -5°C to +5°C cycle, the sensor 1 and sensor 2 reached to ~4°C within six days after the start of thawing while the sensor 5 showed soil temperature near to +4°C after ten days thawing was started (Figure 11). Percolation started immediately after water content reached to more than 10% at all depths for this cycle (Figure 12). Percolation was fast due to the low heat gradient at all depths. The average percolation rate of the total pumping period was 0.006 cm/min. The percolation reached to a constant level at the end of pumping which was73 to 74 cm (Figure 12). Although air temperature shortly increased to +2.52°C due to ice chamber defrosting function during the freezing period of -10ºC, soil temperatures stayed below -6°C at that time and lowered further down after the problems in the ice chamber were fixed (Figure 13). This event proved the insulation of the system worked very

well so that heat transfer was effectively limited from the side and from below. Figure 14showed that percolation for this cycle reached to a constant level when soil moisture up to 87 cm reached to the ±10% of the soil VWC. The rate of percolation was not steady until the soil at all level of the soil column reached to +5ºC (Figure 17). That happened after 9 days since pumping and thawing period started. Immediately after the pumping of water stopped, total height of the percolated water became steady within 89 cm to 91 cm (Figure 14). Figure 16showedthatpercolation reached to a steady state level of 95 cm to 97 cmfor -15ºC to +5ºC cycles. By this time soil temperature at all depth was reached nearly at +5ºC (Figure 15) and pumping was stopped. The average percolation rate during the pumping period was found 0.005 cm/min for this cycle. The existence of latent heat was clearly visible in all freezing periods at all depth of the soil column(Figure 11, Figure 13 and Figure 15).

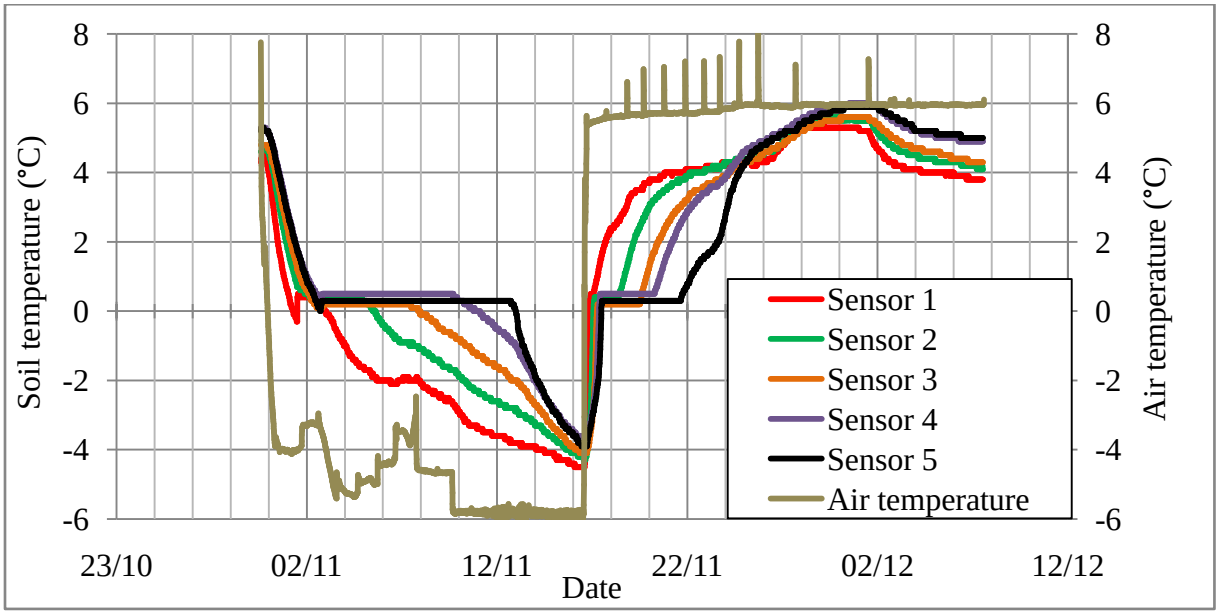

Figure 11: Soil temperature at different depths when air temperature changed from -5°C to +5°C

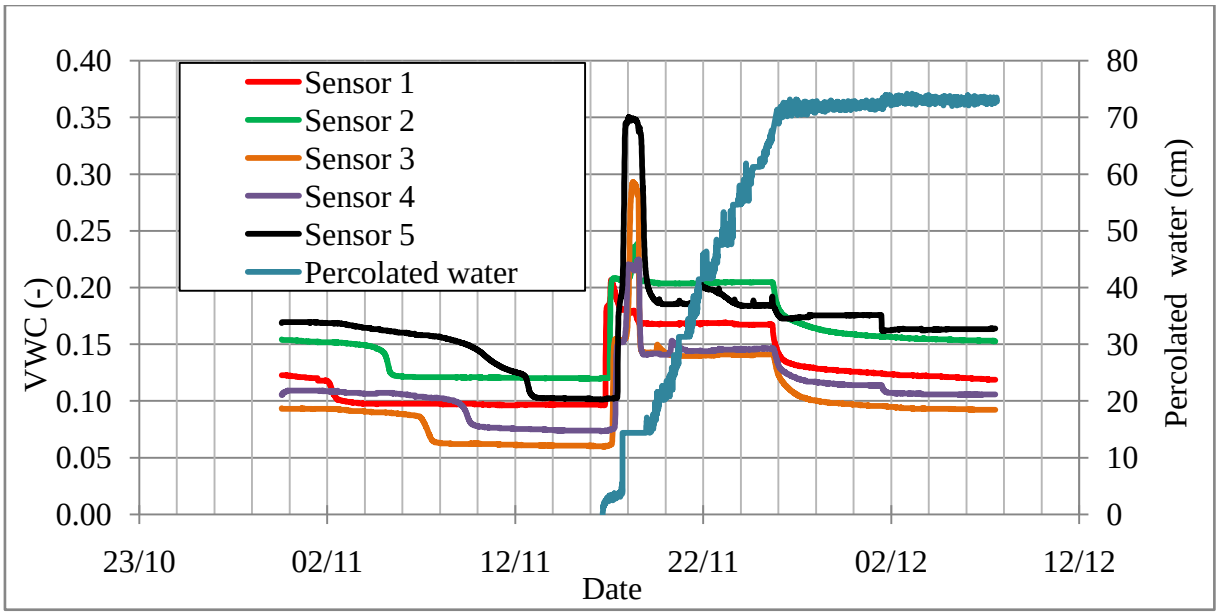

Figure 12: Soil moisture at different depths when air temperature changed from -5°C to + 5°C

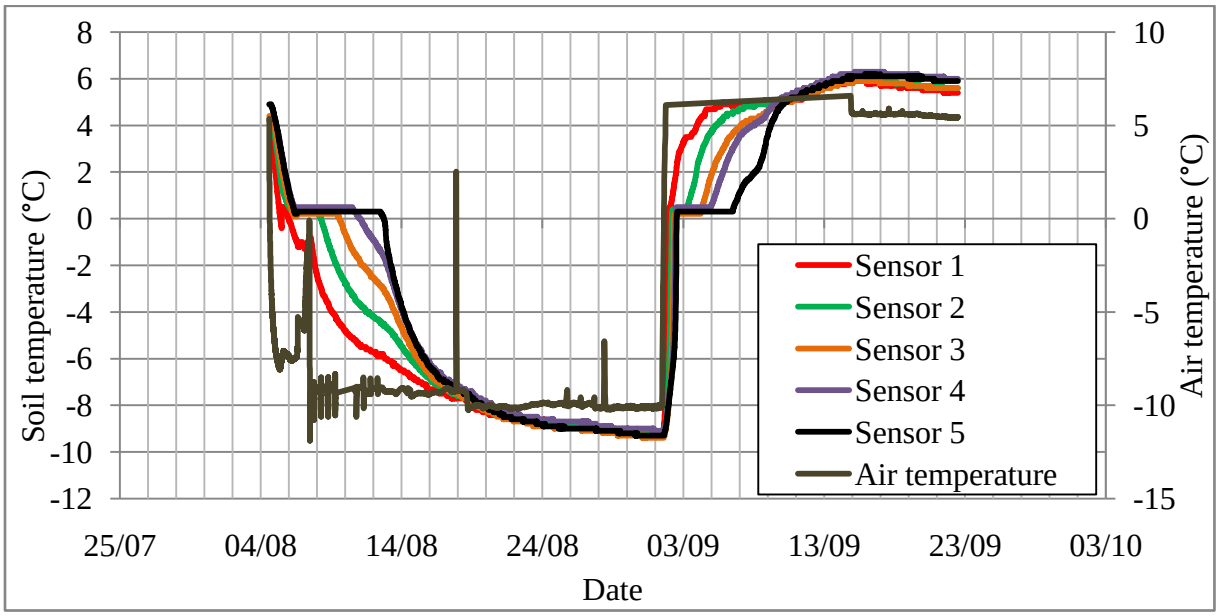

Figure 13: Soil temperature at different depths when air temperature changed from -10°C to +5°C

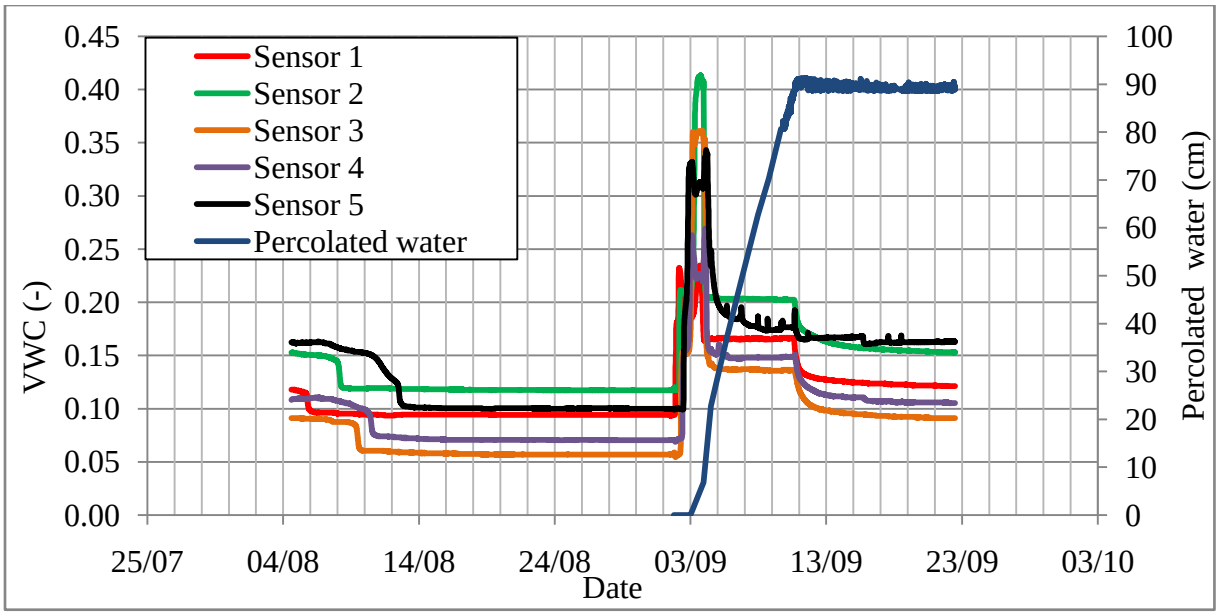

Figure 14: Soil moisture at different depths when air temperature changed from -10°C to + 5°C

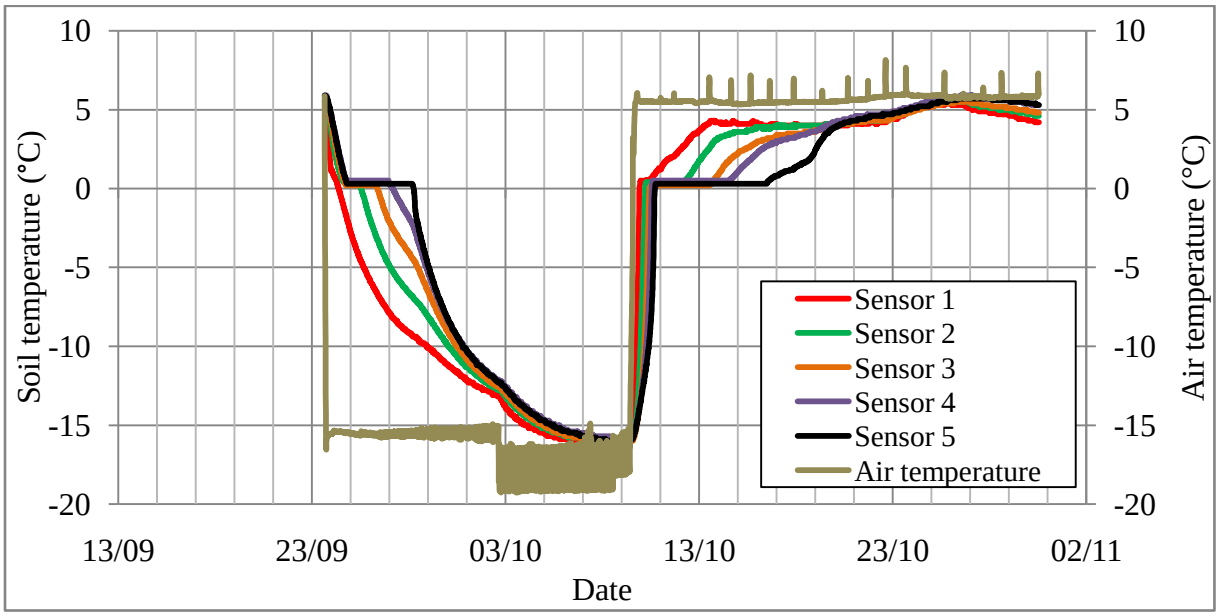

Figure 15: Soil temperature at different depths when air temperature changed from -15°C to +5°C

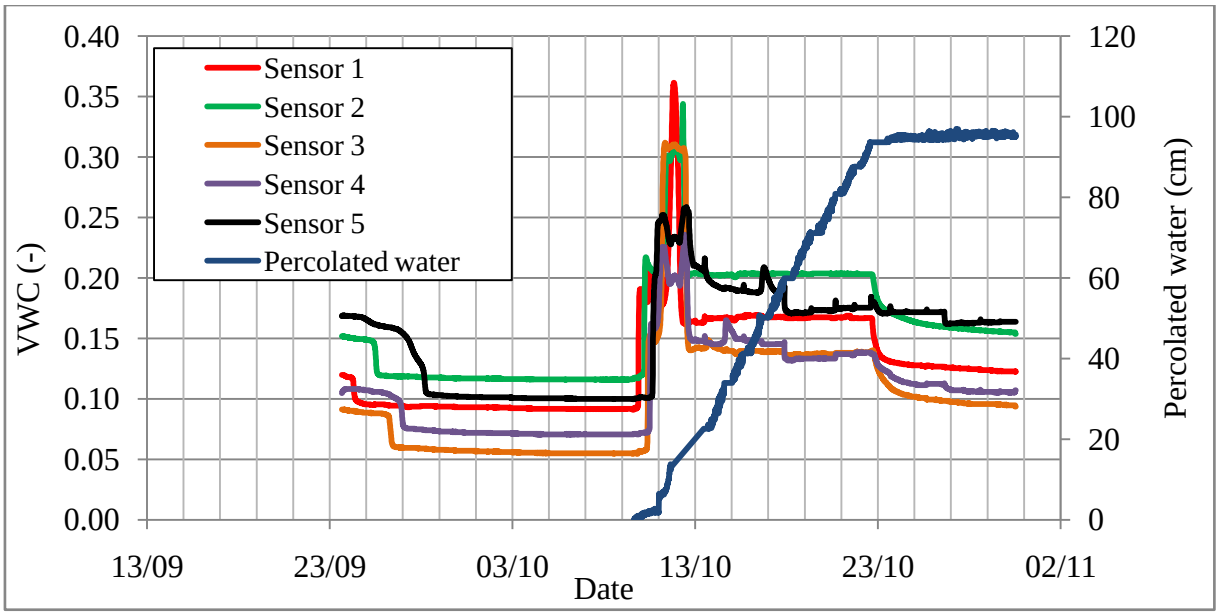

Figure 16: Soil moisture at different depths when air temperature changed from -15°C to + 5°C

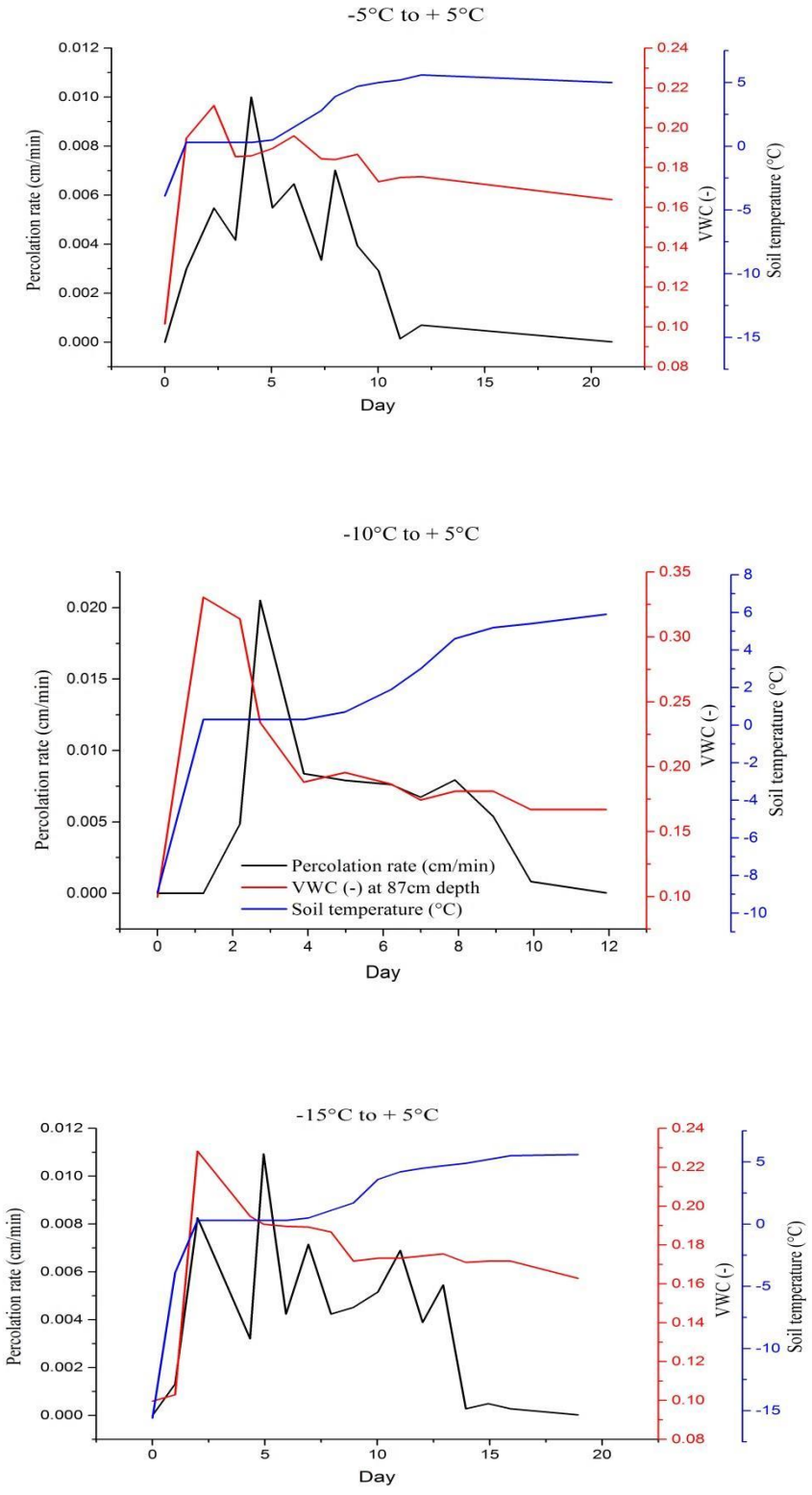

Figure 17: Percolation rate at different freezing and thawing cycles

4.3 Unsaturated soil hydraulic properties

The soil water retention curve that relates the volumetric water content to the pressure potential was developed by using both the lab experiment and the VGM model. TheVGM parameters (Table 2) were determined by fitting the retention model to the observed data using the parameter optimization program in Excel. The variance of the measured value θ_v was calculated. From the variance, the coefficient of determination (R^2) of the curve was found 0.936. The best fit of the variables (θ_r, θ_s, α, n, m) were recorded in Table 2. $K_s$was measured by constant head permeability test while l was an empirical parameter which was assumed to be 0.5 (Mualem 1976; Schaap et al. 2001). In order to evaluate the retention curve measured by VGM, two statistical methods were used: root mean square error (RMSE) and geometric mean error ratio (GMER) (Kanzari et al. 2012). If the RMSE and GMER values were equal to 0 and 1 respectively means there was a perfect match between the observed values from the lab experiment and VGM model values. If the GMER value was less than 1, that means the model underestimates. If it was greater than 1, that means the model overestimates. The correlation between the measured and fitted curves was strong as the coefficient of correlation R^2 was found to be 0.967. The RMSE and GMER were found 0.003 and 0.776respectively. As GMER was well below of 1, the laboratory method slightly underestimated the soil water retention curve. However, RMSE of 0.002 proved no significant difference between the observed and fitted values of SWC curve. Figure 18showed the calculated unsaturated hydraulic conductivity for the fine sand from the VGM model at pF 1 and pF 2.

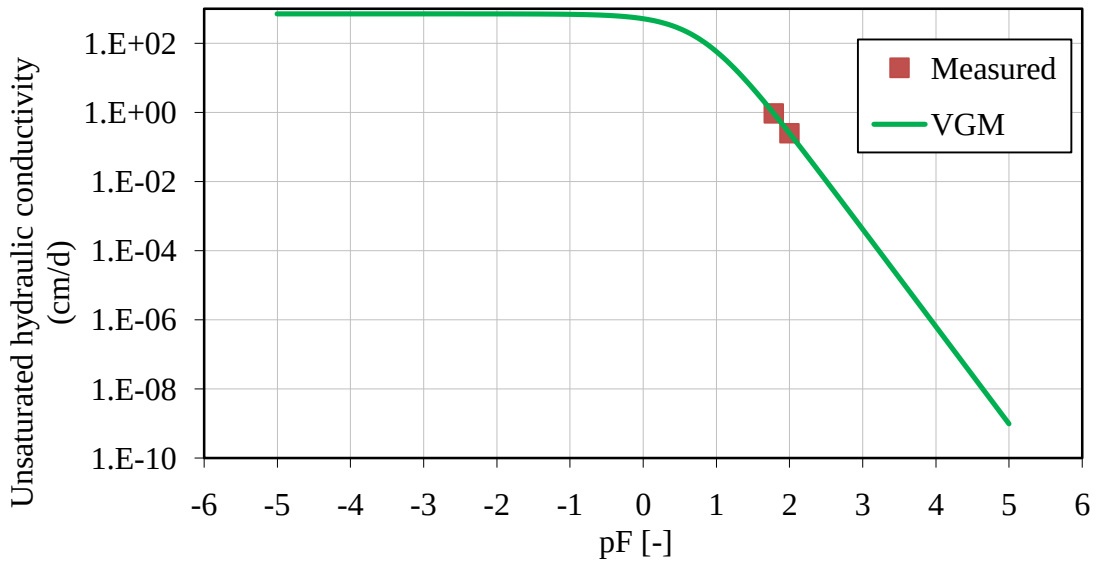

Figure 18: Unsaturated hydraulic conductivity of the fine sand calculated from VGM model

Table 2: Parameterization of unsaturated soil hydraulic properties from VGM model

Parameter	Value
θ_r [-]	0.0089
θ_s [-]	0.3
α [1/cm]	0.15
n [-]	1.15
m [-]	0.9
l [-]	0.5
K_s [cm/d]	709.17

4.4 Simulation results

Unsaturated soil hydraulic properties determined from the lab experiments were used as the initial parameters in the vadose zone modeling using HYDRUS-1D. The modeling of the soil column in different freezing and thawing condition were conducted in two stages: In the first stage the model was built and ran using the standard version of HYDRUS-1D (version 4.18) where the observed data set was used in the inverse calibration process of the model to optimize the results and calibrate the parameters required to simulate water flow and heat transport in partially frozen soil. For this purpose, the observed data set was chosen for that time period of the soil column experiments in each freezing and thawing cycle when the freezing temperature wasjust started moving towards the thawing temperature and precipitation was started once the temperature in the surrounding environment moved to above 0^{o}C. In the second stage, calibrated parameters (taken from stage 1) were directly used to simulate soil moisture and soil temperature using Hansson's model in HYDRUS-1D to verify the prediction performance. However, Hansson's model was not able to run with these calibrated parameters due to numerical instability. Thus, the VGM and heat transport parameter were changed according to the default values of the soil included in HYDRUS-1D. Further calibration of the soil hydraulic properties and heat transport parameters were not performed for Hansson's model as the inverse calibration function which was used in this study for the calibration purpose was not included in the Hansson's model. Hansson's model was an additional module of the standard HYDRUS-1D which was in the experimental and development phase. The model was not developed as a complete package of HYDRUS-1D. Since it was a model which was still in the experimental phase, it was used in this study only to identify the model performance in respect of benchmark data set in order to investigate how the model performs to re-predict the benchmark data set.

4.4.1 Standard HYDRUS-1D

First, the model was built using standard code of HYDRUS-1D, and a series of graphs for different freezing to thawing conditions were produced. The simulated data sets for the soil temperature and soil moisture were plotted in Figure 19 to Figure 24. In these figures, OSM, SSM, OST and SST stands for observed soil moisture, simulated soil moisture, observed soil temperature and simulated soil temperature respectively. The calibrated parameters for the water movement and heat transport equation were shown in Table 3 and Table 4. The error analysis between the simulated data set and benchmark data set were shown in Table 5. The calibrated parameters (unsaturated soil hydraulic properties and heat transport parameters) were very crucial for the accurate prediction of the soil moisture content and soil temperature in the partially frozen soil. The unsaturated soil hydraulic properties were the most sensitive parameters for the modeling of the water movement in soil. Besides soil hydraulic properties, heat transport parameters had also a significant impact to address the heat exchange between the soil particles, ice and infiltrated water. The calibrated values of the unsaturated soil hydraulic properties and heat transport parameters for all the freezing and thawing cycle which were calibrated using the inverse calibration function of HYDRUS-1D were shown in Table 3 and Table 4 respectively. In case of calibrated heat transport parameters, although b_1, b_2 and b_3 values of each freezing to thawing cycles stayed very close to each other, C_n values showed large difference from one cycle to another (Table 4). From the results of the inverse calibration for all experiments, large changes from the initial to the calibrated values for θ_s, α and n were found; K_s value changed little (Table 2 and Table 3). The initial values of the soil hydraulic parameters were taken from the laboratory experiment (Table 2). There were no laboratory experiments performed to investigate the heat transport parameters of the fine sand. Therefore, the initial values of the heat transport parameter

for fine sand were directly taken from the research of Chung and Horton (1987). Comparison of the simulated results with the observed data set was made using different error analysis tool. The calibration was successful since a low RMSE and MAE (Table 5) were found. However, a low range of NSE value (-5.483 to -0.431) was observed for soil VWC at all five depths of three different freezing to thawing cycles. The average difference of water content between observed and measured data was less than 6% for all freezing and thawing cycles. Simulated and observed soil moisture showed for the -5°C to +5°C experiment a minimum RSME of 6.3% at sensor 3 and a maximum RMSE of 7.2% at sensor 5. Similar performance was found in the other cycles. The simulated and observed soil temperature showed for the -5°C and the -10°C to +5°C cycle a better match so that the minimum RMSE was calculated to 0.55°C at sensor 1 (-10°C to +5°C cycle) and the maximum RMSE was 2.11°C at sensor 5 for the same experiment. However, the experiment of the -15°C to +5°C cycles showed a decreased performance so that the maximum RMSE became 3.53°C (sensor 5). Overall, the error increased with increased depth of the sensors.

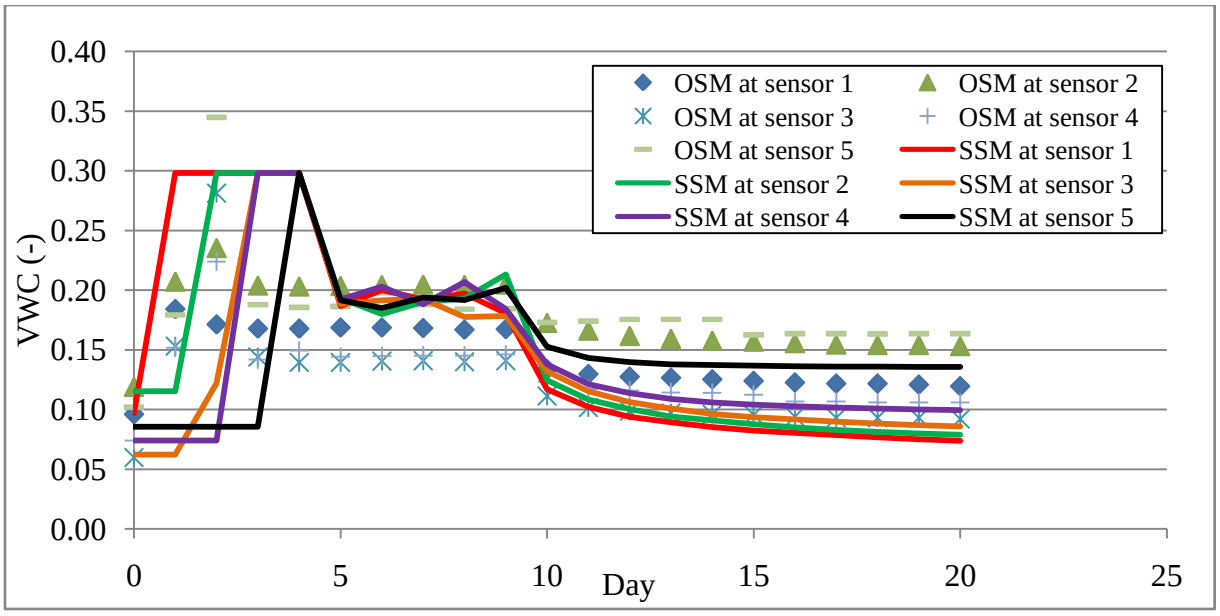

Figure 19: Observed and simulated soil moisture after calibration while air temperature was changing from -5°C to +5°C

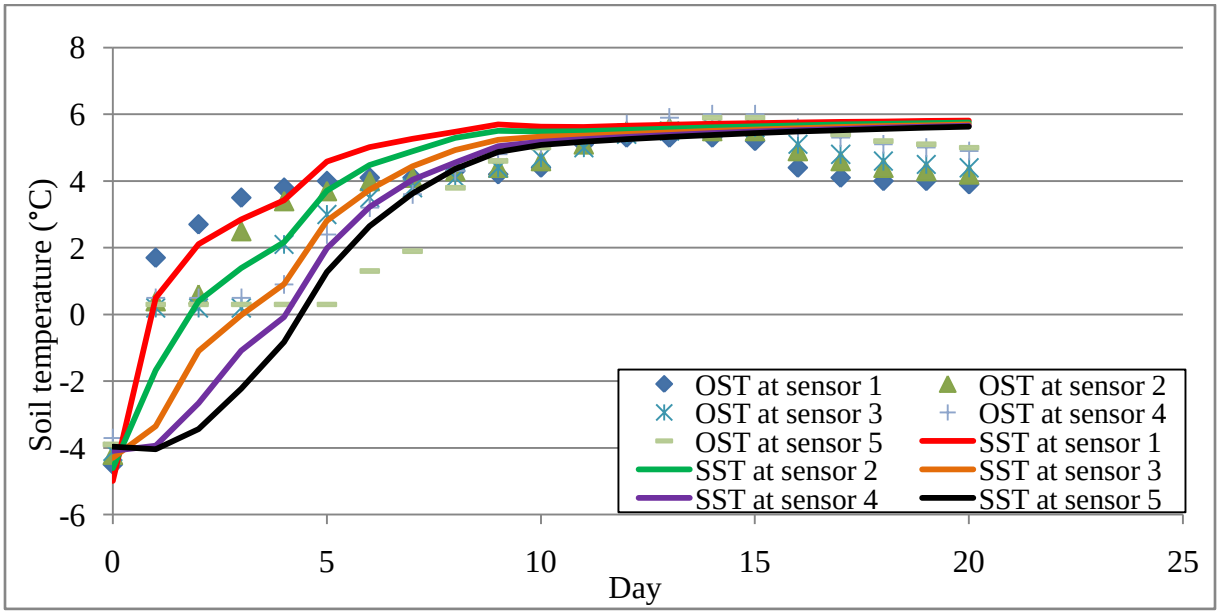

Figure 20: Observed and simulated soil temperature after calibration while air temperature was changing from -5°C to +5°C

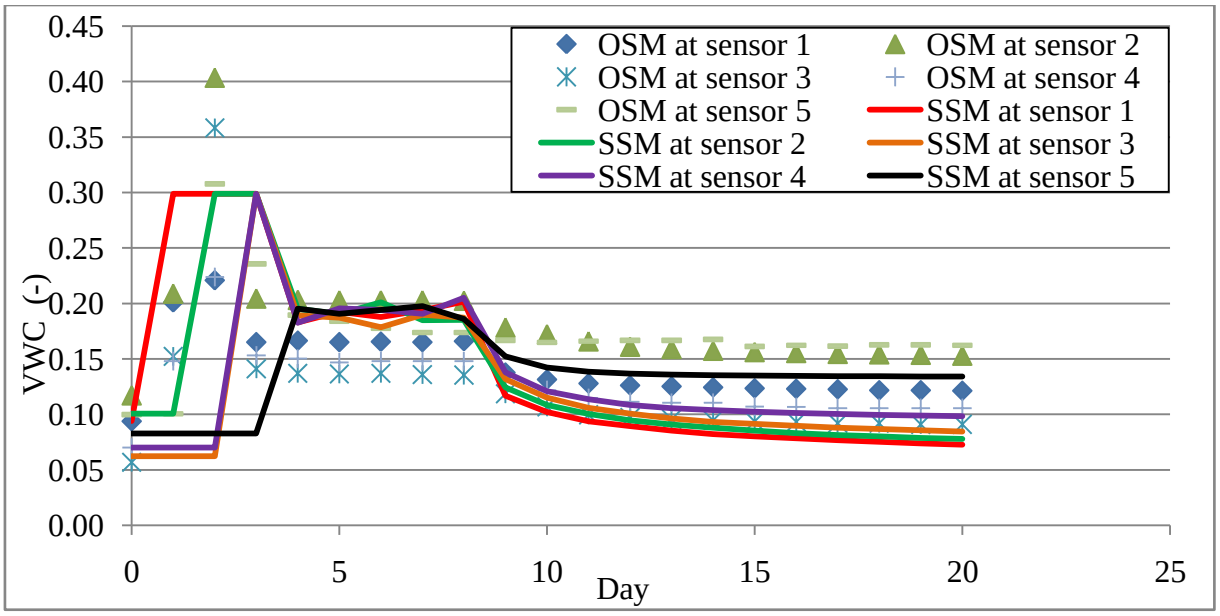

Figure 21: Observed and simulated soil moisture after calibration while air temperature was changing from -10°C to +5°C

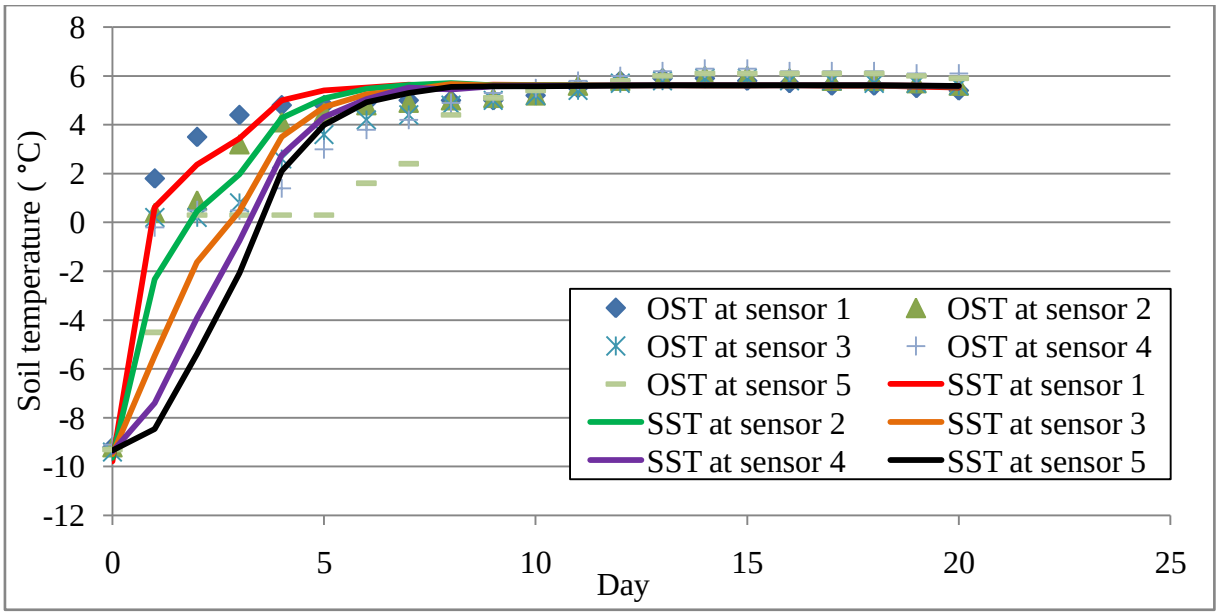

Figure 22: Observed and simulated soil temperature after calibration while air temperature was changing from -10°C to +5°C

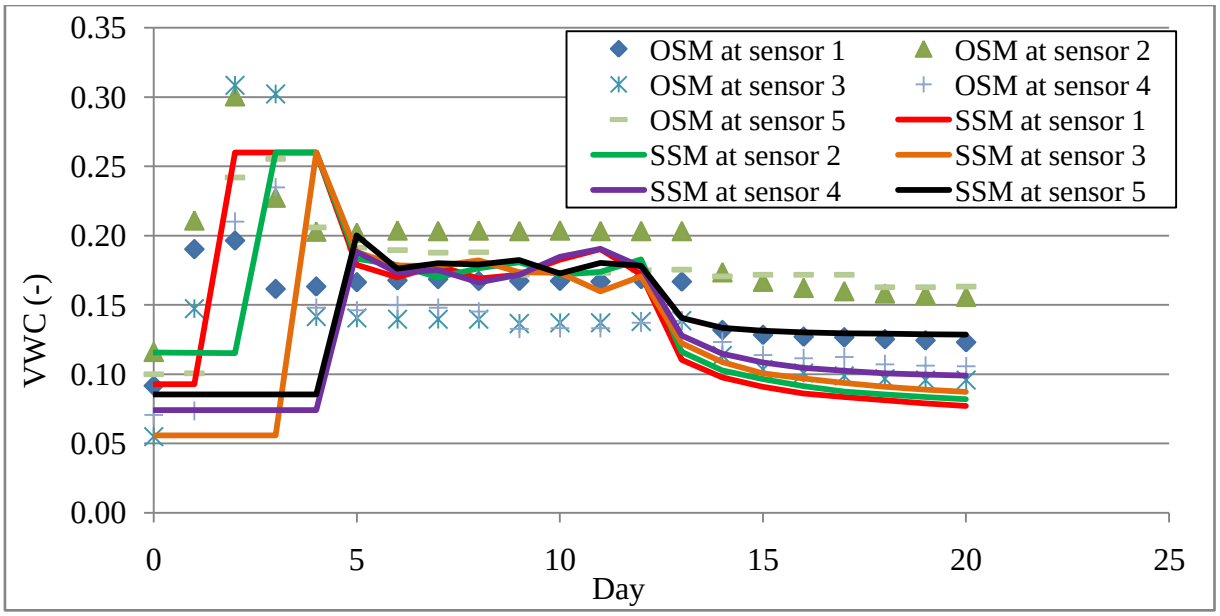

Figure 23: Observed and simulated soil moisture after calibration while air temperature was changing from -15°C to +5°C

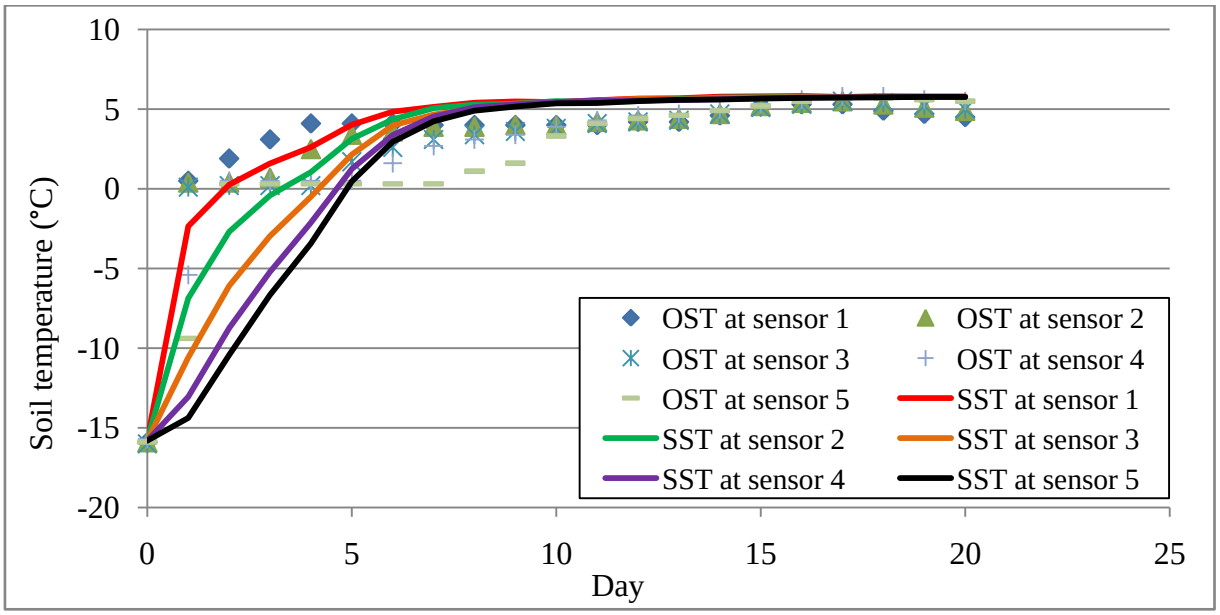

Figure 24: Observed and simulated soil temperature after calibration while air temperature was changing from -15°C to +5°C

Table 3: Calibrated soil hydraulic properties

Parameter	-5°C to +5°C	-10°C to +5°C	-15°C to +5°C
θ_r [-]	0.010	0.010	0.011
θ_s [-]	0.298	0.299	0.260
α [1/cm]	0.146	0.151	0.151
n [-]	1.736	1.730	1.645
l [-]	0.567	0.588	0.629
K_s [cm/d]	716.8	749.6	720.3

Table 4: Calibrated heat transport parameters

Parameter	-5°C to +5°C	-10°C to +5°C	-15°C to +5°C
b_1	1.51E+16	1.51E+16	1.65E+16
b_2	-1.54E+17	-1.59E+17	-1.55E+17
b_3	3.28E+17	3.20E+17	3.30E+17
C_n	3.20E+14	1.30E+14	1.27E+14

Table 5: Error analysis (RMSE, MAE, and NSE) for simulated soil moisture and temperature data at different freezing and thawing condition

Soil VWC					Soil temperature				
	Sensor	RMSE	MAE	NSE		Sensor	RMSE (ºC)	MAE (ºC)	NSE
-5 ºC	1	0.063	0.050	-5.483	-5 ºC	1	1.114	0.983	0.699
	2	0.062	0.055	-3.806		2	0.957	0.768	0.817
	3	0.067	0.041	-1.354		3	1.052	0.723	0.808
	4	0.065	0.040	-3.900		4	1.309	0.778	0.728
	5	0.072	0.046	-2.084		5	1.514	0.962	0.373
-10 ºC	1	0.052	0.044	-2.053	-10 ºC	1	0.549	0.424	0.970
	2	0.066	0.058	-0.431		2	0.761	0.509	0.948
	3	0.080	0.041	-0.895		3	1.400	0.737	0.837
	4	0.054	0.032	-2.165		4	1.993	1.173	0.693
	5	0.064	0.038	-1.488		5	2.105	1.394	0.726
-15 ºC	1	0.048	0.037	-2.515	-15 ºC	1	1.310	1.164	0.911
	2	0.068	0.056	-2.610		2	1.968	1.304	0.805
	3	0.087	0.050	-1.172		3	2.971	1.783	0.567
	4	0.055	0.035	-1.224		4	3.122	1.899	0.581
	5	0.062	0.040	-2.286		5	3.526	2.279	0.540
Max		0.087	0.058	-5.483	Max		3.526	2.279	0.373
Min		0.048	0.032	-0.431	Min		0.549	0.424	0.970

4.4.2 Hansson's model

Simulated soil temperature profiles from Hansson's model were plotted with the benchmark data set of the laboratory experiments in Figure 25 to Figure 27for all three different freezing to thawing cycles. The deviation between the simulated and observed data set were compared based on error analysis, and results were presented in Table 7 for Hansson's model. All calibrated soil hydraulic and heat transport parameters (Table 3and Table 4) were directly used as initial parameter in the Hansson's model. As the model showed numerical instability with the calibrated parameters, default values (Table 6) from HYDRUS-1D were used in Hansson's model. These values were included in the HYDRUS-1D soil catalog based on Carsel and Parrish (1988) for soil hydraulic properties and based on Chung and Horton (1987) for heat transport parameters. Only θ_r and θ_s values were changed to 0.02 and 0.3 respectively, according to the soil testing. It was found numerically stable at these θ_r and θ_s values. Although Hansson's model was not successful to simulate soil moisture content profile in right order of magnitude, it can simulate the soil temperature profile. Therefore, model performance was verified based on the error analysis between the observed and simulated soil temperature profile. Hansson's model showed same results for the moisture content profile of all different freezing to thawing cycles and it is already reported that Hansson's model had numerical problems to model soil moisture movement (Šimůnek et al. 2016). For an example,Figure 28showed the graph for the simulated moisture content of the -10ºC to +5ºC cycle. Therefore, error analysis was performed only between the simulated and observed values of soil temperature data for different freezing to thawing condition. The model performance of Hansson's model was better without any calibration compared to the standard version of HYDRUS-1D with calibration. For example, the maximum mean absolute error was reduced to 1.598ºC from 2.279ºC and the maximum error

based on RMSE reduced to 3.077°C from 3.526°Cin the soil temperature profile of Hansson's model among all freezing to thawing cycles. However, the maximum NSE value was found almost same for the soil temperature profile of both models.

Table 6: Soil hydraulic properties and heat transport parameters for Hansson's model

Soil hydraulic properties	
θ_r [-]	0.02
θ_s [-]	0.3
α [1/cm]	0.145
n [-]	2.68
l [-]	0.5
K_s [cm/d]	712.8
Heat transport parameters	
b_1	1.47E+16
b_2	-1.55E+17
b_3	3.17E+17
C_n	1.43E+14

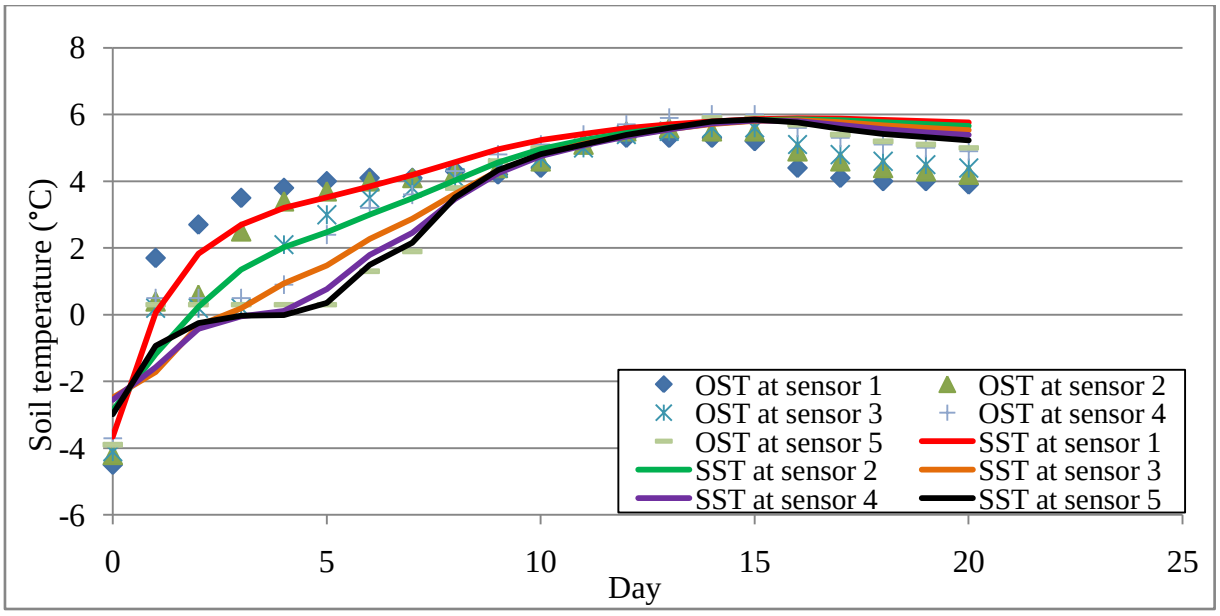

Figure 25: Observed and simulated soil temperature without calibration and using Hansson's model while air temperature was changing from -5°C to +5°C

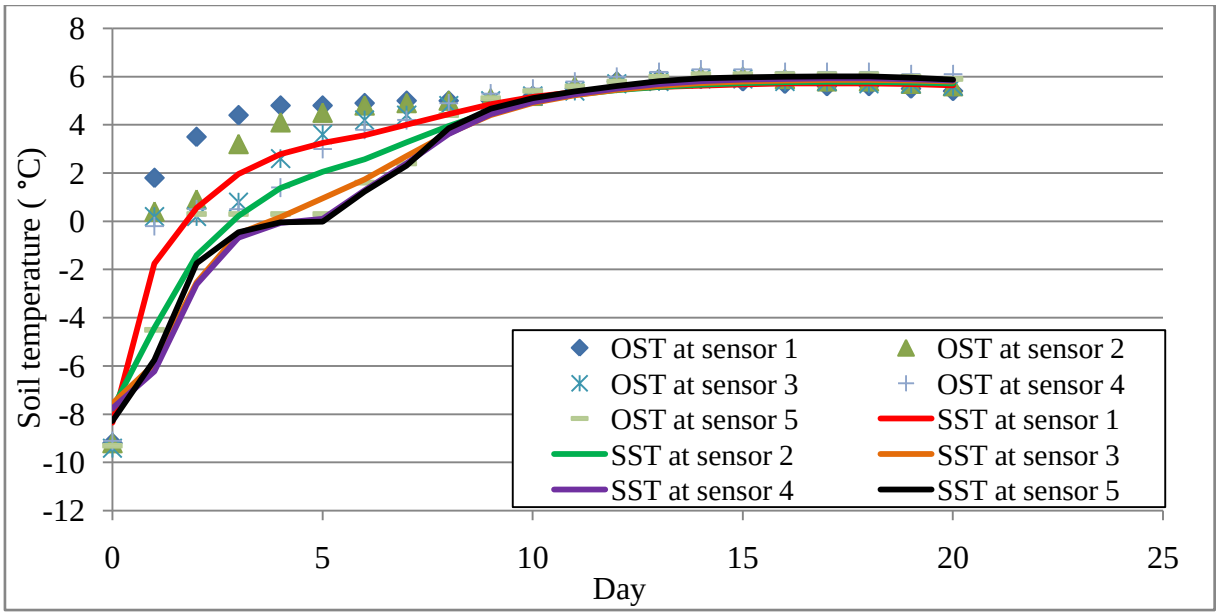

Figure 26: Observed and simulated soil temperature without calibration and using Hansson's model while air temperature was changing from -10°C to +5°C

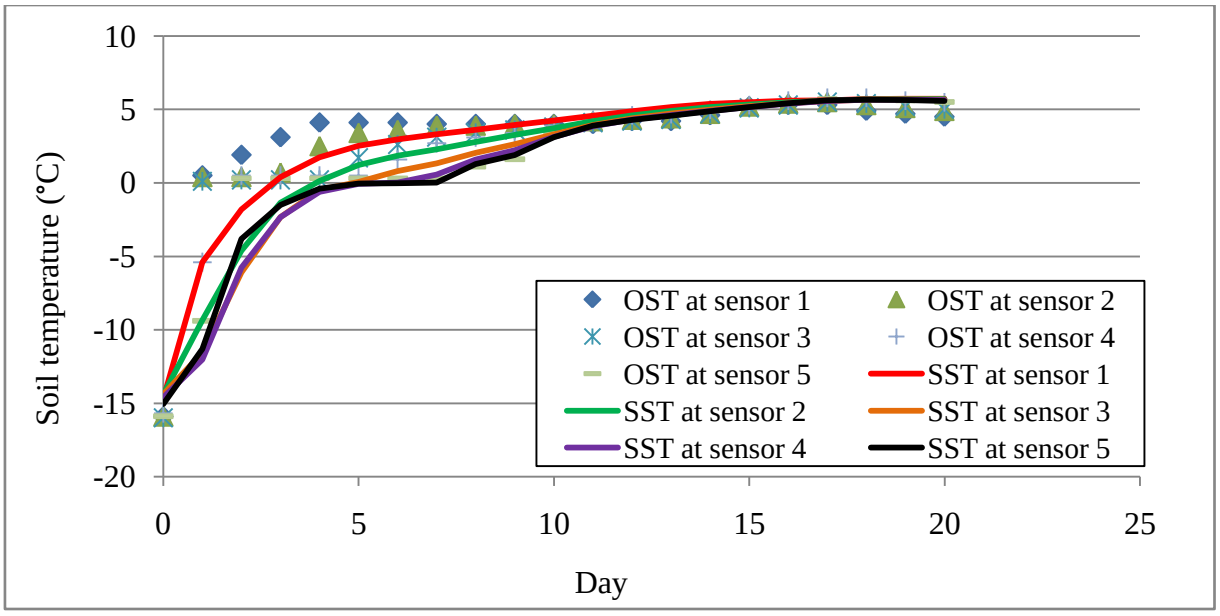

Figure 27: Observed and simulated soil temperature without calibration and using Hansson's model while air temperature was changing from -15°C to +5 °C

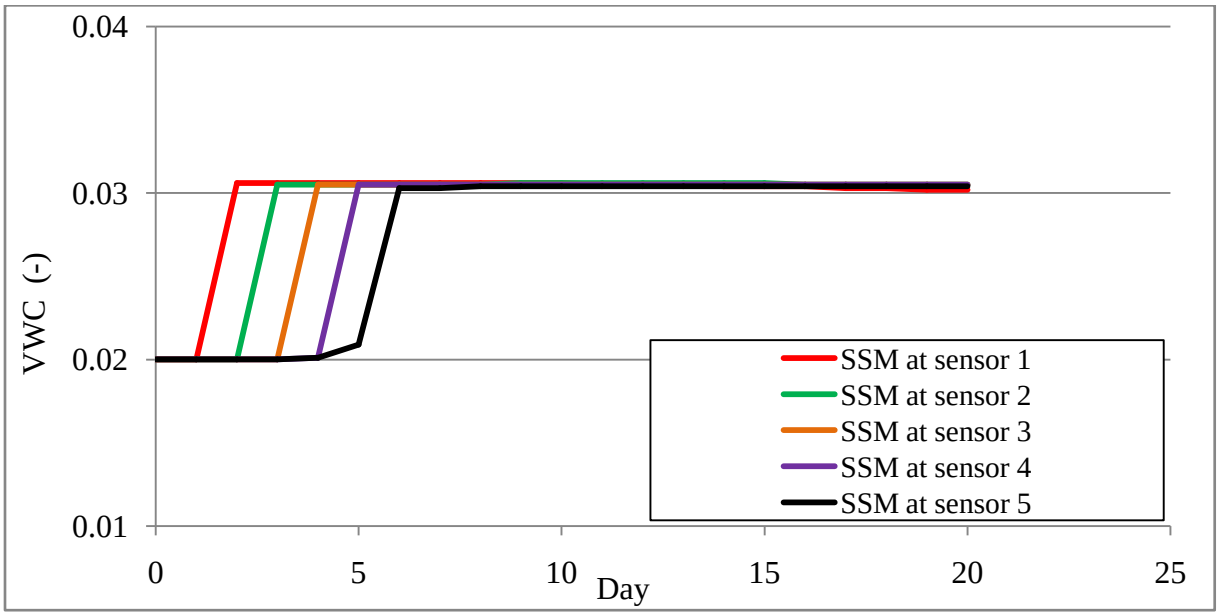

Figure 28: Simulated soil moisture without calibration and using Hansson's model while air temperature was changing from -10°C to +5°C

Table 7: Error analysis (RMSE, MAE, and NSE) for simulated temperature data at different freezing and thawing condition using Hansson's model

	Sensor	RMSE (ºC)	MAE (ºC)	NSE
-5°C	1	0.993	0.830	0.761
	2	0.801	0.614	0.872
	3	0.921	0.590	0.853
	4	1.273	0.813	0.743
	5	1.425	0.920	0.395
-10°C	1	1.344	0.870	0.820
	2	1.725	1.160	0.734
	3	1.878	1.180	0.707
	4	1.870	1.275	0.730
	5	0.635	0.418	0.975
-15°C	1	1.870	1.287	0.818
	2	2.643	1.513	0.649
	3	3.077	1.598	0.535
	4	2.248	1.318	0.783
	5	1.105	0.559	0.955
Max		3.077	1.598	0.395
Min		0.635	0.418	0.975

CHAPTER 5

DISCUSSIONS

In this chapter, the reliability of the insulation of the soil column experiment, the movement of soil moisture and the change of soil temperature along with the percolation characteristics, phase change of water molecules and the numerical analysis of the soil column experiment over the different freezing to thawing periods were discussed. The theory of water flow and heat transport was explained from the results of the freezing and thawing cycle. Obvious conclusions were drawn about the migration of moisture content and heat exchange during different freezing and thawing cycle. The benchmark data set which was developed for soil temperature and soil moisture in the partially frozen condition were later applied in vadose zone modeling using theHYDRUS-1D standard code and the parameters needed to simulate water flow and heat transport were calibrated. These calibrated parameters were used later in the Hansson's model to verify further the model performance in the modified equation of water flow and heat transport used byHansson et al. (2004). All these results were analyzed and discussed in this chapter to justify the model performances and evaluate the physical process of the laboratory experiments.

5.1 Reliability of the insulation for the soil column

Soil temperature profile for all freezing to thawing cycles showed that, while air temperature was increasing above 0°C, soil temperature stayed at 0°C for a couple of days due to latent heat released by soil-water. The air temperature at the beginning of each thawing cycle raised up to 5ºC within 4 to 6 hours while the first sensor of each freezing to thawing cycle showed that, it took several days for the first 27cm of the soil column to reach at 5ºC. Sensors at the lower

depth took more time to reach at 5ºC compared to the first sensor. For example: the first sensor at the beginning of -5ºC to +5ºC thawing cycle took 4 days to reach at +5ºC from -5ºC including the time with the release of latent heat. At the same time the temperature at the lowest depth of the soil column was almost constant at 0.3ºC as shown by the sensor 5. Similar behaviour was found for -10ºC and -15ºC to +5ºC cycles. These events proved that heat transfer from the top of the soil column to the bottom of the soil column did not happen immediately after raising the room temperature to +5ºC. It took considerable amount of time depending on the freezing temperature of the soil to move towards +5ºC including the time of latent heat exchange as shown by each sensors. That clearly proved the reliability of the insulation of the soil column. Therefore, due to the insulation materials at the peripheral area and at the bottom of the soil column, heat exchange only happened vertically from the top of the soil surface to the bottom of the soil column. Moreover the sequential change of temperature with depth in the event of freezing, latent heat exchange and thawing period for each three cycles also proved that insulation worked very well in this soil column lab experiment. The heat flux at the lower soil column was strongly limited due to the overlying soil.

5.2 Soil water movement and soil temperature at different freezing to thawing cycles

The difference in soil moisture content in the -5ºC to +5ºC cycle between sensor 1 and sensor 5 was noticeable (Figure 12) as they were placed at a distance of 60 cm from each other. For example, the differences in the moisture content and temperature of sensor 1 and sensor 5 were found 6.06% and 5% respectively on the 1st day of the thawing cycle while on the 2nd day it was found 2.75% and 140% respectively. After one day of pumping 3.7L percolated water was measured in total. That clearly showed the movement of moisture towards the freezing front was very fast due to a low-temperature difference at the beginning of pumping. Another reason was

the existence of weak thermal gradient with the poor release of latent heat (Figure 11). Once the freezing period started, the moisture content changed in the soil due to the development of ice lenses in the soil. It was also due to the poor release of latent heat (Figure 11and Figure 12).

The initial water content was ±10% when the thawing was started. As soon the moisture content increased, the latent heat initiated and by the time soil temperature increased above 0ºC, soil moisture started decreasing and returned to the initial ±10% (Figure 17). That means, water could infiltrate towards the freezing front at the lower depth, if the soil was enriched with moisture content up to saturation with the advancement of the thawing front after the latent heat was released. However, the development of ice lenses along with the heaving of soil can be assumed during freezing period, and it was already shown by Kane and Stein (1983). For -5ºC to +5 º C, sensor 5 reached to saturation (~30% VWC) earlier compared to the -10ºC and -15ºC to +5ºC cycles (Figure 12, Figure 14 and Figure 16). In case of the -10ºC to +5ºC cycle, sensor 2 and sensor 3 reached to saturation before sensor 5 and for -15ºC to +5ºC, sensor 1, sensor 2 and sensor 3 reached to saturation while sensor 4 and sensor 5 could not reached to saturation due to equilibrium percolation rate within the soil column. That means, thawing front and corresponding soil moisture movement were restricted due to frozen soil at the bottom end of the soil column. The colder the freezing temperature, the retardation due to frozen soil increased and caused saturation in the upper and middle level of the soil column (Figure 14 and Figure 16). By the time soil moisture reached to the bottom of soil column, the soil was completely thawed (all sensors showed positive temperature) which resulted in equilibrium percolation rates so that sensor 4 and sensor 5 could not reach to saturation (Figure 16).

Soil temperature data has been presented in Figure 11; it can be seen that the soil temperature has been extended to below 0°C for all sensors sequentially according to their placement from the

top. That caused the sudden peak of moisture change that was found in all sensors during the thawing cycle when the temperature had been increased to +5°C (Figure 12). This was because of the movement of water due to pumping and the water that converted into liquid from frozen condition in the soil pores once the soil received heat from thawing cycle.

For -10°C to +5°C, the difference between sensor 1 and sensor 5 at the beginning of the thawing cycle for moisture content and temperature were 6.19% and 1.1%, respectively. On the second day of thawing cycle, the difference changed to 33.33% and 85.7%. That means the soil column was frozen uniformly from top to bottom with a little variation of initial moisture content between the top and the bottom. The movement of the thawing front was rather slow in this cycle compared to the -5°C freezing cycle. That was the reason why the difference between the temperature value of the top and the bottom sensor raised that much (1.1% to 85.7%) within one day of thawing. The top portion of the column showed higher moisture content than the bottom, as the movement of the thawing front was slow due to the partially frozen soil at the bottom. The amount of percolated water after 2 days of pumping was approximately 6 L with a percolation rate of 0.002 cm/min while the average percolation rate at the end of pumping period was 0.007 cm/min (Figure 17). There was no percolation at the first two days of thawing. However, the rate of percolation increased with the downward movement of soil moisture (Figure 14)once the bottom soil reached to above 0°C.

For the freezing condition of -15°C, all sensors had a temperature below -16°C (Figure 15). However, the difference of soil moisture at the beginning of thawing between sensor 1 and sensor 5 was 8.3%, which was the smallest difference between top and bottom soil moisture of the soil column among all cycles on the first day of the thawing period. This was due to the non-existence of the thermal gradient between these two sensors. Following that, on the second day

of the thawing cycle, the difference between sensor 1 and sensor 2 values for soil moisture and temperature changed to 62% and 180% respectively. That means water was supplied to the downward thawing front on the first 27 cm of the soil column as the soil was enriched with high moisture content due to the release of heat from soil particles which resulted melting of the ice lenses as well during the thawing cycle. Since the bottom portion was still frozen, there was no significant change in moisture content until the 2nd day of the thawing cycle (Figure 16). Appreciable warming (above +0°C) of the soil has been developed at the bottom within 4 days of the thawingperiod; the moisture content increased at the bottom sensor higher than the top sensor. After 4 days of pumping, 19.6 L percolated water was collected. Thus, a rapid increase in the percolation rate occurred a few days after the start of the thawing period. However, that was observed for a short time only as the percolation rate returned to the equilibrium level when soil temperature at all depth reached to ~4ºC (Figure 15 and Figure 17). This was because soil water accumulated in the first 72cm of the soil columnwhen the bottom layer of the soil was frozen and increased the unsaturated hydraulic conductivity once the bottom layer thawed completely. Thus, water moved downwards suddenly and increased the soil moisture at the bottom layer. By this time, the surplus water (melted ice) was percolated from the bottom of the soil column. Following that event, the outflow became limited by the newly infiltrated water resulting a reduced percolation rate that eventually reached to a constant level once pumping of water stopped. Another reason was due to an increase in the hydraulic gradient as the wetting front reached to the drier level of the soil column.

5.3 Latent heat due to the phase change of water molecules at different freezing to thawing conditions

In all three freezing to thawing cycles, the moisture migrated toward the thawing front, and the peaks in moisture content were found at various levels in the soil profile. The position of these peaks depends on the rates of two processes: heat transfer and moisture transfer. If the soil column was wet and thawed, the unsaturated hydraulic conductivity would be quite high due to the nonexistence of ice lenses. Therefore, the rate of the downward migration of soil water will be increased. That event was found at every thawing cycle of the soil column experiment once the pumping started. Before each freezing period was started, the soil column was completely thawed and the moisture content at all depth stayed at ±10%. There were no ice lenses at the beginning of the freezing as there was no thermal gradient exist between sensor 1 and sensor 5. As soon as temperature dropped down to ±0ºC, the soil moisture started decreasing from the ±10% of the moisture content. This was because water in the soil pores started converting into ice lenses. The presence of latent heat during the both freezing and thawing periods proved the event of conversion of soil water into ice lenses and ice lenses into water. During this period, water converted from solid phase to liquid phase or vice versa and released heat which was carried out further by the soil particles and water molecules and contributed to the change of both soil moisture content and soil temperature later on. However, the extent of the existence of latent heat varied according to the depth and the freezing temperature. For example, the latent heat existed longer at the bottom of the soil column as per reading of sensor 5 at different freezing period compared to the first 72 cm of the soil column. However, the extent of the presence of latent heat increased subsequently with the depth of soil column, the longest presence of the latent heat was found for the lowest freezing temperature of -15ºC which was 6 days at the last

20 cm of the soil column while it was 3 days in case of -5ºC freezing period. That means, therelease of latent heat was rather poor in -5ºC compared to the other freezing period based on the graph in Figure 11, Figure 13 and Figure 15. The soil column was frozen, and it started gaining heat (energy) once the thawing period started. In that case, the frozen soil column was receiving energy and increasing the soil temperature by convection and conduction. The pumping water was additionally supplying heat to the soil column since the infiltrated water had a temperature of 5°C. Overall, the heat exchange happened between the soil particles, infiltrating water and the ice formed in the soil. Thus the temperature increased in the soil column gradually during the thawing period. Once the pump started, water tried to penetrate through the frozen soil which depend largely on the soil gradation, initial water content, and soil compaction(Moghadas et al. 2015).

5.4 Percolation in respect of soil moisture and soil temperature at diiferent freezing to thawing cycles

Percolation of water largely depends on the soil moisture and soil temperature at different freezing to thawing cycles. For example, it can be seen in Figure 17, at the depth of 87 cm, percolation started 1 day after pumping started for the -5°C to +5°C cycle. The corresponding soil moisture was also increased after one day of pumping. The highest rate of percolation was found 0.01 cm/min at the 4^{th} day of thawing when the soil temperature at 87 cm depth was at 0.3°C. The percolation rate was not steady until the pumping was stopped and the soil temperature reached to ~5°C. Once pumping stopped at the 9^{th} day of thawing, the percolation rate decreased. Similar behaviour was observed for -10°C to +5°C and -15°C to +5°C cycle. For -10°C, percolation started after two days of pumping. The percolation rate got a sudden peak while soil temperature was ~0°C at 87 cm depth. Corresponding soil moisture also showed a

sudden peak just one day before the percolation rate got the peak. Similar behaviour was found for the -15°C to +5°C cycle (Figure 17). Although, percolation happened 1 day after the thawing cycle started, the rate was very limited at 0.0013 cm/min which increased to 0.01 cm/min on the 4^{th} day of pumping in this cycle when the soil temperature at 87cm depth was at 0.3°C. In both cycles, percolation rate was not at steady stated level during the whole pumping period and percolation rate decreased once the pumping stopped. By that time the whole soil column was thawed completely. For the first appearance of percolation in the three different freezing to thawing cycles, the temperature at the first 72 cm of the soil column was ~3°C while it was nearly 0°Cfor the next 35 cm. As the water started infiltrating downward the temperature of soil increased close to 0°C. That is why the soil moisture increased in the first 72 cm of the soil column while the soil moisture in the last 35 cm of the soil column was still at 10% (Figure 12, Figure 14 and Figure 16). It took more or less one day for the first 27 cm of the soil column to reach above 0°C for all the thawing cycle but the whole soil column reached to nearly +5°C in more or less than 10 days for all freezing to thawing cycles. During that time the pumping water travelled through the whole soil column and the first percolation was observed. However, for each freezing and thawing cycle, the time of the first appearance of percolation was different. This was because the movement of the thawing front depended on the exchange of heat between the soil particles, ice lenses, and pumping water. For -10°C, it took 2 days to reach to the bottom of the soil column as the percentage of ice was higher than -5°C. Next, the duration of latent heat release was also higher at -10°C and -15°Ccompared to -5°C (Figure 15). For all three cycles, the percolation rate was increased once the first outflow was observed and the highest peak in the percolation rate was observed when the soil temperature reached nearly 0ºC at the bottom soil layer. Immediately before the highest peak in percolation rate was observed in all three cycles,

the soil moisture content at the bottom layer of the soil column was decreased and eventually reached to a steady state condition. Similarly for all three cycles' percolation rates reached to an equilibrium state once the soil temperature at the bottom layer reached nearly at +5ºC. Following this, percolation rate decreased immediately after stopping the pump (Figure 17). All these events proved that, water could percolate even soil temperature remain constant near to 0ºC and percolation rate could get equilibrium state with the equilibrium rate of infiltration once the soil column is completely thawed. The amount of energy required to change the state of water from ice to liquid was high. This can be seen from Figure 11, Figure 13, and Figure 15. The first 27 cm of the soil column reached to nearly 2°C within one day of thawing, while the whole soil column completely thawed after 9, 9 and 13 days for -5°C, -10°C and -15°C respectively since the temperature of the system brought to +5°C. Once the soil column was reached to nearly 1°C, more water was percolated which increased the percolation rate; more blocked pores opened as the ice changed to liquid, and therefore more heat transfer happened and the percolation rate got a sudden peak. Once the pumping was stopped as the whole soil column thawed completely, the percolation rate decreased for all the cycles similarly. This indicated that all soil was unfrozen and no impermeable zone due to freezing was available. The rate of the sudden peak was different for different freezing to thawing cycle as the rate of heat transfer was different depending on the freezing depth and freezing temperature.

5.5 Numerical analysis of water flow and heat transport in partially frozen soil

One of the most important processes in water flow through partially frozen soil was the change of material phase from solid to liquid with the movement of the thawing front. Since the partially frozen soil was receiving heat from both the pumping water and the latent heat, the movement of the thawing front was increased subsequently with depth. Apparently, the total water content

reduced when the soil column was freezing for all the freezing cycle i.e. -5°C, -10°C and -15°C (Figure 12, Figure 14 and Figure 16respectively). The water content was increased once the soil pore was opened since the ice blockage was removed due to heat exchange between the pumped water and ice lenses in the soil pores. The simulated water content showed almost the same physical behaviour as the observed data from lab experiments. However, the soil temperature profile simulated by using the standard code of HYDRUS-1D was not able to predict the release of latent heat during the phase change of water which was visible in the Hansson's model. This was because of the second term in the modified heat transport equation (equation 41) of the Hansson's model which expressed the change in the amount of latent energy stored in the ice (Hansson et al. 2004). With the increasing heat transport of soil particles, the water content was increasing in all the thawing cycles. However, the starting of the thawing font was variable depending on the freezing depth. For example: in the case of -5°C, -10°C and -15°C , the peak in soil moisture content was found in 2 days for the first 20 cm of the soil column. This peak was visible for 42 cm, 57 and 72 cm in 3, 4 and 5 days respectively. However, for the lowest depth of the soil column at 87 cm, the peak in soil moisture was found after 6 days (Figure 19, Figure 21 and Figure 23). This scenario was more or less same for all the freezing to thawing cycles. That proved, while the thawing front was clearly visible up to 72 cm of the soil column, the bottom of the column was still partially frozen. Although both the standard code of HYDRUS-1D and the Hansson's model were not able to simulate the temperature profile for all experiments adequately, the Hansson's model was able to show the presence of latent heat in the soil temperature (Figure 25, Figure 26 and Figure 27). The presence of latent heat affected the model performance in both models at different depths in all freezing to thawing cycles. For example: in case of -10ºC to +5ºC, the SST at sensor 1 had a steep thermal gradient so that the energy

required for latent heat was added in a very short time period. This resulted in a good match with the OST at sensor 1 for standard code of HYDRUS-1D since latent heat did not play any role due to large thermal gradient. However, the SST at sensor 5 showed a bad match with the OST at sensor 5 (Figure 22) since the thermal gradient was rather low and phase impacted by latent heat was much longer. The standard code of HYDRUS-1D was not able to simulate latent heat at all. This resulted a strong RMSE of 0.549 at sensor 1 and a much weaker RMSE of 2.105 at sensor 5 for standard code of HYDRUS-1D (Table 5). In the Hansson's model, the SST at sensor 1 had a low thermal gradient which gave a bad match with the OST at sensor 1 while SST at sensor 5 had a good match with the OST at sensor 5 due to the presence of latent heat at both SST and OST of sensor 5 (Figure 26). This resulted high RMSE value of 1.344 at sensor 1 and low RMSE value of 0.635 at sensor 5. Thus, both model performances behave vice-versa directed (Table 5 and Table 7). Similar behaviour was found for -15ºC to +5ºC e.g., RMSE value at sensor 5 was reduced to 1.105 in Hansson model from 3.526 value of RMSE in standard code of HYDRUS-1D. Due to the presence of latent heat, temperature gradient at the lower depth of the soil column was slow which resulted good match with the OST in Hansson's model. On the other hand the standard code of HYDRUS-1D showed good match of SST with OST at the upper portion of the soil column due to the steep gradient of temperature of SST and less duration of latent heat in OST. Therefore, the lower the temperature, the longer the duration of latent heat was observed at the lower depth of the soil column which was predicted well in Hansson's model that made the model performance better compared to the standard code of HYDRUS-1D. However, the weak RMSE in the upper portion of the soil column derived from Hansson's model might be only due to the simulation method in this research since Hansson's model could not be calibrated. I claim

that calibration of the VGM and the thermal parameters in Hansson's model would increase the match between simulated and observed temperature.

The soil profile became saturated after starting the thawing cycle at different depth at different times depending on the freezing temperature and movement of thawing front as discussed in section 5.2. The standard code of HYDRUS-1D showed saturation after the thawing period started. However, it was not able to able to simulate that event close to the observed data since the simulated duration of saturation was predicted longer than observed. E.g. in the -15°C to 5°C experiment, the standard code predicted at sensor 1 three days, at sensor 2 two days and at sensor 3 one day of saturation (Figure 23). The observed duration was about one day at all sensors. The reason for the extended time of saturation was the reducing prediction quality of temperature in the lower portions of the soil column (compare last paragraph). E.g., the saturation at sensor 1 reduced after simulated soil temperature at sensor 2 became unfrozen (Figure 24). This follows; the key process for exact soil moisture prediction is the correct heat transfer simulation.

The Hansson's model could not simulate soil moisture at all (Figure 28). It was well known that Hansson's model failed to simulate soil moisture at saturation (Šimůnek et al. 2016), it was also observed that the model failed to simulate soil moisture at a much lower soil moisture content (3% VWC instead of saturation at 30% VWC). This research found that any infiltration of water into the soil column resulted into a direct malfunction of the soil moisture routine in Hansson's model.From Figure 25, Figure 26 and Figure 27, it can be said that, release of latent heat was clearly visible in the simulated soil temperature profile at different freezing and thawing cycle, which was not visible at the temperature profile simulated by the standard code of HYDRUS-1D (Figure 20, Figure 22and Figure 24). Heat transfer by both conduction and convection were well addressed in Hansson's model which yielded better model performance for the lower depth of

the soil column at the lower freezing temperature for the soil temperature profile. However, the water content profile was not being simulated by Hansson's model for this specific case due to numerical instability, further improvement in the coding may allow this prediction in the same freezing and thawing condition. Comparing the results between the simulated versus observed data from Hansson's model and calibrated versus observed data by the standard code of HYDRUS-1D from Table 5 and Table 7, it can be also said that Hansson's model yielded a good result for the soil temperature at partially frozen soil by simulating the latent heat. For example: in Table 5, the maximum values of RMSE and MAE in all three cycles at five different positions of the soil column were found 3.526 and 2.279 respectively. On the other hand, these values came down to 3.077 and 1.598 for RMSE and MAE respectively in the error analysis results of the Hansson's model. Therefore, calibration of Hansson's model will further reduce the deviation between the observed and simulated data set. If the problem of numerical instability at saturation can be solved in Hansson's model, it might be able to produce a better prediction of moisture content in the partially frozen soil as the corresponding heat exchange was well addressed in Hansson's model by simulating the latent heat during the phase change of water.

CHAPTER 6

SUMMARY AND CONCLUSIONS

6.1 Summary

Based on the soil column experiments in the laboratory on the partially frozen soil, standardized data set were developed for soil moisture and soil temperature at different freezing to thawing temperatures. Decagon 5TE sensors were calibrated successfully prior to the soil column experiments and calibrated equations were applied to convert the measured dielectric permittivity into VWC during the soil column experiments. In order to simulate the water flow and heat transport in the standard code of HYDRUS-1D and Hansson's model, unsaturated soil hydraulic properties of the soil were measured from the VGM model by using laboratory developed SWC curve for fine sand. The presented laboratory based standardized data set was successfully used to simulate and calibrate flow and heat transport using both the standard code of HYDRUS-1D and the Hansson's model from freezing and thawing module of HYDRUS-1D. The standard code of HYDRUS-1D predicted both the soil moisture and soil temperature data in partially frozen and thawed soil. The simulated results showed that the prediction of soil moisture was depended on the heat exchange procedure in the corresponding soil profile. However, the code of Hansson's model showed numerical instability in terms of soil moisture prediction while it could predict the soil temperature better than the standard code of HYDRUS-1D in the lower depth of the soil column for low freezing temperature by simulating the presence of latent heat. The code was successful to cope with the rapidly changing boundary condition with the heat exchange in the partially frozen soil column.

6.2 Conclusions

Prior to the laboratory test, soil specific calibration was carried out for the 5TE sensors that worked based on the frequency domain reflectometry and were used to measure soil moisture and soil temperature at five deferent depth of the soil column. All five sensors for five different depths were tested and calibrated equations were developed based on the linear regression analysis for all of them as the Actual VWC showed significant deviation from the Sensor's VWC. Therefore, calibrated equations were directly applied to convert the measured dielectric permittivity into VWC of the different freezing to thawing cycle of the laboratory based soil column experiments. Thus, this research recommends soil-specific calibration of FDR sensors prior to installing them in soils.

It was found that the soil system did not remain in the isothermal state during the thawing cycle. Therefore, the distribution of moisture was greatly influenced by the temperature gradient. Moreover, gravitational gradient were mainly responsible for the infiltration into the partially frozen soil. High rate of soil moisture distribution was found for dryer soil, and low distribution of soil moisture occurred at the freezing front due to frozen soil. The soil water content was one of the important factors for the infiltration of water into the partially frozen soil as it can affect the thawing process. The initial soil moisture converted into ice and blocked the open pores of the soil during freezing period. Melting of this pore blocking ice required a high amount of energy. This energy was provided by convection and conduction process. Hence, the thawing period of the soil column depend on thenumber of ice lenses presented on it which was variable depending on the freezing period and the initial water content. As the initial water content for all three freezing and thawing cycle was same (±10%), it depended on the freezing temperature. From this study, it was proved that if the initial moisture content remained within ±10% VWC,

the thawing process was mainly affected by the freezing temperature. That means melting the ice in the pores and attaining a steady percolation rate required different time period from different freezing to thawing period. This study proved that percolation can be totally stopped until the soil particles reached to a temperature close to 0°C. Once the soil temperature reached nearly 0°C, the ice in the soil pores started melting due to heat exchange by conduction and convection process and therefore, it opened pores to create a passage for the movement of the water. In this study, depending on the freezing temperature it took 1-2 days. This timeduration could increase depending on the temperature of the pumping water. Percolation could not attain a steady state condition until all ice got melted and got a free passage for the downward movement of water. As a result, pumping water may create an overflow in the upper soil surface. The total time for the whole process of melting the ice by heat exchange between soil and water system and attaining a steady percolation rate might be possible to calculate using the energy balance equation for the soil/water system. Slow percolation rate was observed at the beginning of each thawing cycle. However, percolation rate increased suddenly once the soil temperature reached to nearly 0ºC at the bottom of the soil column for all the freezing to thawing cycle. From the sudden peak in moisture content at different thawing cycle, the percolation started decreasing and reached to a steady state level shortly. That was because heat exchange between soil particles and pumping water took some time and this was the time required for the water to breakthrough the soil column. Once the pumping water broke through the frozen soil column at all depth, a sudden increase in percolation observed which eventually decreased when the whole soil column thawed completely by melting the ice lenses and opening the blocked pores. The time for water breakthroughs was different at different freezing temperature. Depending on that time, the starting time of percolation varies as well. In this study, the water breakthrough time for

a 107 cm soil column filled with fine sand was found approximately 1, 2 and 1 day for -5ºC, -10ºC and -15ºC freezing temperature respectively.

Unsaturated soil hydraulic properties for fine sand were taken from VGM model and were determined for the fitted values of VGM parameter with the SWC curve developed based on the laboratory experiment for fine sand. These values were used as the initial value of unsaturated soil hydraulic properties in the numerical modeling of the soil column experiment by HYDRUS-1D. These values of the soil hydraulic properties were later calibrated using inverse calibration function of HYDRUS-1D (standard code) and adjusted by validating the model using the benchmark data set from the laboratory-based soil column experiments. After the validation of the numerical model, adjusted and calibrated parameters were used as the initial input in the Hansson's model of HYDRUS-1D. As Hansson's model was not able to simulate any data with the calibrated parameters due to the numerical instability, default values from the soil catalog of HYDRUS-1D were used as initial parameter in the Hansson's model instead of the calibrated parameters from the standard code of HYDRUS-1D. Although Hansson's model was not successful for predicting the soil moisture in different freezing to thawing cycles, the model was able to simulate the soil temperature profile in different freezing to thawing cycles by showing the presence of latent heat which was absent in the simulation results of the soil temperature profile by the standard code of HYDRUS-1D. This model was again successfully validated using the benchmark data set from the laboratory experiments, and a good fit was found between the observed and simulated data set of soil temperature at the lower depths of the soil column at low freezing temperature. The new expression used for thermal conductivity in the freezing and thawing module (Hansson's model) of HYDRUS-1 D which was a function of water content and heat transport was applicable for the partially frozen soil to some extent. The outcome of this

study asks for the further optimization of this model by following these steps: measuring the soil specific heat transport parameters for the optimization of the results and further calibration, measuring the amount of unfrozen water content to calculate the decrease in total water content in freezing temperature.

This study improved the understanding of the soil moisture movement process into the partially frozen soil as well as the capability of the physically-based processes that can be used in the hydrological models. A new standardized data set was needed since existing data sets are generally created to verify a certain numerical model as done in several studies (e.g., Flerchinger and Saxton 1989a). The benchmark data sets developed from this study is useful for the validation of numerical models and for developing scientific knowledge to suggest potential code variations or new code development in numerical models. The numerical study will provide useful insight into the appropriate large-scale hydrological situations by parameterizing all the models in the same way.

CHAPTER 7

RECOMMENDATIONSFOR FUTURE WORKS

In laboratory-based soil column experiments some other factors that can affect the soil moisture movement in partially frozen soil need to be addressed. For example, experiments can be carried out on various types of soil having a different gradation. This was because impact on coarse graded soil were different than finely graded soil due to freeze/thaw process as there was a significant difference in the soil water redistribution process based on the gradation (Moghadas et al. 2015). Next, the size and number of macropores, as the formation of frozen layer during soil freezing can be retarded due to the presence of macropores(Watanabe and Kugisaki 2016). Moreover, addressing these major effects can lead to an accurate estimation of energy exchange based on the energy balance equation. Therefore, more accurate prediction of the time required for thawing the whole soil column system, estimation of the volume of water that can percolate through the partially frozen soil and the total energy required to melt the ice blocks in soil pores will be possible to analyze from this study. Moreover, the presence of unfrozen water content in frozen soil was not addressed in this study. This unfrozen water content of the frozen soil can be addressed using a dielectric mixing model (equation 3) since dielectric permittivity of the frozen soil can be decreased if the temperature and the unfrozen water content decreased (Watanabe and Wake 2009). These events were also found during the freezing cycle of the lab experiments in this study (Figure 12 and Figure 14). Therefore, the data set developed from this laboratory experiments for frozen soil can be used to measure the amount of the unfrozen water content from the frozen soil using dielectric mixing model which can be later validated by using NMR

technology. Thus a proper estimation of unfrozen water content and ice content in a frozen soil could be possible.

In order to simulate laboratory based soil column freeze/thaw experiments, it was important to measure all the physical properties of soil such as unsaturated soil hydraulic properties and heat transport parameters. In this study, unsaturated soil hydraulic properties for fine sand were measured. However, instead of measuring heat transport parameters for fine sand, they were directly taken and used from the research of Chung and Horton (1987). For future study, it was recommended that, soil specific heat transport parameters should be measured in order to calibrate and validate modeling results more accurately. Moreover, it should reduce the model prediction uncertainties as all necessary input parameters could be soil specific which could also improve model performance. For this study, although Hansson's model showed numerical instability while simulating water content at different freeze/thaw process, it performed well in this study for simulating the soil temperature profile. Considering this obstacle, further development of the code in Hansson's model is needed in order to reduce the numerical instability so that it can work quite well to address the soil moisture along with the prediction of soil temperature at different freezing and thawing conditions. It was also recommended that numerical simulation of the current study, which was conducted using HYDRUS-1D should also be conducted using other numerical tools such as CoupMODEL(Jansson and Moon 2001) and SHAW (Flerchinger and Saxton 1989a). Since sensitivity analysis was not carried out in this study, using SHAW on the benchmark dataset developed from the laboratory experiments will further allow addressing the effect of changes in the input parameters of the model in the simulation results. Moreover, it would be also possible to parameterize some numerical models of soil freeze-thaw by using the same standardized data set.Therefore, it will be helpful to reduce

the uncertainties in model prediction and to identify some more potential physical properties that need to be addressed in the currently developed numerical tool for simulating the freezing and thawing behavior of soil more precisely.

REFERENCES

Abbott, M.B., J.C. Bathurst, J.A. Cunge, P.E. O'Connell, and J. Rasmussen. 1986. An introduction to the European Hydrological System — Systeme Hydrologique Europeen, "SHE", 1: History and philosophy of a physically-based, distributed modelling system. *Journal of Hydrology* 87 no. 1–2: 45-59.

Anderson, D.M., and N.R. Morgenstern. 1973. Physics, chemistry, and mechanics of frozen ground: A review. In *Second International Conference of Permafrost*, 257-288.

Arnold, J.G., R. Srinivasan, R.S. Muttiah, and J.R. Williams. 1998. Large area hydrologic modeling and assessment part I: model development. *Journal of the American Water Resources Association* 34 no. 1: 73-89.

ASTM. 2006a. Standard test method for sieve analysis of fine and coarse aggregates. In *ASTM C136-06*. West Conshohocken, Pennsylvania: American Society for Testing and Materials.

———. 2006b. Standard test method for permeability of granular soils (constant head). In *ASTM D2434-68*. West Conshohocken, Pennsylvania: American Society for Testing and Materials.

Bandaranayake, W., L. Parsons, M. Borhan, and J. Holeton. 2007. Performance of a capacitance-type soil water probe in a well-drained sandy soil. *Soil Science Society of America Journal* 71 no. 3: 993-1002.

Bathurst, J.C., and K.R. Cooley. 1996. Use of the SHE hydrological modelling system to investigate basin response to snowmelt at Reynolds Creek, Idaho. *Journal of Hydrology* 175 no. 1–4: 181-211.

Bittelli, M., M. Flury, and G.S. Campbell. 2003. A thermodielectric analyzer to measure the freezing and moisture characteristic of porous media. *Water Resources Research* 39 no. 2.

Blonquist, J., S.B. Jones, and D. Robinson. 2005. Standardizing characterization of electromagnetic water content sensors. *Vadose Zone Journal* 4 no. 4: 1059-1069.

Bogena, H., J. Huisman, C. Oberdörster, and H. Vereecken. 2007. Evaluation of a low-cost soil water content sensor for wireless network applications. *Journal of Hydrology* 344 no. 1: 32-42.

Borsi, I., R. Rossetto, C. Schifani, and M. Hill. 2013. Modeling unsaturated zone flow and runoff processes by integrating MODFLOW-LGR and VSF, and creating the new CFL Package. *Journal of Hydrology* 488 no. 0: 33-47.

Bouyoucos, G.J., and M.M. McCool. 1916. Further studies on the freezing point lowering of soils: Michigan Agricultural College, Experiment Station.

Brooks, R.H., and A.T. Corey. 1964. Hydraulic properties of porous media. Colorado State University 37.

Brooks, R.H., and A.T. Corey. 1966. Properties of porous media affecting fluid flow. *Journal of the Irrigation and Drainage Division* 92 no. 2: 61-90.

Bruce, R. 1972. Hydraulic conductivity evaluation of the soil profile from soil water retention relations. *Soil Science Society of America Journal* 36 no. 4: 555-561.

Brun, E., E. Martin, V. Simon, C. Gendre, and C. Coleou. 1989. An energy and mass model of snow cover suitable for operational avalanche forecasting. *Journal of Glaciology* 35 no. 121: 333-342.

Burdine, N. 1953. Relative permeability calculations from pore size distribution data. *Journal of Petroleum Technology* 5 no. 03: 71-78.

Campbell, G.S. 1974. A simple method for determining unsaturated conductivity from moisture retention data. *Soil Science* 117 no. 6: 311-314.

Campbell, G.S., G.W. Gee, and A. Klute. 1986. Water potential: miscellaneous methods. *Methods of soil analysis. Part 1. Physical and Mineralogical Methods*: 619-633.

Cannell, G.H., and W.H. Gardner. 1959. Freezing-point depressions in stabilized soil aggregates, synthetic soil, and quartz sand. *Soil Science Society of America Journal* 23 no. 6: 418-422.

Carsel, R.F., and R.S. Parrish. 1988. Developing Joint Probability Distributions of Soil Water Retention Characteristics. *Water Resources Research* 24 no. 5: 755-769.

Celia, M.A., E.T. Bouloutas, and R.L. Zarba. 1990. A general mass-conservative numerical-solution for the unsaturated flow equation. *Water Resources Research* 26 no. 7: 1483-1496.

Chai, T., and R.R. Draxler. 2014. Root mean square error (RMSE) or mean absolute error (MAE)?–Arguments against avoiding RMSE in the literature. *Geoscientific Model Development* 7 no. 3: 1247-1250.

Chai, T., H.-C. Kim, P. Lee, D. Tong, L. Pan, Y. Tang, J. Huang, J. McQueen, M. Tsidulko, and I. Stajner. 2013. Evaluation of the United States national air quality forecast capability experimental real-time predictions in 2010 using air quality system ozone and NO_2measurements. *Geoscientific Model Development* 6 no. 5: 1831-1850.

Chambers, C. 2015. Decagon Support, ed. M. Islam.

———. 2016. Decagon Support, ed. M. Islam.

Chandler, D., M. Seyfried, M. Murdock, and J. McNamara. 2004. Field calibration of water content reflectometers. *Soil Science Society of America Journal* 68 no. 5: 1501-1507.

Cheng, Q., Y. Sun, S.B. Jones, V.I. Vasilyev, V.V. Popov, G. Wang, and L. Zheng. 2014. In situ measured and simulated seasonal freeze–thaw cycle: A 2-year comparative study between layered and homogeneous field soil profiles. *Journal of Hydrology* 519, Part B no. 0: 1466-1473.

Chung, S.O., and R. Horton. 1987. Soil heat and water flow with a partial surface mulch. *Water Resources Research* 23 no. 12: 2175-2186.

Clark, M.P., and J.A. Vrugt. 2006. Unraveling uncertainties in hydrologic model calibration: Addressing the problem of compensatory parameters. *Geophysical Research Letters* 33 no. 6: L06406.

Clausnitzer, V., and J. Hopmans. 1995. General-purpose optimization code based on the Levenberg-Marquardt algorithm. Land, Air, Water Resources Paper.

Cobos, D. 2014. Measurement volume of decagon volumetric water content sensors.

Connecticut, U.o. LAB #3 – Measurement of soil water characteristic curve-sensor pairing and laboratory methods. University of Connecticut.

Constantz, J. 1982. Temperature dependence of unsaturated hydraulic conductivity of two soils. *Soil Science Society of America Journal* 46 no. 3: 466-470.

Cutforth, H., E. O'Brien, J. Tuchelt, and R. Rickwood. 2004. Long-term changes in the frost-free season on the Canadian Prairies. *Canadian Journal of Plant Science* 84 no. 4: 1085-1091.

Dane, J.H., C. Topp, G.S. Campbell, R. Horton, W.A. Jury, D.R. Nielsen, H.M. van Es, P.J. Wierenga, and G.C. Topp. 2002. Part 4. Physical Methods. *Methods of Soil Analysis. Soil Science Society of America, Madison, WI*: 1692.

Dash, J., H. Fu, and J. Wettlaufer. 1995. The premelting of ice and its environmental consequences. *Reports on Progress in Physics* 58 no. 1: 115.

Davis, J., and A. Annan. 1977. Electromagnetic detection of soil moisture: Progress report I. *Canadian Journal of Remote Sensing* 3 no. 1: 76-86.

Day, P.R. 1942. The moisture potential of soils. *Soil Science* 54 no. 6: 391-400.

De Marsily, G. 1986. Quantitative hydrogeology. Paris School of Mines, Fontainebleau.

Decagon Devices, I. 2007-2010. 5TE operator's manual, 1-38. 2365 NE Hopkins Court, Pullman WA 99163: Decagon Devices, Inc.

DeVries, D. 1963. Thermal properties of soils. In 'Physics of plant environment'.(Ed. WR van Wijk) pp. 210–235. John Wiley & Sons: New York, NY.

Fayer, M.J. 2000. UNSAT-H version 3.0: Unsaturated soil water and heat flow model. Theory, user manual, and examples. *Pacific Northwest National Laboratory* 13249.

Feddes, R.A., E. Bresler, and S.P. Neuman. 1974. Field-test of a modified numerical-model for water uptake by root systems. *Water Resources Research* 10 no. 6: 1199-1206.

Feddes, R.A., P. Kabat, P.J.T. Van Bakel, J.J.B. Bronswijk, and J. Halbertsma. 1988. Modelling soil water dynamics in the unsaturated zone — State of the art. *Journal of Hydrology* 100 no. 1–3: 69-111.

Flerchinger, G., T. Caldwell, J. Cho, and S. Hardegree. 2012. Simultaneous heat and water (SHAW) model: model use, calibration, and validation. *Transactions of the ASABE* 55 no. 4: 1395-1411.

Flerchinger, G., and K. Cooley. 2000. Snowmelt simulation with the simultaneous heat and water (SHAW) model *American Geophysical Union*.

Flerchinger, G., C. Hanson, and J. Wight. 1996. Modeling evapotranspiration and surface energy budgets across a watershed. *Water Resources Research* 32 no. 8: 2539-2548.

Flerchinger, G.N., and K.E. Saxton. 1989a. Simultaneous heat and water model of a freezing snow-residue-soil system I. Theory and development. *Transactions of the ASABE* 32 no. 2: 573-576.

———. 1989b. Simultaneous heat and water model of a freezing snow-residue-soil system. II. Field verification. *Transactions of the American Society of Agricultural Engineers* 32 no. 2: 573-578.

Fortin, J.-P., R. Turcotte, S. Massicotte, R. Moussa, J. Fitzback, and J.-P. Villeneuve. 2001. Distributed watershed model compatible with remote sensing and GIS data. I: Description of model. *Journal of Hydrologic Engineering* 6 no. 2: 91-99.

Frauenfeld, O.W., T. Zhang, R.G. Barry, and D. Gilichinsky. 2004. Interdecadal changes in seasonal freeze and thaw depths in Russia. *Journal of Geophysical Research: Atmospheres* 109 no. D5.

Freeze, R.A. 1969. The mechanism of natural ground-water recharge and discharge 1. One-dimensional, vertical, unsteady, unsaturated flow above a recharging or discharging ground-water flow system. *Water Resources Research* 5 no. 1: 1-19.

Freeze, R.A., and J. Banner. 1970. The mechanism of natural ground-water recharge and discharge 2. Laboratory column experiment and field measurements. *Water Resources Research* 6 no. 1: 1 to 18.

French, H., and A. Binley. 2004. Snowmelt infiltration: monitoring temporal and spatial variability using time-lapse electrical resistivity. *Journal of Hydrology* 297 no. 1–4: 174-186.

Green, R., and J. Corey. 1971. Calculation of hydraulic conductivity: a further evaluation of some predictive methods. *Soil Science Society of America Journal* 35 no. 1: 3-8.

Hanson, B., and D. Peters. 2000. Soil type affects accuracy of dielectric moisture sensors. *California Agriculture* 54 no. 3: 43-47.

Hansson, K., J. Šimůnek, M. Mizoguchi, L.-C. Lundin, and M.T. Van Genuchten. 2004. Water flow and heat transport in frozen soil. *Vadose Zone Journal* 3 no. 2: 693-704.

He, H., and M. Dyck. 2013. Application of multiphase dielectric mixing models for understanding the effective dielectric permittivity of frozen soils. *Vadose Zone Journal* 12 no. 1.

Hirota, T., Y. Iwata, M. Hayashi, S. Suzuki, T. Hamasaki, R. Sameshima, and I. Takayabu. 2006. Decreasing soil-frost depth and its relation to climate change in Tokachi, Hokkaido, Japan. *Journal of the Meteorological Society of Japan. Ser. II* 84 no. 4: 821-833.

Hivon, E., and D. Sego. 1990. Determination of the unfrozen water content of saline permafrost using time-domain reflectometry (TDR). In *Proceedings of the 5th Canadian Permafrost Conference*, 257-262.

Hoekstra, P., and A. Delaney. 1974. Dielectric properties of soils at UHF and microwave frequencies. *Journal of Geophysical Research* 79 no. 11: 1699-1708.

Holländer, H.M., T. Blume, H. Bormann, W. Buytaert, G.B. Chirico, J.-F. Exbrayat, D. Gustafsson, H. Hölzel, P. Kraft, C. Stamm, S. Stoll, G. Blöschl, and H. Flühler. 2009. Comparative predictions of discharge from an artificial catchment (Chicken Creek) using sparse data. *Hydrology and Earth System Sciences* 13 no. 11: 2069-2094.

Holländer, H.M., H. Bormann, T. Blume, W. Buytaert, G.B. Chirico, J.F. Exbrayat, D. Gustafsson, H. Hölzel, T. Krauße, P. Kraft, S. Stoll, G. Blöschl, and H. Flühler. 2014.

Impact of modellers' decisions on hydrological a priori predictions. *Hydrology and Earth System Sciences* 18 no. 6: 2065-2085.

Hopmans, J.W., and J.H. Dane. 1986. Combined effect of hysteresis and temperature on soil-water movement. *Journal of Hydrology* 83 no. 1–2: 161-171.

Hyndman, R.J., and A.B. Koehler. 2006. Another look at measures of forecast accuracy. *International Journal of Forecasting* 22 no. 4: 679-688.

Ishizaki, T., M. Maruyama, Y. Furukawa, and J.G. Dash. 1996. Premelting of ice in porous silica glass. *Journal of Crystal Growth* 163 no. 4: 455-460.

Iwata, Y., M. Hayashi, and T. Hirota. 2008. Comparison of Snowmelt Infi ltration under Different Soil-Freezing Conditions Influenced by Snow Cover. *Vadose Zone Journal*: 1-8.

Iwata, Y., M. Hayashi, S. Suzuki, a. T. Hirota, and S. Hasegawa. 2010. Effects of snow cover on soil freezing, water movement, and snowmelt infiltration: A paired plot experiment. *Water Resources Research* 46 no. W09504: 1-11.

Jackson, R.D. 1972. On the calculation of hydraulic conductivity. *Soil Science Society of America Journal* 36 no. 2: 380-382.

Jackson, R.D., R. Reginato, and C. Van Bavel. 1965. Comparison of measured and calculated hydraulic conductivities of unsaturated soils. *Water Resources Research* 1 no. 3: 375-380.

Jansson, P.-E., and D.S. Moon. 2001. A coupled model of water, heat and mass transfer using object orientation to improve flexibility and functionality. *Environmental Modelling & Software* 16 no. 1: 37-46.

Jeppson, R.W. 1974. Axisymmetric infiltration in soils, I. Numerical techniques for solution. *Journal of Hydrology* 23 no. 1: 111-130.

Jones, S.B., and D. Or. 2004. Frequency domain analysis for extending time domain reflectometry water content measurement in highly saline soils. *Soil Science Society of America Journal* 68 no. 5: 1568-1577.

Kane, D.L., and J. Stein. 1983. Water movement into seasonally frozen soils. *Water Resources Research* 19 no. 6: 1547-1557.

Kanzari, S., M. Hachicha, and B. Rachida. 2012. Laboratory method for estimating water retention properties of unsaturated soil. *Walailak Journal of Science and Technology (WJST)* 9 no. 4: 361-367.

Kelleners, T., D. Robinson, P. Shouse, J. Ayars, and T. Skaggs. 2005b. Frequency dependence of the complex permittivity and its impact on dielectric sensor calibration in soils. *Soil Science Society of America Journal* 69 no. 1: 67-76.

Kelleners, T., M. Seyfried, J. Blonquist, J. Bilskie, and D. Chandler. 2005a. Improved interpretation of water content reflectometer measurements in soils. *Soil Science Society of America Journal* 69 no. 6: 1684-1690.

Kelleners, T., R. Soppe, J. Ayars, and T. Skaggs. 2004. Calibration of capacitance probe sensors in a saline silty clay soil. *Soil Science Society of America Journal* 68 no. 3: 770-778.

Kirkham, D., and W.L. Powers. 1972. *Advanced soil physics*: Wiley.

Kizito, F., C. Campbell, G. Campbell, D. Cobos, B. Teare, B. Carter, and J. Hopmans. 2008. Frequency, electrical conductivity and temperature analysis of a low-cost capacitance soil moisture sensor. *Journal of Hydrology* 352 no. 3: 367-378.

Kool, J., J. Parker, and M.T. Van Genuchten. 1985. ONESTEP: A nonlinear parameter estimation program for evaluating soil hydraulic properties from one-step outflow experiments. *Bulletin-Virginia Agricultural Experiment Station, Virginia Polytechnic Institute and State University (USA)*.

———. 1987. Parameter estimation for unsaturated flow and transport models—A review. *Journal of Hydrology* 91 no. 3-4: 255-293.

Lea-Cox, J., A. Ristvey, F. Arguedas Rodriguez, D. Ross, J. Anhalt, and G. Kantor. 2008. low-cost multihop wireless sensor network, enabling real-time management of environmental data for the greenhouse and nursery industry. In *International Symposium on High Technology for Greenhouse System Management: Greensys2007*.

Li, R., H. Shi, G.N. Flerchinger, T. Akae, and C. Wang. 2012. Simulation of freezing and thawing soils in Inner Mongolia Hetao Irrigation District, China. *Geoderma* 173–174 no. 0: 28-33.

Logsdon, S. 2005. Time domain reflectometry range of accuracy for high surface area soils. *Vadose Zone Journal* 4 no. 4: 1011-1019.

Lundin, L.-C. 1990. Hydraulic properties in an operational model of frozen soil. *Journal of Hydrology* 118 no. 1: 289-310.

Madsen, H.B., C.R. Jensen, and T. Boysen. 1986. A comparison of the thermocouple psychrometer and the pressure plate methods for determination of soil water characteristic curves. *Journal of Soil Science* 37 no. 3: 357-362.

Malmberg, C., and A. Maryott. 1956. Dielectric constant of water from 0°C to 100°C. *Journal of Research of the National Bureau of Standards* 56: 1-8.

Marquardt, D.W. 1963. An algorithm for least-squares estimation of nonlinear parameters. *Journal of the society for Industrial and Applied Mathematics* 11 no. 2: 431-441.

McKeen, S., J. Wilczak, G. Grell, I. Djalalova, S. Peckham, E.Y. Hsie, W. Gong, V. Bouchet, S. Menard, and R. Moffet. 2005. Assessment of an ensemble of seven real-time ozone forecasts over eastern North America during the summer of 2004. *Journal of Geophysical Research: Atmospheres* 110 no. D21.

Miller, E., and R. Miller. 1956. Physical theory for capillary flow phenomena. *Journal of Applied Physics* 27 no. 4: 324-332.

Miller, R.D. 1980. Freezing phenomena in soils. *Applications of Soil Physics* 278: 283.

Millington, R., and J. Quirk. 1961. Permeability of porous solids. *Transactions of the Faraday Society* 57: 1200-1207.

Milly, P.C.D. 1982. Moisture and heat transport in hysteretic, inhomogeneous porous media: A matric head-based formulation and a numerical model. *Water Resources Research* 18 no. 3: 489-498.

Moghadas, S., A.M. Gustafsson, P. Viklander, J. Marsalek, and M. Viklander. 2015. Laboratory study of infiltration into two frozen engineered (sandy) soils recommended for bioretention. *Hydrological Processes* 30 no. 8: 1251-1264.

Mualem, Y. 1974. A conceptual model of hysteresis. *Water Resources Research* 10 no. 3: 514-520.

———. 1976. A new model for predicting the hydraulic conductivity of unsaturated porous media. *Water Resources Research* 12 no. 3: 513-522.

Nash, J.E., and J.V. Sutcliffe. 1970. River flow forecasting through conceptual models part I — A discussion of principles. *Journal of Hydrology* 10 no. 3: 282-290.

Nemali, K.S., F. Montesano, S.K. Dove, and M.W. van Iersel. 2007. Calibration and performance of moisture sensors in soilless substrates: ECH2O and Theta probes. *Scientia Horticulturae* 112 no. 2: 227-234.

Neuman, S.P., R.A. Feddes, and E. Bresler. 1974. Finite element simulation of flow in saturated-unsaturated soils considering water uptake by plants.

Noborio, K., K. McInnes, and J. Heilman. 1996. Two-dimensional model for water, heat, and solute transport in furrow-irrigated soil: I. Theory. *Soil Science Society of America Journal* 60 no. 4: 1001-1009.

Ojo, E.R., P.R. Bullock, J. L'Heureux, J. Powers, H. McNairn, and A. Pacheco. 2015. Calibration and evaluation of a frequency domain reflectometry sensor for real-time soil moisture monitoring. *Vadose Zone Journal* 14 no. 3: 0.

Oreiller, M., D.F. Nadeau, M. Minville, and A.N. Rousseau. 2014. Modelling snow water equivalent and spring runoff in a boreal watershed, James Bay, Canada. *Hydrological Processes* 28 no. 25: 5991-6005.

Parsons, L.R., and W.M. Bandaranayake. 2009. Performance of a new capacitance soil moisture probe in a sandy soil. *Soil Science Society of America Journal* 73 no. 4: 1378-1385.

Paterson, D. 1995. Biogenic structure of early sediment fabric visualized by low-temperature scanning electron microscopy. *Journal of the Geological Society* 152 no. 1: 131-140.

Patterson, D., and M. Smith. 1981. The measurement of unfrozen water content by time domain reflectometry: Results from laboratory tests. *Canadian Geotechnical Journal* 18 no. 1: 131-144.

———. 1983. Measurement of unfrozen water content in saline permafrost using time domain reflectometry. In *Proceedings of the 4th International Conference on Permafrost. Fairbanks, Alaska*.

———. 1985. Unfrozen water content in saline soils: results using time-domain reflectometry. *Canadian Geotechnical Journal* 22 no. 1: 95-101.

Persson, M., and R. Berndtsson. 1998. Texture and electrical conductivity effects on temperature dependency in time domain reflectometry. *Soil Science Society of America Journal* 62 no. 4: 887-893.

Philip, J., and D. De Vries. 1957. Moisture movement in porous materials under temperature gradients. *Eos, Transactions American Geophysical Union* 38 no. 2: 222-232.

Plauborg, F., B.V. Iversen, and P.E. Lærke. 2005. In situ comparison of three dielectric soil moisture sensors in drip irrigated sandy soils. *Vadose Zone Journal* 4 no. 4: 1037-1047.

Polyakov, V., A. Fares, and M. Ryder. 2005. Calibration of a capacitance system for measuring water content of tropical soil. *Vadose Zone Journal* 4 no. 4: 1004-1010.

Rao, B.H., and D. Singh. 2011. Moisture content determination by TDR and capacitance techniques: a comparative study. *International Journal of Earth Sciences and Engineering* 4 no. 6: 132-137.

Robinson, D., C. Campbell, J. Hopmans, B. Hornbuckle, S.B. Jones, R. Knight, F. Ogden, J. Selker, and O. Wendroth. 2008. Soil moisture measurement for ecological and hydrological watershed-scale observatories: A review. *Vadose Zone Journal* 7 no. 1: 358-389.

Robinson, D., I. Lebron, S. Lesch, and P. Shouse. 2004. Minimizing drift in electrical conductivity measurements in high temperature environments using the EM-38. *Soil Science Society of America Journal* 68 no. 2: 339-345.

Rodríguez, F.R.A. 2009. Calibrating capacitance sensors to estimate water content, matric potential, and electrical conductivity in soilless substrates, Department of Plant Science and Landscape Architecture, University of Maryland, 789 East Eisenhower Parkway.

Savage, N., P. Agnew, L. Davis, C. Ordóñez, R. Thorpe, C. Johnson, F. O'Connor, and M. Dalvi. 2013. Air quality modelling using the Met Office Unified Model (AQUM OS24-26): model description and initial evaluation. *Geoscientific Model Development* 6 no. 2: 353-372.

Scanlon, B.R., K. Keese, R.C. Reedy, J. Simunek, and B.J. Andraski. 2003. Variations in flow and transport in thick desert vadose zones in response to paleoclimatic forcing (0–90 kyr): Field measurements, modeling, and uncertainties. *Water Resources Research* 39 no. 7.

Schaap, M.G., F.J. Leij, and M.T. van Genuchten. 2001. ROSETTA: A computer program for estimating soil hydraulic parameters with hierarchical pedotransfer functions. *Journal of Hydrology* 251 no. 3-4: 163-176.

Schofield, R., and J.B. Da Costa. 1938. The measurement of pF in soil by freezing-point. *The Journal of Agricultural Science* 28 no. 04: 644-653.

Schulla, J., and K. Jasper. 2007. Model Description WaSiM. ETH Zurich 181.

Seyfried, M.S., and M.D. Murdock. 2004. Measurement of soil water content with a 50-MHz soil dielectric sensor. *Soil Science Society of America Journal* 68 no. 2: 394-403.

Simunek, J., R. Angulo-Jaramillo, M.G. Schaap, J.-P. Vandervaere, and M.T. van Genuchten. 1998. Using an inverse method to estimate the hydraulic properties of crusted soils from tension-disc infiltrometer data. *Geoderma* 86 no. 1-2: 61-81.

Simunek, J., M. Sejna, and M.T. van Genuchten. 1999. The HYDRUS-2D software package for simulating the two-dimensional movement of water, heat, and multiple solute in variably-saturated porous media. Riverside, Calofornia, USA: U.S. Salinity Laboratory Agricultural Research Service, U.S. Department of Agriculture.

Simunek, J., M.T. van Genuchten, and M. Sejna. 2013. The HYDRUS-1D software package for simulating the movement of water, heat, and multiple solutes in variably saturated media Department of Environmental Sciences, University of California Riverside, Riverside, California, USA.

Šimůnek, J., M.T. van Genuchten, and M. Šejna. 2016. Recent developments and applications of the HYDRUS computer software packages. *Vadose Zone Journal* 15 no. 7.

Smith-Rose, R. 1933. The electrical properties of soil for alternating currents at radio frequencies. *Proceedings of the Royal Society of London. Series A, Containing Papers of a Mathematical and Physical Character* 140 no. 841: 359-377.

Smith, M.W., and A.R. Tice. 1988. Measurement of the unfrozen water content of soils. comparison of NMR (Nuclear Magnetic Resonance) and TDR (Time Domain Reflectometry) methods. DTIC Document.

Sophocleous, M. 1979. Analysis of water and heat flow in unsaturated-saturated porous media. *Water Resources Research* 15 no. 5: 1195-1206.

Spaans, E.J., and J.M. Baker. 1996a. The soil freezing characteristic: Its measurement and similarity to the soil moisture characteristic. *Soil Science Society of America Journal* 60 no. 1: 13-19.

Spaans, E.J.A., and J.M. Baker. 1996b. The soil freezing characteristics: its measurement and similarity to the soil moisture characteristic: E. J. A. Spaans & J. M. Baker, Soil Science Society of America Journal, 60(1), 1996, pp 13–19. *International Journal of Rock Mechanics and Mining Sciences & Geomechanics Abstracts* 33 no. 7: A300.

Spelman, D., K.-D. Kinzli, and T. Kunberger. 2013. Calibration of the 10HS soil moisture sensor for southwest florida agricultural soils. *Journal of Irrigation and Drainage Engineering* 139 no. 12: 965-971.

Stähli, M., L. Nyberg, P.-E. Mellander, P.-E. Jansson, and K.H. Bishop. 2001. Soil frost effects on soil water and runoff dynamics along a boreal transect: 2. Simulations. *Hydrological Processes* 15 no. 6: 909- 926.

Suzuki, K. 2013. Estimation of snowmelt infiltration into frozen ground and snowmelt runoff in the mogot experimental watershed in East Siberia. *International Journal of Geosciences, 2013, 4, 1346-1354*: 1346-1354.

Thompson, R., M. Gallardo, M. Fernandez, L. Valdez, and C. Martinez-Gaitan. 2007. Salinity effects on soil moisture measurement made with a capacitance sensor. *Soil Science Society of America Journal* 71 no. 6: 1647-1657.

Tian, H., C. Wei, H. Wei, and J. Zhou. 2014. Freezing and thawing characteristics of frozen soils: Bound water content and hysteresis phenomenon. *Cold Regions Science and Technology* 103 no. 0: 74-81.

Topp, G., S. Zegelin, and I. White. 2000. Impacts of the real and imaginary components of relative permittivity on time domain reflectometry measurements in soils. *Soil Science Society of America Journal* 64 no. 4: 1244-1252.

Topp, G.C., J.L. Davis, and A.P. Annan. 1980. Electromagnetic determination of soil water content: Measurements in coaxial transmission lines. *Water Resources Research* 16 no. 3: 574-582.

Travis. 2015. Re: Urgent: Re: Contact Us - Montasir Islam - Canada.

Van Dam, J., J. Stricker, and P. Droogers. 1994. Inverse method to determine soil hydraulic functions from multistep outflow experiments. *Soil Science Society of America Journal* 58 no. 3: 647-652.

Van Genuchten, M.T. 1980. A closed-form equation for predicting the hydraulic conductivity of unsaturated soils. *Soil Science Society of America Journal* 44 no. 5: 892-898.

———. 1981. Non-equilibrium transport parameters from miscible displacement experiments.

van Genuchten, M.T., and D. Nielsen. 1985. On describing and predicting the hydraulic properties of unsaturated soils. *Annales Geophysicae* 3 no. 5: 615-628.

Vogel, T., M. Cislerova, and J.W. Hopmans. 1991. Porous media with linearly variable hydraulic properties. *Water Resources Research* 27 no. 10: 2735-2741.

Walker, J.P., G.R. Willgoose, and J.D. Kalma. 2004. In situ measurement of soil moisture: a comparison of techniques. *Journal of Hydrology* 293 no. 1: 85-99.

Watanabe, K., and Y. Kugisaki. 2016. Effect of macropores on soil freezing and thawing with infiltration. *Hydrological Processes*.

Watanabe, K., and M. Mizoguchi. 2002. Amount of unfrozen water in frozen porous media saturated with solution. *Cold Regions Science and Technology* 34 no. 2: 103-110.

Watanabe, K., and T. Wake. 2009. Measurement of unfrozen water content and relative permittivity of frozen unsaturated soil using NMR and TDR. *Cold Regions Science and Technology* 59 no. 1: 34-41.

Zhang, X., S. Sun, and YongkangbXue. 2007. Development and testing of a frozen soil parameterization for cold region studies. *Journal of Hydrometeorology* 8 no. 4: 690-701.